# COMPRESSED ENCODING OF SIGNALS AND ACTIVITY DETECTION BASED ON LEVEL-CROSSING SAMPLING

**A THESIS**

***Submitted to the University of Calicut***

***By***

**PREMANAND B.**

(No. 11890/2014/CU)

*Under the Supervision of*

**Dr. SHEEBA V. S.**

*for the fulfilment of the award of the degree*

**DOCTOR OF PHILOSOPHY**


**DEPARTMENT OF ELECTRICAL AND ELECTRONICS ENGINEERING**

**GOVERNMENT ENGINEERING COLLEGE THRISSUR**

**UNIVERSITY OF CALICUT**

**KERALA - INDIA**

**JANUARY 2021**

# Certificate

This is to certify that the suggestions / corrections from the adjudicators as per Ref. No. 3176/RESEARCH-E-ASST-3/2021/Admn, dated 25/08/2021 from the Director of Research, University of Calicut, have been incorporated in the thesis **"Compressed Encoding of Signals and Activity Detection based on Level-Crossing Sampling"** done by **Mr. Premanand B.**, under my supervision and guidance at Department of Electrical and Electronics Engineering, Govt. Engineering College, Thrissur in partial fulfilment of the requirement for the Degree of Doctor of Philosophy under Faculty of Engineering, University of Calicut.

September 2021

GOVT ENGINEERING COLLEGE
Department of Electrical Engineering
THRISSUR

Dr. Sheeba V. S
Retired Principal,
Govt. Engineering College, Thrissur.
(Research Supervisor)

# BONAFIDE CERTIFICATE

This is to certify that the work reported in this thesis entitled **"Compressed Encoding of Signals and Activity Detection based on Level-Crossing Sampling"** that is being submitted by Mr. PREMANAND B. for the award of the Degree of Doctor of Philosophy, to the University of Calicut, is based on the bonafide research work carried out by him under my supervision and guidance in the Department of Electrical and Electronics Engineering, Government Engineering College, Thrissur, University of Calicut. The results embodied in this thesis have not been included in any other thesis submitted previously for the award of any degree or diploma of any other University or Institution.

**Dr. SHEEBA V. S.**
(Supervising Guide)
Department of Electrical and Electronics Engineering,
Government Engineering College, Thrissur.

GOVT. ENGINEERING COLLEGE
Department of Electrical Engineering
THRISSUR

**Head of Department**
Electrical and Electronics Engineering
Government Engineering College, Thrissur.

**Place: Thrissur – 9**

Date: 6th January 2021

# DECLARATION

I hereby declare that this thesis entitled Compressed Encoding of Signals and Activity Detection based on Level-Crossing Sampling, submitted to the University of Calicut, for the award of Degree of Doctor of Philosophy under the Faculty of Engineering is an independent work done by me under the supervision and guidance of Dr. SHEEBA V. S, Professor, Department of Electrical and Electronics Engineering, Research Centre, Government Engineering College Thrissur, University of Calicut.

I also declare that this thesis contains no material which has been accepted for the award of any other degree or diploma of any University or Institution and to the best of my knowledge and belief, it contains no material previously published by any other person, except where due references are made in the text of the thesis.

**Premanand B.**

11890/RESEARCH-B-SO/2014/CU,
Research Scholar
Department of Electrical and Electronics Engineering
Government Engineering College, Thrissur

6th January 2021

# ACKNOWLEDGEMENT

*This thesis would not have been possible without the support and guidance of several people and I would like to take this opportunity to express my sincere gratitude towards them.*

*My deepest gratitude goes first to my supervisor Dr. (Prof). Sheeba V.S., Principal, G.E.C Thrissur, for her sincere and timely support and guidance throughout the research. Amid her busy routine responsibilities as the head of a large institution, she found time to evaluate, correct, and lead my research on the right path with continuous and consistent inputs. I remain indebted to her encouragements, continuous support, timely suggestions, and discussion throughout my research work. I take this opportunity to express my heartfelt thanks to her for all the technical and moral help that she has offered.*

*I am grateful to the Director and all the staff members of the Directorate of Research, Calicut University for their timely support to complete the work and in the final submission of the thesis.*

*I use this opportunity to thank my Doctoral committee members Dr. Suresh K., Professor, Government Engineering College Barton Hill, and Dr. K. Meenakshy, Professor, Government Engineering College, Thrissur for providing me timely directions in carrying out my research work.*

*I am also obliged to Dr. M. Nandakumar, Dr. Reji P, Dr. B. Jayanand, and Prof. Preetha K.P who in their capacity as the Heads of the Department of Electrical and Electronics Engineering have helped me by providing the facilities in the department for carrying out my research work. I am also grateful to Dr. B. Jayanand for his help in simulating the basic models. I am thankful to Dr. Shalij P.R., Professor in Production Engineering for helping me to format the thesis.*

*The encouragement and support by Prof. Mrinalini C.P., Dr. Thajudhin AhamedV.I., and Dr. Anilkumar C.D. in their capacity as Heads of Department of Electronics & Communication Engineering is worth mentioning. The support extended to me by Mr. Job Chunkath, Professor, G.E.C Thrissur, Mr. Jayadevan R, Professor G.E.C Palakkad, and Mrs. Jeeva K. A, Prof. VAST is also worth mentioning.*

*I am thankful to all the faculty members and staff members of the Department of Electronics and Communication Engineering, Govt. Engineering College, Thrissur, for their help and motivation throughout the research period.*

*Finally, I would like to acknowledge the unconditional love and support of my family. Without them, this thesis could not have been accomplished.*

Thrissur – 9

6th January 2021 PREMANAND B

# ABSTRACT

Classical data acquisition systems are based on uniform sampling, and they do not exploit the signal variations. Many samples are generated while sampling low-activity sporadic signals without any relevant information, which increase the system activity and power consumption. The Nyquist rate for sampling is specified for a general signal, and for efficient encoding, the sampling rate must be specific to signals and applications. Level-crossing sampling (LCS) is an activity-dependent sampling method that results in the compressed encoding of sparse and bursty signals. The systems that have scarcity in computational power, bandwidth, and memory will be benefited from LCS. Presently LCS methods have been widely applied for sampling bio-potential signals. While sampling speech signals, LCS with a constant temporal resolution demands the time-to-digital converter (TDC) to have wide dynamic ranges resulting in increased bits per sample.

Vibration signals are utilized to monitor the mechanical systems and have the highest frequency among all the other sensor outputs. The analysis of these signals becomes extremely difficult due to the enormous amount of vibration data acquired at the Nyquist rate. Besides, there is a limitation on the available bandwidth in launch vehicles and wireless nodes. Wireless transmissions in sensor nodes consume a significant portion of its power, and hence data compression must be done before transmission. Traditional data compression methods have to operate on all the samples acquired at the uniform rate, which increase the computational complexity at the transmitter.

This thesis explores the application of level-crossing methods for (i) the compressed encoding of speech and vibration signals and (ii) the activity detection of the signals. The concept of frequency-scaling is applied to LCS, adaptive LCS, and extremum sampling to achieve multiple resolutions in time.

Due to the reduction in the dynamic range of TDC, the number of bits per sample and the total data size are decreased. Extremum sampling is proposed for the encoding of vibration signals that results in excellent compression. Since the level-crossing sampling accomplishes compression during the sampling process, the additional burden at the transmitter for subjecting all the acquired samples to a compression algorithm is evaded.

Faults in the machines usually create an increase in the frequency or the amplitude of the vibration signal. This thesis proposes anomaly detection in mechanical systems with average level-crossing rate (*ALCR*), a parameter indicating the rate of change of the vibration signals. *ALCR* is also applied for detecting the activity of signals, based on which specific control action can be triggered. A voice-controlled audio mixer is simulated, in which the activity of the input speech signal is monitored with its *ALCR* values. Based on the *ALCR*, the attenuation of a background music signal is controlled. An acoustic feedback suppressor in which the feedback detection is performed with *ALCR* and the feedback frequency estimation with zero-crossing time, has been simulated. The feedback suppression is performed with notch and low-pass filters. The methods based on *ALCR* work on the analog output of sensor and does not require the conventional steps like sampling, framing, feature extraction, classification, or computation of the spectrum.

# TABLE OF CONTENTS

# LIST OF FIGURES

**Figure No Description** **Page**

**Figure No Description** **Page**

# LIST OF TABLES

# LIST OF SYMBOLS

| | |
|---|---|
| $\Delta v$ | Inter-level distance in LCS |
| $f_{max}$ | Maximum frequency |
| $W$ | Bandwidth of the signal |
| $a$ | Activity factor |
| $C$ | Value of switched capacitance |
| $V$ | Value of supply voltage |
| $f_c$ | Frequency of the clock |
| $t_q$ | Time quantum |
| $f_{Nyq}$ | Nyquist frequency |
| $m$ | Number of non-zero samples of the signal in a domain |
| $n$ | Original signal size specified in CS |
| $x$ | discrete time input signal |
| $y$ | output signal |
| $\phi$ | Measurement matrix |
| $\psi$ | Ortho-normal basis function |
| $\alpha$ | Coefficient sequence of input in a domain |
| $\theta$ | Sensing matrix |
| $\mu$ | Coherence |
| $l_n$ | $n^{th}$ reference level in LCS |
| $L_n$ | Digital count corresponding to a level $l_n$ |
| $dt_n$ | Interval between adjacent level-crossing instants |
| $dt_{max}$ | Maximum value of $dt_n$ |
| $Dt_n$ | Digital equivalent of $dt_n$ |
| $Dt_{max}$ | Digital equivalent of $dt_{max}$ |
| $L$ | Total number of reference levels in LCS |
| $T_C$ | Time period of clock signal |
| $DIR$ | Direction bit in ALCS |
| $t_n$ | $n^{th}$ time instant |
| $x(t)$ | Continuous-time signal |
| $T$ | Time interval between two events |
| $\overline{T}$ | Quantized time interval |

| | |
|---|---|
| $\delta t$ | Error in time quantization |
| $\delta v$ | Error in amplitude corresponding to $\delta t$ |
| $SNR$ | Signal-to-quantization noise ratio |
| $P(x)$ | Power of the input signal $x$ |
| $P(\delta v)$ | Noise power due to quantization |
| $d$ | Delay in conversion loop |
| $d_{max}$ | Maximum loop delay |
| $p(x)$ | Probability density of input |
| $ADA$ | Indication bit for adaptive mode |
| $S_n$ | Polariy indication bit for the peak value |
| $P_n$ | The distance between adjacent peaks (in terms of $\Delta v$) in ES |
| $V_H$ | Upper threshold value at input comparator |
| $V_L$ | Lower threshold value at input comparator |
| $R_i$ | Approximated value of $x(t)$ |
| $B$ | Word size of the TDC counter |
| $K$ | Frequency-scaling factor |
| $CLK$ | Clock input |
| $L(j,t_0)$ | Level-crossing rate of a particular level |
| $N$ | Total number of reference levels in LCS |
| $N_t$ | Number of level-crossings in a duration t |
| $\Delta t$ | Duration for which $ALCR$ is calculated |

# LIST OF ABBREVIATIONS

| | |
|---|---|
| ADC | Analog-to-digital converter |
| CS | Compressed Sensing |
| ZCR | Zero-Crossing Rate |
| ALCR | Average Level-Crossing Rate |
| LCD | Level-Crossing Detector |
| TDC | Time-to-Digital Converter |
| ES | Extremum Sampling |
| ALCS | Adaptive Level-Crossing Sampling |
| CMOS | Complementary Metal Oxide Semiconductor |
| CT-DSP | Continuous-Time Digital Signal Processing |
| DCT | Discrete Cosine Transform |
| PHM | Prognostics and Health Management |
| CBM | Condition-Based Maintenance |
| RUL | Remaining Useful Life |
| STE | Short-Term Energy |
| PTPR | Peak-to-Threshold Power Ratio |
| PAPR | Peak-to-Average Power Ratio |
| PHPR | Peak-to-Harmonic Power Ratio |
| PNPR | Peak-to-Neighbouring Power Ratio |
| IPMP | Inter-frame Peak Magnitude Persistence |
| IMSD | Inter-frame Magnitude Slope Deviation |
| SNR | Signal-to-Noise Ratio |
| CCSDS | Consultative Committee for Space Data Systems |
| MSE | Mean-Square Error |
| PSNR | Peak Signal-to-Noise Ratio |
| $R^2$ | R-square value |
| CR | Compression Ratio |
| AFC | Adaptive Frequency Cancellation |
| AGC | Automatic Gain Control |
| AEQ | Automatic Equalisation Method |
| FFT | Fast-Fourier Transform |

# CHAPTER 1

# INTRODUCTION

In most data acquisition systems, analog signals are sampled at the Nyquist rate, which is twice the highest frequency $f_{max}$ present in the signal. It is a uniform sampling method, in which the sampling rate is independent of the instantaneous frequency of the input signal. The conventional sampling is inefficient while sampling sparse and bursty signals. Signals are over-sampled if the instantaneous frequency is much less than $f_{max}$. Non-uniform and event-driven sampling methods have advantages compared to uniform and synchronous sampling while processing sparse and bursty signals. Non-uniform sampling methods reduce the sampling and computation costs, taking advantage of the sparsity of the signals.

Conventional data compression methods are based on a two-step process: sample-then-compress, which consume the already limited resources. Many samples are discarded at a later stage, wasting resources like storage and computation. Non-uniform sampling methods generate a compressed set of samples with which the input signal can be reconstructed accurately. In compressed sensing (CS), the signal reconstruction is possible with fewer samples than those acquired at the Nyquist rate. The signal is reconstructed by finding a solution to an under-determined linear system of equations. The reconstruction methods are based on optimization algorithms, which make the real-time reconstruction difficult. The sensing part may also involve multiplication by large size matrices.

Level Crossing Sampling (LCS) is a form of non-uniform sampling in which a sample is generated when the amplitude of the signal crosses any of the fixed numbers of reference levels. It is an activity-dependent sampling method,

in which more samples are acquired when the signal is bursty, and none during the idle period. The signal need not be passed through an anti-aliasing filter to limit its frequency. LCS has inherent noise reduction property because amplitude variations within the limits of two nearby reference levels are automatically removed. Several signals, including telemetry, biopotential, and speech, are sparse in time. For a sparse signal, LCS combines sampling and compression into a single step. It results in economic consumption of power and is suitable for battery-operated implantable or wearable devices.

Vibration signals are used for the condition monitoring of mechanical systems. Among all the telemetry signals from a launch vehicle, vibration signals have the highest frequency and must be sampled at higher sampling frequencies. In industries, vibration data must be sent to remote servers for processing. Hence, there is a necessity for compressing vibration signals to reduce the total data size and transmission bandwidth.

Most engineering systems have rotating parts, and various parameters must be closely monitored to maintain their health. The situation is very critical in systems such as aircraft and spacecraft in which failure may cause loss of lives. The faults of machines used in industries must be detected long before they become severe to schedule the planned repair work. Most of the faults such as imbalance, resonance, misalignment, looseness, drive belt problems, and eccentricity occurring in machines cause a few variations in the vibration signals. Hence vibration analysis serves as a means for identifying machine deterioration. Further damage and its severe effects can be avoided if preventive maintenance is carried out soon after a warning signal is received.

Fault diagnosis and prognosis are mainly dependent on sensors and their sensing strategies. A wide variety of sensors are used for condition monitoring of equipments nowadays. The data output from the sensors must be processed to extract useful information about the machine's health. For vibration data,

frequency or wavelet domain are suitable for fault detection or condition monitoring. Failures in the systems cause changes in power, entropy, spectrum, and amplitude. From the massive data, useful information must be extracted for detecting anomalies or faults. All the present methods for anomaly detection involve either sophisticated analysis or require processing on a massive amount of data collected for this purpose. The number of vibration signals transmitted to the ground can be reduced to a minimum if on-board anomaly detection is used, and its output alone needs to be transmitted to earth instead of sending the real sensor data.

The zero-crossing rate (*ZCR*) and energy of the signals are usually employed for the activity detection of the signals. Both *ZCR* and energy are computed with the digital samples of the input signal. Average level-crossing rate (*ALCR*) measured from the analog input signal can be used for activity detection in speech signals. Voice-controlled mixers used in radio stations and other announcement systems attenuate the background signal depending upon the intensity of speech signal. Another application for which *ALCR* has been used in this thesis is for the howling detection. Public address systems usually suffer from acoustic feedback, and annoying howling noise is generated. Presently used howling detection systems require sampling, digitization, and framing of the acoustic signal.

## 1.1 MOTIVATION

The primary motivations for carrying out this research work are summarized as follows:

- There exist non-uniform sampling methods that are economical compared to conventional sampling methods.
- LCS has been employed successfully for the compressed encoding of biopotential signals.

- An efficient encoding of the level-crossing time is essential for reducing the dynamic range of the time-to-digital converter (TDC) employed in LCS while sampling speech signals.
- Extremum sampling can generate compressed samples of signals which have an oscillatory nature, including vibration signals.
- The parameter, "average level-crossing rate (*ALCR*)," can be employed for real-time activity detection and abnormality detection using vibration signals.

## 1.2 OBJECTIVES

The objectives of this work are to:

1. Design non-uniform samplers which employ Level-Crossing Sampling (LCS), adaptive LCS, and extremum Sampling for speech signals and compare their performance in compressing the signals.
2. Design level-crossing samplers with multiple resolutions in time to reduce the dynamic range of the TDC and minimize the bits per sample.
3. Design a non-uniform sampler based on extremum sampling to produce a compressed set of samples from vibration signals.
4. Use Level-Crossing Rate for
    - the identification of the speech activity
    - acoustic feedback detection
    - the anomaly detection in mechanical systems using vibration signals

## 1.3 CONTRIBUTIONS

Level-crossing methods have been applied for the compressed encoding of the signals and activity detection. Speech and vibration signals have been

encoded with level-crossing sampling methods. Activity detection has been performed based on the level-crossing rate of the input signals. The following are the contributions of this thesis.

1. Designed and simulated a level-crossing sampling (LCS) system for the compressed encoding of speech signals that perform sampling, quantization, encoding, and compression in a single step.

2. Simulated 2-level adaptive level-crossing sampler (ALCS) in which the inter-level distance $\Delta v$ is varied according to the slope of the input signal. The data size is reduced compared to LCS.

3. Simulated sampler based on extremum sampling (ES) in which a signal is represented with its peak values and the interval between the peaks. ES has been applied to speech and vibration signals. ES has resulted in the highest compression ratio compared to LCS and ALCS.

4. Simulated LCS, ALCS, and ES with multiple temporal resolutions to reduce the dynamic range of the time-to-digital converter. The concept of frequency-scaling is introduced to adaptively change the clock frequency during the active and silent portions of the speech signal. The frequency-scaling has resulted in the reduction of the bits per sample and also the overall data size. The dynamic power consumption in a system is directly proportional to the clock frequency, and hence, decreasing the clock frequency during inactive periods saves power, increases battery life, and reduces the heat emission.

5. Devised a method for the real-time anomaly detection in mechanical systems based on the parameter, average level-crossing rate (*ALCR*) of the vibration signals. Abnormalities in the bearings cause an increase in the amplitude and frequency of the signals,

which produce a corresponding increase in the *ALCR*. The proposed system works on the analog output of the sensor and does not require conventional steps like sampling, feature extraction, classification, or computation of the spectrum.

6. A voice-controlled audio mixer has been simulated in which the background music is attenuated based on the intensity of the speech signal. Instead of measuring both the zero-crossing rate and the signal's energy, variations in the *ALCR* are sufficient for activity detection.

7. Simulated an acoustic feedback suppression system, in which the feedback discrimination is performed with *ALCR*, and howling frequency identification with the zero-crossing time. In conventional methods, the frequency resolution and delay are dependent on the frame size. The method based on *ALCR* works on the analog input, and the sampling, encoding and framing are evaded.

## 1.4 THESIS ORGANIZATION

The remaining chapters of the thesis are organized as follows.

Chapter 2 provides a comprehensive review of the literature on non-uniform sampling and level-crossing sampling. The review is divided into four sections. These sections are the literature on

1. level-crossing sampling
2. compression of vibration signals
3. anomaly detection using vibration signals and
4. voice-controlled mixer and acoustic feedback detection.

Chapter 3 gives an overview of the sampling process, starting with uniform sampling and its limitations. A brief history of non-uniform sampling methods is also provided. The chapter is concluded with an introduction to the random sampling method known as compressed sensing.

Chapter 4 introduces LCS, various blocks for its implementation, and the design procedure for the sampler. The signal-to-noise ratio due to the quantization error in time is explained in this chapter. Adaptive and extremum sampling methods are also introduced. The effect of noise in level-crossing samplers, and samplers with hysteresis are discussed in this chapter.

Chapter 5 introduces LCS with multiple temporal resolutions, which provides an efficient encoding of the silence regions in speech signals. The concept of frequency-scaling, which is used for achieving multi-temporal resolution, is also explained. The performance comparison of frequency-scaled LCS, adaptive LCS, extremum sampling and the reconstruction algorithm for each type are also detailed in this chapter.

Chapter 6 deals with the application of level-crossing methods on vibration signals. The compressed representation of vibration signals achieved with extremum sampling is demonstrated. The chapter also explains the anomaly detection of mechanical systems performed by monitoring the variations in the *ALCR* of the signal.

Chapter 7 presents the applications of *ALCR* for activity detection in speech or audio signals. The applications explained are voice-controlled audio mixer and acoustic feedback detection in public address systems. The use of *ALCR* for feedback discrimination and zero-crossing time for howling frequency estimation is illustrated.

## 1.5 SUMMARY

This chapter summarizes the limitations of the conventional sampling techniques and the advantages offered by non-uniform sampling. Among various non-uniform sampling methods, level-crossing sampling has gained popularity in sampling biopotential signals. There is further scope for improving the efficiency of LCS while sampling the speech signals. The organization of the remaining chapters is also provided. The next chapter presents a literature review on non-uniform sampling, level-crossing sampling, compression methods for vibration signals, anomaly detection using vibration signals, and voice-activity detection for mixer and howling- noise detection.

# CHAPTER 2

# LITERATURE REVIEW

This chapter presents a review of the literature available on various sampling methods, compression schemes for vibration signals, anomaly detection in mechanical systems using vibration signals, and activity detection.

## 2.1 INTRODUCTION

Sampling is the process of converting an analog signal into a discrete-time signal, which is the primary step in digital signal processing or digital communication. Shannon, in his paper [1], specifies the condition for the exact reconstruction of the input signal from the samples. Uniform sampling methods acquire samples even if there is no variation in the signal amplitude. Drawbacks of uniform sampling methods are detailed in [2, 3]. The factors on which dynamic power consumption of CMOS circuit depends are explained in [4]. Battery-operated devices such as implantable devices are available in the form of microchips, usually implemented with CMOS logic. The dynamic power consumption in a CMOS device is proportional to the activity factor. Devices based on level-crossing sampling (LCS) are asynchronous circuits in which the switching rate is proportional to the activity of the signal. Hence the average switching rate is less in circuits which are based on LCS compared to synchronous circuits. Activity-dependent sampling methods minimize the dynamic power consumption of a system exploiting the local properties of the signal. The power-savings achieved with non-uniform sampling techniques have been presented in [5, 6]. Signal-dependent sampling methods are suitable for wireless sensor nodes with minimal resources [7]. The development of event-based signal processing techniques has led to the concept of continuous-time digital signal processing (CT-DSP) [8, 9].

Compressed sensing was introduced for acquiring a reduced number of samples from a sparse signal compared to that obtained at the Nyquist rate [10-13]. It involved multiplication by large-sized matrix for encoding, and optimization algorithms for reconstruction of the signal.

## 2.2 LEVEL-CROSSING SAMPLING

Level-crossing sampling (LCS) is another non-uniform sampling scheme suitable for sparse signals, which is easy to implement. LCS was first introduced as a data compression technique in [14]. Analog-to-digital converter based on LCS was proposed in [15]. In [16], a level-crossing detector (LCD) which resembles the flash type analog-to-digital converter is employed. Instead, LCD can also be implemented as an asynchronous delta modulator [17]. Different realizations of time-to-digital converters are detailed in [18].

The design of a level-crossing sampler is explained in [19]. Several structures for analog-to-digital conversion based on LCS have been proposed in literature [20-22]. Continuous -time LCS with charge sharing has been proposed in [23].

Adaptive LCS, in which the inter-level distance is varied according to the slope of the input signal, is introduced in [24]. Peak sampling was introduced in [25] for signals which have an oscillatory nature. Peak sampling is also known as extremum sampling [2] and minimax sampling [26]. Peak sampling can be implemented with level-crossing sampling [27].

LCS has been used for sampling signals in low-power IoT devices in [28] and has been successfully employed for sensing biopotential signals [29-34]. A single-chip implementation of LCS has been done in [35] for acquiring ECG signals. QRS detection from ECG has been performed with LCS in [36]. Digital filters have been implemented in [37], that operate on the samples acquired with

LCS. The processing of signals using the samples obtained with LCS is introduced in [38].

Speech signals have been applied to LCS in [15,19,39-41], in which the use of time-to-digital converters (TDC) with a constant temporal resolution has resulted in a large number of bits per sample. LCS with multiple temporal resolutions achieved with the frequency-scaling technique is proposed in this thesis. Frequency-scaling is employed in computer architecture for the dynamic power reduction based on the CPU activity [42-44].

## 2.3 COMPRESSION OF VIBRATION SIGNALS

Data compression is used to reduce memory space requirements, communication bandwidth, and power consumption [45]. Compression algorithms are generally classified into lossless and lossy. Vibration signals are employed to detect the anomaly in mechanical systems and have the highest frequency among other telemetry signals. Hence, there is a high demand for compressing vibration signals. Lossless compression has been applied to the accelerometer signals in [46], where time delay estimation with differential pulse code modulation is used. However, the compression gained is less and is approximately equal to 70%. An adaptive compression scheme for vibration signals is proposed in [47], which applies lifting discrete wavelet transform with set-partitioning of embedded blocks. The compression of vibration signals from wireless sensor nodes with a modified discrete cosine transform has been proposed in [48]. Run-length encoding has been applied to telemetry data in a multichannel acquisition system in [49]. However, the method involves oversampling and averaging before performing run-length encoding. The compression of vibration signals collected from airplane engines has been achieved in [50] using discrete cosine transform. In [51], the authors propose a compression method referred to as sub-band adaptive quantization for vibration signals from aircraft engines. In all the above methods, samples are acquired at

the Nyquist rate based on the maximum signal frequency $f_{max}$, and most of the samples are discarded during the compression process, wasting the resources.

CS has been employed for encoding vibration signals in [52] for high-speed rail monitoring in China. Vibration signals are found to have a sparse representation in discrete cosine transform (DCT). A sparsity-adaptive subspace pursuit CS algorithm has been applied in [53] to represent vibration signals from the wireless sensors, used for the health monitoring of structures. Even though CS stands for sensing the signals in a compressed form, in most cases, the vibration signals are first uniformly sampled and encoded. Subsequently, they are multiplied with a measurement matrix using the sparsity of the signal in a particular domain.

## 2.4 ANOMALY DETECTION USING VIBRATION SIGNALS

Various approaches for condition-based maintenance (CBM) of systems and prognostics and health management (PHM) are explained in [54]. In CBM, conditions of the machines are determined from the run-time data to schedule repair and maintenance. PHM predicts future behaviour, the remaining useful life (RUL) from the present data, and schedule the steps needed for the machine to operate for a long time. The general approaches for CBM and PHM are classified into (i) model-based methods, (ii) data-driven methods, and (iii) hybrid methods. In the model-based method, a mathematical model is created to describe the damage in the equipment [55]. In the data-driven approach, the measured data is used for fault detection or prediction [56]. Hybrid methods make use of both techniques [57].

Vibration signals are used for anomaly detection because the damages in moving parts, especially the bearing faults, create changes in vibration. Various feature extraction methods are used for this purpose. Time-domain methods have been applied for fault detection in the planetary gear set in [58], which is based on the change in the peak amplitude of the stator current. In another time-domain

method [59], artificial modulation of the current signal is done to extract the frequency components due to faults. However, the accuracy of failure detection is dependent on the careful selection of the frequency and measurement of the time gap between the zero-crossings.

Features extracted from the vibration signals have been used for bearing fault detection. Statistical features in the time domain were used in [60], and time domain and frequency domain features were used in [61]. Fifty-nine features from the time, frequency, and wavelet domains were used in [62]. Empirical mode decomposition and time-domain statistics were used to extract features from vibration signals in [63]. Several wavelet-based methods are also available in the literature [64-66].

Even though efforts have been made to reduce the amount of data by employing compressed sensing [67, 68], the process involved for feature extraction is very much involved. Damage-detection using the vibration signal is not limited to machines only but extended to civil structures also [69]. Machine learning techniques have been used for anomaly detection in [70]. Even though several deep-learning methods have been developed [71-74] for anomaly detection in machines, they need vast numbers of normal and faulty data for training. A simple mechanism for anomaly detection from the analog input signal is proposed in this thesis.

## 2.5 VOICE-CONTROLLED MIXER AND ACOUSTIC FEEDBACK DETECTION

Voice-activity detection has been employed for the separation of speech and silence into different time intervals. There are certain situations in which intensity of a particular signal is monitored, and a control action is initiated if the intensity crosses a threshold value. One such application is a voice-controlled mixer in which a background signal is suppressed, either entirely or partially, if another signal of sufficient intensity appears from a different source. For

implementing an automatic voice-controlled audio amplifier, envelope detection is used for activity detection [75]. Short-term energy (STE) and zero-crossing rate (ZCR) are used in [76] for detecting the speech signal for controlling the background music. Another more straightforward method based on the average level-crossing rate is proposed in chapter 7.

Howling noise is produced in public address systems due to the acoustic feedback, and is quite annoying to the audience. In notch-based howling suppression, the first step is to identify the feedback signal. The peak spectral component is picked, and it is compared with other components. The feature, Peak-to-Threshold Power Ratio, is used in [77], and in [78], Peak-to-Average Power Ratio is used to detect feedback signal. Similarly, Peak-to-Harmonic Power Ratio [79] and Peak-to-Neighbouring Power Ratio [80] are also employed. Literature is available, where Inter-frame Peak Magnitude Persistence [81] and Inter-frame Magnitude Slope- Deviation [82] are used for detecting the feedback. In frame-based methods, the frequency resolution increases with the length of the frame, but the delay also increases. A technique based on the average level-crossing rate, which detects howling directly from the analog signal, is proposed in Chapter 7.

## 2.6 SUMMARY

This chapter reviews the literature on level-crossing sampling, compression of vibration signals, and anomaly detection in mechanical systems using vibration signals. Non-uniform sampling methods are gaining popularity since they generate a compressed set of samples. Processing based on the samples acquired with non-uniform sampling has been proposed in various literature available. Most of the compression methods for vibration signals are based on a sample-then compress scheme, discarding most of the acquired samples, wasting the resources like power and storage. Even though speech signals are applied to LCS, the dynamic range of TDC is very high, resulting in

higher bits per sample and data size. Hence there is a requirement for efficiently encoding the samples acquired with LCS, which is addressed in this thesis. Anomaly detection in mechanical systems is based on the complex processing of a massive amount of vibration data. A simple method based on the level-crossing rate is proposed in this thesis for anomaly detection. Basics of uniform sampling scheme, its limitations, and the evolution of non-uniform sampling are discussed in the next chapter.

# CHAPTER 3

# SAMPLING PROCESS-A REVIEW

## 3.1 INTRODUCTION

In the real world, all the signals appear in the analog form. Present-generation computers store and process the signals in the digital domain. Moreover, noise and interference have lesser effect on digital signals during the transmission. Hence analog signals must be converted into the corresponding digital equivalent. Sampling is the first step for this conversion, in which a continuous-time signal is converted into a discrete-time signal, satisfying the conditions for the perfect reconstruction. Due to the robust technology and ease of processing, uniform sampling has been adopted as the standard sampling scheme for more than half a century.

Very often, uniform sampling leads to a number of redundant samples being acquired, which have to be further reduced to a compact form with the help of suitable compression techniques. Researches for acquiring samples from analog signals, which are just sufficient for the reproduction, have led to the invention of several non-uniform sampling techniques. In this chapter, a review of uniform sampling scheme, its limitations, and the evolution of non-uniform sampling are presented. Compressed sensing, a method which samples the signal in a compressed form, making use of the sparsity of the input signal is introduced.

## 3.2 UNIFORM SAMPLING

The foundation for digital communication was set with the paper published by Shannon in 1949 [1]. According to Shannon, if a function $x(t)$ contains no frequencies higher than $f_{max}$ Hz, it is completely determined by giving its ordinates at a series of points spaced $1/(2f_{max})$ seconds apart. The rate,

$2f_{max}$ samples per second is known as the Nyquist rate. The function $x(t)$ can be reconstructed using $sinc\ (2\pi.\ f_{max}.t)$, which is $sin\ (2\pi.\ f_{max}.t)/\ 2\pi.\ f_{max}.t$. In frequency domain, this is equivalent to an ideal low pass filter which has a flat pass band up to $f_{max}$ Hz, and stop-band with gain zero outside this band. Analog-to-digital converters (ADC) are the interface between the real-world analog signals and digital signals which are stored and processed by computers. Sampling theorem is the basis for the conversion of analog quantity to digital. Once the sampling frequency is chosen as $2f_{max}$, any frequency component above $f_{max}$ Hz present in the input signal causes spectral overlap called aliasing during the sampling process. Hence it is a necessity to limit the frequency of the input signal to $f_{max}$ Hz using a filter known as anti-aliasing filter.

In Shannon's paper, there was no restriction that samples are to be uniformly spaced in time. But standard rates were fixed for acquiring regularly spaced samples from band-limited signals. For example, 8 kHz was selected as the sampling rate for telephone signals and 16 kHz for some other applications. The ease of sampling and reconstruction, and the existence of the well-established theory have been the basic reasons for most of the existing digital systems to be based on uniform sampling. Even today, the number of samples selected for converting an analog signal into its digital equivalent is based on the Nyquist–Shannon sampling theorem.

### 3.2.1 Need for compression

A uniformly sampled and digitized data may not be represented in an efficient manner. The representation is said to be inefficient because there is redundant data which do not convey any information. In general, data compression is termed as the process of redundancy-reduction. Redundancy-reduction is a reversible process because the removed redundancy can be reinserted into the data afterwards. There are always situations in which the resources such as memory, transmission bandwidth, and energy for transmission

are limited. For efficient utilization of the resources, data compression is a necessity. Wireless sensor networks consist of a number of wireless nodes that are employed for the monitoring of various parameters such as temperature, pressure, vibration, etc. The sensor nodes have constrained resources like processing speed, memory capacity, and communication bandwidth. Wireless transmissions in sensor nodes consume the major portion of its power, and hence data must be compressed before transmission. The basic techniques for data compression are run-length encoding, statistical methods, dictionary methods, and specific methods for audio, image and video data [45].

Conventional data compression methods have to operate on all the samples acquired at the Nyquist rate, which increases the computational complexity at the transmitter, and consumes more battery power [7]. This extra burden at the transmitter side can be minimized if samples are acquired such that they are just sufficient for the reproduction of the signal. Generating a lesser number of samples leads to lesser computation, storage, communication, and power requirements.

### 3.2.2 Limitations of uniform sampling

In the conventional sampling methods, the sampling rate is independent of the instantaneous frequency of the signal. It is inefficient because the part of the signal with frequency content much less than the highest frequency is over-sampled by this method. Another drawback is that, in order to avoid aliasing, the signal is band-limited to half of the sampling frequency, which can cause missing of any abrupt change present in it. Therefore, sampling must be specific to the signals and their applications. Systems with multiple sampling rates and systems with distributed computing face severe difficulties with fixed sampling rates [2]. The complexity of the multi-rate systems depends critically on the ratio between different sampling rates. The clocks must be synchronized in distributed systems where jitter and delays create difficulties.

Electrocardiogram and seismic signals fall in the category of sparse and bursty signals. A signal is said to be sparse in a domain if it has few numbers of non-zero elements in that domain. However, there may be sudden changes in amplitude in the form of bursts occurring for short durations. If sampling is done at the Nyquist rate, redundant samples are generated during the quiescent period also [3]. Hence signal-dependent sampling methods are more adequate for these classes of signals.

The common issues associated with the synchronous circuits are higher dynamic power consumption, the clock distribution problem, electromagnetic emission, etc. [3]. The synchronous logic circuits have reached the technical limits in dealing with these problems. The asynchronous circuits have emerged as an alternative to the synchronous circuits in many applications. They are having properties like less power consumption, less electromagnetic emission, higher speed of operation, and they are robust against variations in supply voltage and temperature.

## 3.3 NON-UNIFORM SAMPLING (NUS)

Non-uniform sampling has advantages compared to uniform and synchronous sampling while processing low activity signals. There are many situations in which the dynamic power consumption has to be reduced for longer battery life, and the size of the data is to be small to reduce the transmission bandwidth, which is expensive. The dynamic power consumption $P$ in CMOS circuits is stated in Eqn. 3.1.

$$P=aCV^2f_c \tag{3.1}$$

Where $a$ is the activity factor, $C$ denotes the switched capacitance, $V$ denotes the supply voltage, and $f_c$ is the frequency of the clock used [4]. Many studies have been carried out in literature to minimize the dynamic power consumption by reducing the values of $C$, $V$, or $f_c$. Non-uniform sampling allows

the exploitation of the local properties of the signal to avoid sampling at a high rate when the local bandwidth is low thereby reducing the activity factor. For perfect reconstruction from non-uniform samples, the mean sampling rate must exceed the Nyquist rate [83]. Several sampling methods have been evolved, which generate samples at non-uniform rates.

### 3.3.1 A brief history of non-uniform sampling

In non-uniform sampling, samples are not equally spaced in time axis. This idea started appearing in the papers published in the 1950s. Aperiodic sampling was suggested by Ellis [84] in 1959. It was pointed out that periodic sampling was not necessary for transmitting data through a channel. Transmission can take place only when the value of data changes from one possible value to the next. Several papers appeared in the 1960s about increasing the efficiency of the sampling process. Asynchronous delta modulation was invented by H. Inose et al. [85]. Delta modulation is based on a clock signal, and a pulse output is transmitted in synchronization with each clock signal, which depends on whether the amplitude of the signal has changed by a step size or not. However, in asynchronous delta modulation, there is no clock signal, and a pulse output is transmitted only when the signal has changed by a step size, thus reducing the transmission rate. In synchronous delta modulation systems, there will be slope-overload distortion and granular noise occurring at fast changing and quiescent regions of the signals respectively. In asynchronous sampling, in order to minimize the effects of slope-overload and granular noise, input signal is sampled at a higher rate during the fast-changing regions compared to the slowly changing regions. Comparison of uniform and non-uniform sampling was done in [86]. In the event-based sampling methods, analog signals have a discrete representation in terms of the levels which are equally distributed in the amplitude domain. An event could be a significant change in the measured value of a signal. Hence, they are termed as Lebesgue sampling. Uniform sampling is usually termed as Riemann sampling.

A non-uniform sampler based on level-crossing was discovered by Mark and Todd in 1981 [14] which resulted in data compression. It consists of a level-crossing detector (LCD), in which the input signal is compared to a number of uniformly spaced threshold levels. A pulse is generated at the output of the LCD and a sample is taken whenever the input signal crosses any of the threshold levels. If the pulse is transmitted as such, then it is equivalent to an asynchronous delta modulator. However, in a wireless system, the pulse output cannot be transmitted as such without performing the encoding operation. The information about the signal is in the interval between the level-crossing instants, and also in the direction of the level-crossing. The interval is a continuous variable that could not be stored or transmitted. Hence the interval between level-crossing instants is encoded before transmission. Binary strings "00" is used to represent the time between level-crossings and "01" and "10" denote upward and downward level-crossings respectively. $t_q$ is the time quantum with which the interval is measured. Hence an interval is represented as a sequence of "00" followed by either "01" or "10". This representation had long sequences of 0s which was coded with run-length encoding to reduce its length. Fig. 3.1 depicts the block diagram of this method [14].

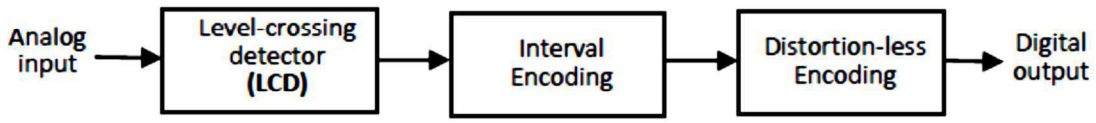


*Fig. 3.1 Block diagram of the non-uniform sampler proposed by Mark et al.*

Fig. 3.2 is the block diagram for non-uniform sampling based on level-crossing sampling suggested for analog-to-digital conversion by Sayiner et al. in [15]. The input signal is compared to 'N' threshold levels. The intervals between level-crossing instants are recorded in terms of the number of clock cycles with frequency $f_c$, which has the total duration equal to this interval. Time resolution is proportional to the value of $f_c$. Output of the quantizer, which are the non-

uniform samples are fed to an interpolator to convert them into uniform samples. These uniform samples are fed to a decimator to convert the rate to Nyquist rate $f_{Nyq}$.

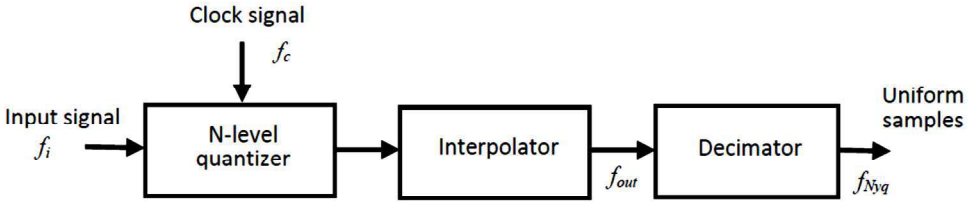


*Fig. 3.2 Block diagram of the non-uniform sampler proposed by Sayiner et al.*

Lebesgue sampling is also known as "Send on delta" scheme in the context of transmission in the sensor networks. It is a signal-dependent sampling method in which the sampling is triggered if the signal has a significant change of 'Δ' volts in its amplitude. Hence, between the samples there is a difference in amplitude which is equal to Δ. The quantitative evaluations of the sampling rate in send-on-delta and the comparison with uniform sampling are given in [87]. This scheme is illustrated in Fig. 3.3.

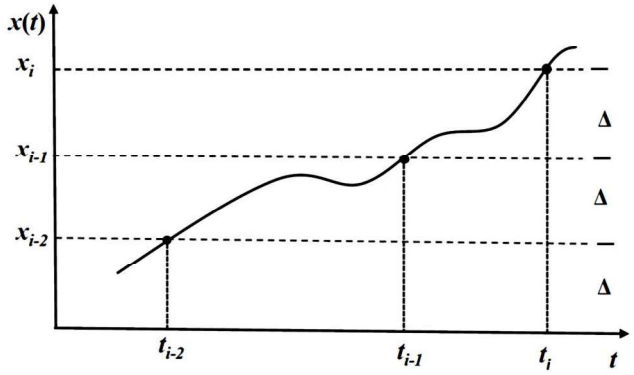


*Fig. 3.3 Illustration of the principle of send-on-delta scheme*

The distance between adjacent levels can be expressed as,

$$|x(t_i)|-|x(t_{i-1})|=\Delta \tag{3.2}$$

Where $x(t_i)$ is the $i^{th}$ sample, $i$=1, 2, .. n.

The threshold Δ determines the resolution of the signal representation. The smaller the value of the threshold Δ, the higher will be the resolution.

The number of samples in the case of periodic sampling and that in the send-on-delta scheme are compared in Fig. 3.4. The resolution in both cases is the same and is equal to 0.2v.

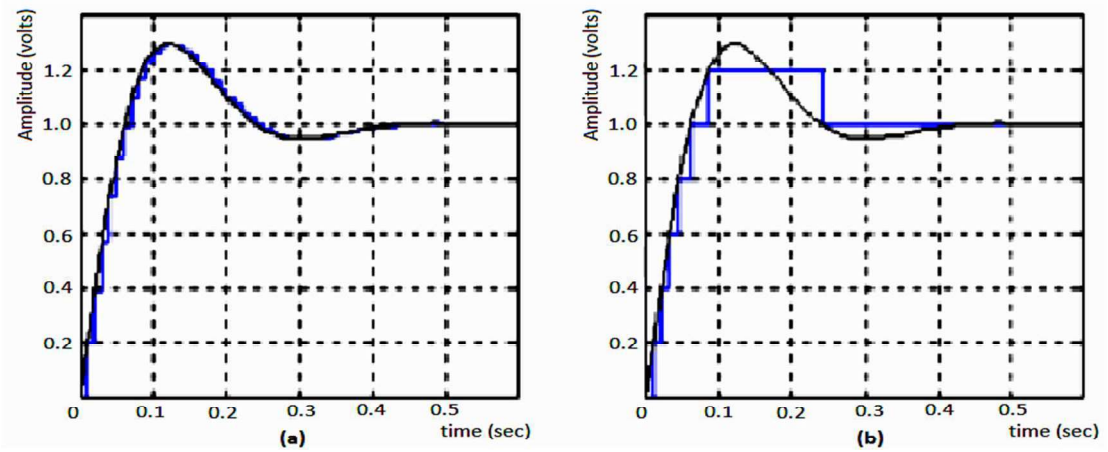


*Fig. 3.4 (a) Number of samples in periodic sampling*
*(b) number of samples in send-on-delta scheme*

A comparison of ADCs based on uniform and level-crossing sampling is shown in table 3.1 [19].

*Table 3.1 Comparison of Uniform and level-crossing sampling*

| **Parameter** | **Uniform sampling** | **Level-crossing sampling** |
|---|---|---|
| Conversion trigger | Clock | Level-crossing |
| Amplitude | Quantized value | Exact value |
| Time | Exact value | Quantized value |
| SNR dependency | Number of bits in the representation | Timer period of TDC |
| Converter output | amplitude | (amplitude, time) |

## 3.4 COMPRESSED SENSING

Compressed sensing (CS), also known as compressive sampling is another sensing technique of acquiring samples at a reduced rate. Candes et al. proved [10] that if a signal has a sparse representation in a particular basis, the number of samples required for perfect reconstruction can be less than that acquired at the Nyquist rate. A signal of length $n$ is said to be sparse in a domain if it has $m<n$ non-zero samples in that domain. The name "compressed sensing" is due to the fact that the data is compressed during the sensing process. In classical sampling, a continuous-time signal which has infinite length is being sampled at the Nyquist rate. However, CS theory does not treat the signal as a continuous one [88]. It projects finite dimensional vectors in $R^n$ to lower dimensional vectors in $R^m$. CS linearly projects a signal to a known basis. The reconstruction of the signal from the CS-domain is done by complex convex-optimization methods, whereas in classical sampling, the reconstruction is done by simple sinc interpolation.

Let $x$ be an input signal with sample vector length $n$. The output $y$ obtained by performing compressed sensing on the input $x$ can be expressed in matrix form as given below.

$$y=\phi x \tag{3.3}$$

The output $y$ is of length $m < n$, and $\phi$ is a measurement matrix of size $m$ x $n$. In most of the cases, the input $x$ will be expressed in terms of an ortho-normal basis function, $\psi$ as shown in Eqn. 3.4.

$$x=\psi\alpha \tag{3.4}$$

$\Psi$ is the $n$ x $n$ sampling basis, and $\alpha$ is the coefficient sequence of length $n$. If $x$ is sparse in wavelet domain, then $\psi$ is the inverse wavelet transform matrix which converts the wavelet coefficients $\alpha$ into $x$.

Eqn. 3.3 and Eqn. 3.4 can be combined as

$$y=\Theta\alpha \tag{3.5}$$

where

$$\Theta=\phi\psi \tag{3.6}$$

which is known as the sensing matrix. Since the number of measurements $m$ is very less than $n$, compression is achieved during the sensing process. The two requirements for implementing CS on a signal $x$ are sparsity and incoherence.

Sparsity- The signal x must be sparse in some domain.

Incoherence- The sampling matrix ψ, and the measurement matrix ϕ must be incoherent.

The coherence between $\psi$ and $\phi$ is expressed as

$$\mu(\psi,\phi)=\sqrt{n}.\max_{0\le k,j<n}\left|\langle\psi_j,\phi_k\rangle\right| \tag{3.7}$$

Coherence is a measure of the largest correlation between any two elements of $\psi$ and $\phi$. The reconstruction of the signal $x$ from $y$ can be performed as

$$\hat{x}=\phi^{-1}y \tag{3.8}$$

However, there are just $m$ known values in $y$ and there are $n$ unknown values of the signal $x$, where $m<n$. Hence the problem is under-determined with many possible solutions. One of the methods for finding the solution is with $l_1$-norm minimization as

$$\min\left|\left|\hat{\alpha}\right|\right|_{l_1}, \text{ subject to } y=\Phi\psi\hat{\alpha} \tag{3.9}$$

where $l_1$-norm of a function $z$ is defined as

$$\left|\left|z\right|\right|_{l_1} = \sum_i |z_i| \tag{3.10}$$

Compressed sensing has applications in various fields including medical imaging. MRI images can be reconstructed from fewer Fourier coefficients using the optimization techniques of compressed sensing. The need for executing complex optimization algorithms have restricted the use of compressed sensing for real-time applications.

## 3.5 SUMMARY

The famous Nyquist-Shannon sampling theorem laid the foundation for analog-to-digital conversion and digital communication. However, uniform sampling is inefficient while sampling sparse signals. Several non-uniform sampling techniques have been developed, which efficiently sample the signals with a rate which is dependent on the activity. The evolution of non-uniform sampling has been discussed in this chapter. Compressed sensing, another technique that allows reconstruction of the signals sampled at sub-Nyquist rates, is also introduced. In CS-based methods, sensing generally requires multiplication by large-sized matrices. In addition to this, the need for iterative optimization methods makes the real-time reconstruction a difficult task. An efficient non-uniform sampling method which is suitable for sparse and bursty signals is level-crossing sampling (LCS) and it is discussed in the next chapter.

# CHAPTER 4

# LEVEL-CROSSING SAMPLING

## 4.1 INTRODUCTION

Level-crossing sampling (LCS) is an efficient non-uniform sampling method which is suitable for sparse and bursty signals. In order to reduce the number of samples acquired while the signal has sudden variations in its amplitude, adaptive level-crossing sampling is used. Extremum sampling is another form of non-uniform sampling in which samples are taken at the local extrema points. In this chapter, basic theory of level-crossing sampling, and the design of LCS sampler are discussed. Adaptive LCS, extremum sampling, and the noise tolerance of level-crossing methods are also introduced.

## 4.2 PRINCIPLE OF LEVEL-CROSSING SAMPLING

The concept of LCS is depicted in Fig. 4.1. The horizontal dotted lines represent different reference levels $l_n$. The signal $x(t)$ is compared with the pre-fixed reference levels. A pulse signal is produced at the output of a level-crossing detector (LCD) whenever the signal crosses any of these reference levels. The LCD output triggers a time-to-digital converter (TDC), to produce a digital count, which is a representation of the interval between level-crossing instants $dt_n$. Each sample is represented by a couple ($L_n$, $Dt_n$), which are the digital representations of a particular threshold level $l_n$ and the time interval between the present and previous level-crossing instants $dt_n$, respectively. Hence the signal is represented by an ordered sequence of amplitude-time pairs with non-uniformly spaced time values.

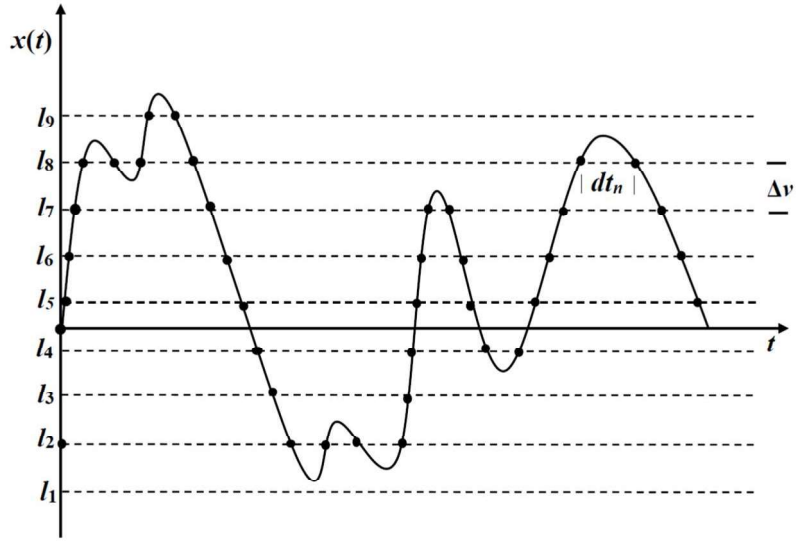


*Fig. 4.1 Illustration of the level-crossing sampling scheme*

The general block diagram of a level-crossing sampler is depicted in Fig. 4.2. The major blocks are (i) a level-crossing detector (LCD) and (ii) a time-to-digital converter (TDC). LCD sets the required number of threshold levels, which spans the dynamic range of the input signal.

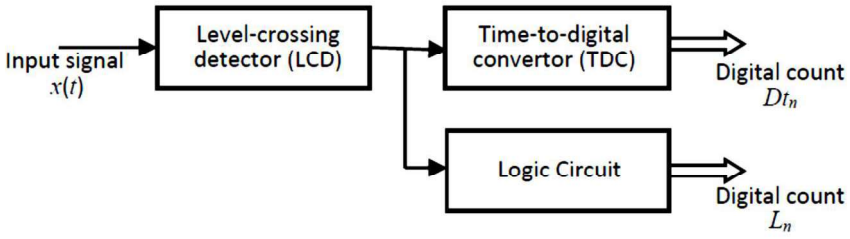


*Fig. 4.2 The block diagram of a general level-crossing sampler*

We require at least $\lceil \log_2 L \rceil$ bits to encode the level which the signal has crossed, where $L$ is the total number of crossing levels, and $\lceil . \rceil$ indicates the rounding operation towards the nearest higher integer. The number of bits needed to represent the time-gap between successive level-crossings is $\left\lceil log_2(dt_n / T_c) \right\rceil$,

where $T_c$ is the time-period of the clock signal used for measuring $dt_n$. The bit representation of each sample is depicted in Fig. 4.3.


*Fig. 4.3 The representation of the samples in LCS*

In order to reduce the number of bits required to represent each level, a differential form can be used as illustrated in Fig. 4.4 [16]. Instead of representing $L_n$ in the couple ($L_n$, $Dt_n$), a single bit '*DIR*' can be used to indicate the direction of change in the input amplitude, and each sample is represented by the pair (*DIR*, $Dt_n$). The advantage of this differential representation is that the amplitude variations in the signal can be monitored by the *DIR* bit. In a wired system, the signal can be reconstructed using the DIR signal alone with the knowledge of $x_0$ and the step size $\Delta v$.

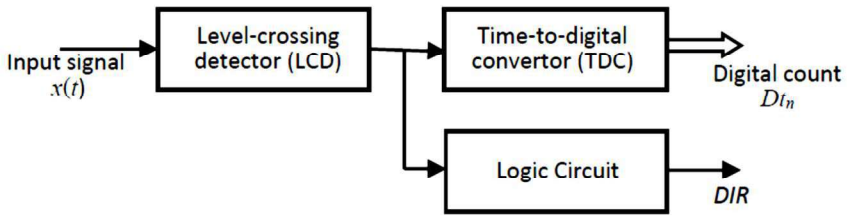


*Fig. 4.4 The block diagram of a level-crossing sampler with differential representation*

The representation of sample values is depicted in Fig. 4.5. The initial value of the input signal $x_0$ must be transmitted before transmitting the *DIR* and $Dt_n$ values of succeeding samples.

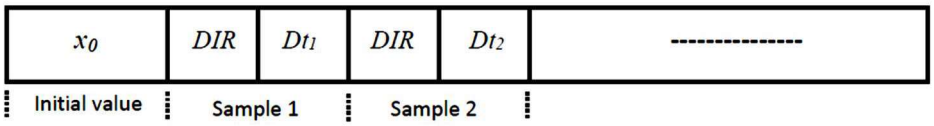


*Fig. 4.5 The bit representation in differential LCS*

Let $t_n$ be the n$^{th}$ time instant at which a non-uniform sample is acquired, $x(t_n)$ the corresponding amplitude of the sample, $\Delta v$ the inter-level distance, and $b_n$ =1 for $DIR$=1 &$b_n$ =-1 for $DIR$=0. The present time $t_n$ is updated from the previous time instant $t_{n-1}$ using the sample value ($DIR$, $Dt_n$) as shown in Eqn. 4.1.

$$t_n = t_{n-1} + Dt_nT_c \tag{4.1}$$

The value of $x(t_n)$ can be updated from the previous value $x(t_{n-1})$ as,

$$x(t_n) = x(t_{n-1}) + b_n\Delta v \tag{4.2}$$

### 4.2.1 Level-crossing detector

Level-crossing detector (LCD) can be implemented with various methods. A number of voltage comparators arranged in the form of a flash type ADC circuit can be used [16] for implementing LCS. As shown in Fig. 4.6, different threshold levels are connected as one of the inputs to each of the comparators, with the signal input connected as the common input. The number of comparators required is equal to the number of threshold levels, and hence the hardware complexity of this type of circuit increases with the number of levels.

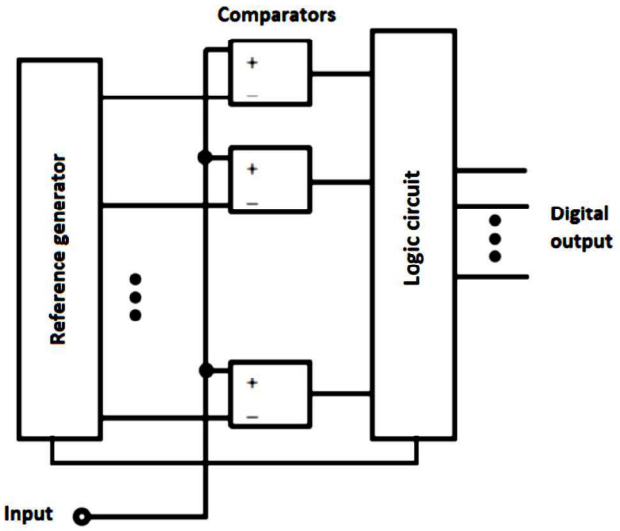


*Fig. 4.6 The block diagram of a flash-type LCD*

LCS can also be realized in the form of an asynchronous delta modulator as depicted in Fig. 4.7, in which the input signal is fed to a window comparator. At any instant, the input amplitude is compared with the present reference levels $V_H$ and $V_L$. $V_H$ and $V_L$ are the upper and lower thresholds, based on the amplitude of the signal during the previous level-crossing instant. Based on the output of the comparators, $V_H$ and $V_L$ are increased or decreased by the step size $\Delta v$. If the input crosses any of the present reference levels, LCD output stores the present count of the TDC counter, resets it, and then starts counting the next interval.

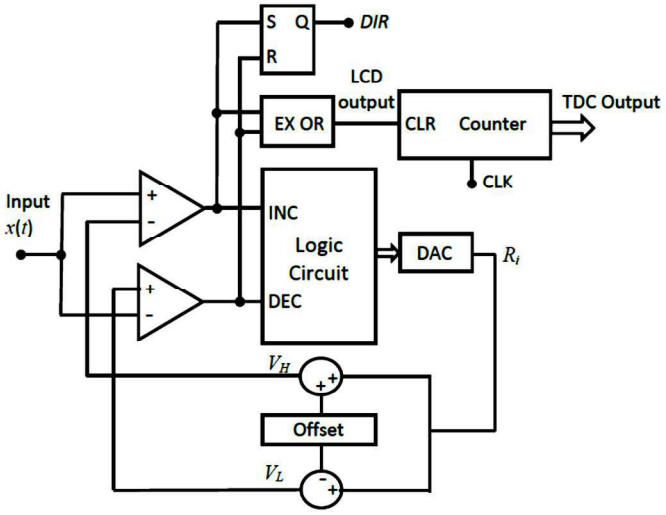


*Fig. 4.7 The block diagram of the level-crossing sampler with differential representation*

### 4.2.2 Time-to-digital converters

Time-to-digital converters (TDC) are used for the measurement of time intervals between physical events in various applications in science and industry. The simplest case of time interval measurement is illustrated in Fig.4.8 [89]. Physical events in the form of variations in temperature, pressure, etc. are detected, which are fed to the time discriminators to produce pulses. The leading edges of the pulses are applied to the START and STOP inputs of the TDC. Instead of having two separate inputs for START and STOP, a common pulse input can also be used. The leading edge of the pulse will trigger the conversion process and the trailing edge will stop the counting. The TDC converts a time

interval into a binary word. There are several areas of applications of TDCs including nuclear physics, dynamic testing of integrated circuits, high-speed data transfer and laser ranging systems.

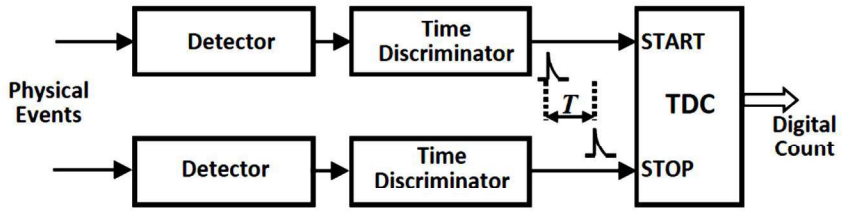


*Fig. 4.8 The block diagram for time interval measurement*

The initial TDCs developed were based on time-to-amplitude converters in which the basic element was a capacitor. Based on this, several analog TDCs were developed which fall into the category of first generation of TDCs [18]. Recently developed converters are completely based on digital approaches.

The important parametrs used to evaluate the performance of a TDC are,

i. Time resolution

It is the minimum time input that a TDC can correctly measure, which depends on the lower significant bit (LSB).

ii. Dynamic range

It indicates the maximum time input that a TDC can measure. For counter-based converters, this parameter is dependent on the number of bits of the counter.

iii. Conversion time

It is the minimum time with which a TDC performs a conversion, which is measured from the beginning of the START trigger. Conversion time is an important parameter for high-speed applications.

iv. Dead time

It is the shortest time needed after the stop event, for a converter to produce the digital word.

The simplest method for time-to-digital conversion is based on a digital counter which is fed with a reference clock signal of time period $T_c$ as shown in Fig. 4.9. The counter must be reset before enabling it for a fresh measurement. The time interval $T$ will be measured in terms of the number of clock pulses. The result will be available as a count $n$ such that

$$\bar{T} = n.T_c \tag{4.3}$$

with a measurement error $\delta t = T - \bar{T}$ which has a value within $[0, T_c]$. The signal-to-noise ratio of LCS due to this measurement error is derived in section 4.3.

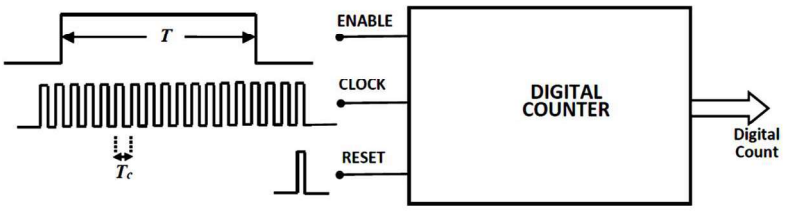


*Fig. 4.9 The block diagram of a TDC based on counter*

The clock signal must be highly stable and the delay in the counter circuit must be very small. In order to increase the resolution of the measurement, each clock cycle can be further sub-divided. A TDC counter with a large dynamic range can be used as a coarse counter, and one or two counters with short dynamic ranges used as fine counters. A ring oscillator with $p$ delay stages can generate $p$ equally spaced versions of the clock signal. Higher values of resolution can be achieved by delaying the clock signal using a series of digital delay elements. In this case the resolution will be dependent on the delay provided by the delay elements. The resolution can be further doubled by making

use of CMOS inverters in place of delay-lines in which both the rising and the falling transitions are used for measurement [18].

## 4.3 SIGNAL-TO-NOISE RATIO (SNR) OF LEVEL-CROSSING SAMPLERS

In classical ADCs, regular sampling is done at the Nyquist rate, and the amplitudes are quantized. Amplitude of each sample is represented by an $N$-bit word, where $N$ is the resolution of the converter. Since the sampling interval is constant, the information regarding the sampling time is not needed. The $SNR$ for classical ADC is specified as shown in Eqn. 4.4.

$$SNR_{\mathrm{dB}} = 1.76 + 6.02N \tag{4.4}$$

In LCS, each sample is taken when the signal amplitude crosses any of the threshold levels. In regular sampling, the uncertainty lies in the amplitude of the samples, and the sample times are exactly known. Assuming that ideal levels are considered, and the amplitudes in LCS are exactly known, the interval between successive samples are quantized with the precision $T_c$ of the timer used for representing $dt_n$ as shown in Fig. 4.10.

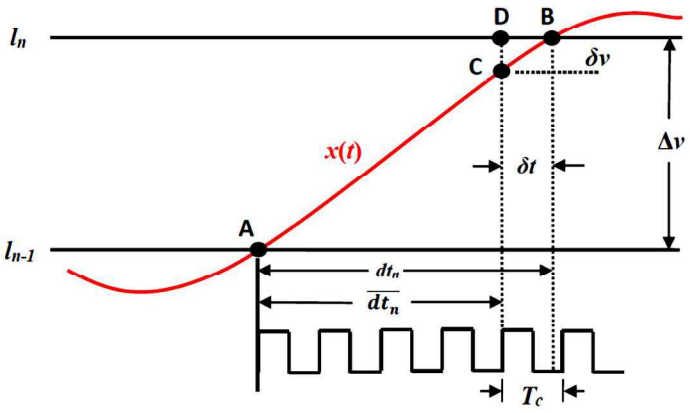


*Fig. 4.10 Illustration of the error due to time quantization*

Input signal $x(t)$ is crossing level $l_{n-1}$ at point A, and the next upper-level $l_n$ at point B. The interval $dt_n$ between these two points is measured as the number

of clock cycles, the total duration of which lie completely within $dt_n$. Since the time measurement is synchronized with the leading edge of the clock as shown in the figure, there is an error in time by a quantity $\delta t$. Instead of $dt_n$, the time interval is measured as $\bar{dt_n}$. $\delta t$ can be any value within the range [0, $T_c$]. In order to find an expression for the SNR, the error $\delta t$ is converted to an equivalent error $\delta v$ in the amplitude [19] as illustrated in figure. Assuming a linear variation of the input signal within $\Delta v$,

$$\delta v = \frac{\mathrm{d}x}{\mathrm{d}t}\delta t \tag{4.5}$$

Where $\frac{\mathrm{d}x}{\mathrm{d}t}$ is the slope of the input signal $x(t)$. $\frac{\mathrm{d}x}{\mathrm{d}t}$ and $\delta t$ can be taken as independent random variables. Then the noise power due to quantization will be,

$$P(\delta v) = P\left(\frac{dx}{dt}\right) P(\delta t) \tag{4.6}$$

$\delta t$ is uniformly distributed in the interval [0, $T_c$].

Therefore,

$$P(\delta t) = \frac{{T_c}^2}{3} \tag{4.7}$$

SNR can be calculated as,

$$SNR_{\mathrm{dB}} = 10\log_{10}\left(\frac{P(x)}{P(\delta v)}\right) \tag{4.8}$$

Thus,

$$SNR_{dB} = 10\log_{10}\left(\frac{3P(x)}{P\left(\frac{dx}{dt}\right){T_c}^2}\right) \tag{4.9}$$

Splitting Eqn. 4.9 into two terms,

$$SNR_{dB} = 10\log_{10}\left(\frac{3P(x)}{P\left(\frac{dx}{dt}\right)}\right) + 20\log_{10}\left(\frac{1}{T_c}\right) \tag{4.10}$$

The first term in Eqn. 4.10 is dependent on the statistical properties of the input signal. In the case of LCS, *SNR* is not dependent on the number of quantization levels, but on the time period $T_c$ of the clock signal used for measuring $dt_n$. By dividing $T_c$ by two, SNR increases by 6.02 dB. From Eqn. 4.4, it is clear that if the number of bits *N* is doubled, the SNR of a synchronous ADC increases by 6.02 dB. Hence dividing the value of $T_C$ by two is equivalent to the addition of a bit in a classical ADC.

## 4.4 DESIGN OF A LEVEL-CROSSING SAMPLER

The complete design methodology of an A/D converter based on level-crossing sampling (LCS) is presented by E. Allier et al. in [19]. A timer with time period $T_C$ is used to represent $dt_n$.

If the converter resolution *M* and the maximum value of the input $V_{max}$ are known, then the inter-level distance $\Delta v$ will be,

$$\Delta v = \frac{V_{max}}{2^M\text{-}1} \tag{4.11}$$

Let *d* be the total delay of the conversion loop, which is the time gap between a level-crossing instant and the time at which the reference levels $V_H$ and $V_L$ are updated. When a conversion is triggered, the input signal must not change its amplitude by $\Delta v$ until the conversion corresponding to the previous level-crossing is reflected in the output. This restriction which is stated as a tracking condition of the asynchronous converter, can be expressed as

$$\left|\frac{dv_{in}}{dt}\right| < \frac{\Delta v}{d} \tag{4.12}$$

The design of the level-crossing sampler is explained below. Characteristics of the input signal and the desired effective number of bits *ENOB*

are the input parameters required. Substituting the expected SNR value in the equation for classical ADCs, *ENOB* can be calculated. Input signal parameters are

i) Power spectral density
ii) Bandwidth, $f_{max}$
iii) Maximum amplitude of the signal, $V_{max}$
iv) Probability density of the input, $p(x)$

The parameters of LC sampler to be computed are

i) Resolution $M$ which fixes the number of quantization levels
ii) The maximum loop delay $d_{max}$, to satisfy the tracking condition
iii) The time period $T_c$ of the timer and
iv) The inter-level distance, $\Delta v$

Design procedure:

(a) Computation of $M$

In synchronous ADCs, the number of samples is selected to satisfy the Nyquist criterion. However, in asynchronous ADCs, the number of samples is dependent on the resolution $M$ which fixes the number of threshold levels. If the value of $M$ is high, the average number of samples per second will be high. As pointed out in section 3.3, the average sampling rate $\overline{f_s}$ must be greater than twice the maximum frequency of the signal. Using statistical methods, the average sampling rate $\overline{f_s}$ can be calculated. In order to minimize the power, the value of $M$ and hence, $\overline{f_s}$ are selected as the minimum values which satisfy the condition for reconstruction.

(b) Computation of $d$ and $\Delta v$

Using the values of $V_{max}$ and $f_{max}$, maximum value of the slope can be found based on Bernstein theorem as

$$\left|\frac{dv_{in}}{dt}\right| \leq 2\pi f_{max} V_{max} \tag{4.13}$$

For a given $M$, the number of quantization levels will be $2^M - 1$. According to the tracking condition (Eqn. 4.12) and the Bernstein inequality (Eqn. 4.13), the loop delay $d$ must be less than $d_{max}$, where

$$d_{max} = \frac{1}{2\pi f_{max}(2^M - 1)} \tag{4.14}$$

$\Delta v$ can be calculated based on the condition for $d_{max}$.

(c) Computation of $T_c$

The first term in Eqn. 4.10 for computing *SNR* can be found from the power spectral density of the input signal. The desired *SNR* for LCS can be calculated from Eqn. 4.4, substituting the equivalent value of $N$ in a synchronous ADC. Then from Eqn. 4.10, the value of $T_C$ can be calculated.

## 4.5 ADAPTIVE LCS

In LCS, the dynamic range of input signals must be known for selecting the crossing levels. The distance between the levels is a constant. Enough samples are not taken if the input signal has a slow variation between two threshold levels. This increases the time between successive level-crossings, causing $Dt_n$ to be a high value. More number of bits are required to represent $Dt_n$ which increases the data size. Similarly, redundant samples are acquired when the input signal has a higher slope. In order to address this problem, an adaptive LCS scheme (ALCS) has been proposed in [24]. The distance between the levels is adapted to the slope of the input signal. In a 2-level ALCS, two values, $d_1$ and $d_2$ with $d_1 > d_2$ are used as distances between the levels. A threshold value for the slope is fixed, and if the slope of the input signal is above the threshold, $d_1$ is used as the inter-level distance. During the portions where the slope is less, $d_2$ is used as the distance ensuring that enough samples are acquired. The representation of $dt_n$ is similar to that of normal LCS. However, we require two

bits to represent each level-crossing, one bit for indicating whether the sample belongs to a low-slope or a high-slope region and the second *DIR* bit to represent the direction of change in the amplitude.

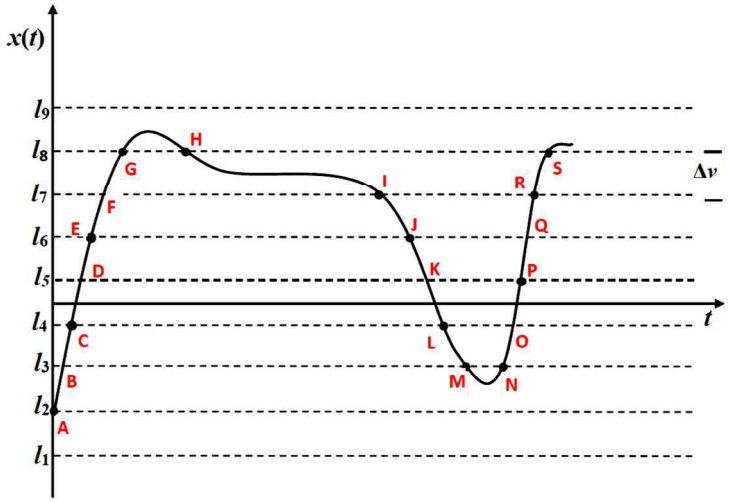


*Fig. 4.11 Illustration of adaptive LCS*

Two-level adaptive LCS is illustrated in Fig. 4.11. The level-crossing instants are shown with alphabets A to S. During the initial portion (from points A to G) the slope is high, and hence samples are not acquired at the intermediate points B, D and F. In this case $d_1$ will be twice the value of $d_2$. Between the adjacent points H and I, the signal slope is low, and hence samples are taken at both the points. For a standard level-crossing scheme, the slope of the signal between two nearby levels can be specified as,

$$\text{slope} = \frac{\Delta v}{dt_n} \tag{4.15}$$

However, the interval between level-crossings is represented as a digital count, $Dt_n$. Hence, the interval can be expressed as

$$dt_n = Dt_n . T_c \tag{4.16}$$

Therefore, the slope becomes

$$\text{slope} = \frac{\Delta v}{Dt_n . T_c} \tag{4.17}$$

If $\Delta v$ and $T_c$ are constant, the slope is dependent on the TDC count $Dt_n$ only, higher will be the slope if $Dt_n$ is less. In this scheme, the inter-level distance is adapted to the signal slope. Distance will be changed to a larger value if the signal slope crosses a threshold. The block diagram for ALCS is similar to that in Fig. 4.7, slightly modified by providing feedback from the counter output to the logic circuit. $Dt_n$ is compared with the threshold, and based on the result, the inter-level distance and the reference voltages to the comparators are updated. An example is a two-level LCS in which the distance changes between $\Delta v$ and $2\Delta v$ depending upon the slope of the input. Additional indication bit is needed to differentiate between different modes. Data representation of a sample value in a differential, adaptive LCS is shown in Fig. 4.12.


*Fig. 4.12 The bit representation in two-level adaptive LCS*

*DIR* is the direction bit, *ADA* is the indication for the inter-level distance, and $Dt_n$ is the TDC count.

In order to reconstruct the signal from ALCS samples, Eqn. 4.2 is modified to include the additional bit, *ADA*. Let $a_n = 2$ if *ADA* is 1, and $a_n = 1$ if *ADA* is 0. The value of $x(t_n)$ can be updated from the previous value $x(t_{n-1})$ as,

$$x(t_n) = x(t_{n-1}) + b_n\, a_n\, \Delta v \tag{4.18}$$

## 4.6 EXTREMUM SAMPLING

The advantage of LCS is that the sampling density adapts to the local activity of the signal. If there is no activity in the signal, LCS does not acquire samples. However, if the value of $\Delta v$ selected is very small, the time interval between successive samples may be very small. If $\Delta v$ is high, there could be a loss of information that increases the error in the reconstruction. In LCS, the

sampling density depends on the input signal, and on the placement of the levels. Hence the advantages of LCS are dependent on the proper placement of the threshold levels within the dynamic range of the input signal. Another non-uniform sampling method for which the sampling density depends only on the input signal is extremum sampling (ES). In extremum sampling (ES), samples are acquired at the zero-crossings of the first derivative of the signal. A sample is captured whenever a local maximum or minimum value of the input signal is detected. The most significant points that characterize a signal are its local extrema. Extremum sampling is suitable for the representation of the signals like speech and vibrations that have an oscillatory nature. ES can be implemented with level-crossing sampling (LCS) [27]. In ES, whenever the input signal crosses a threshold level, it checks whether the slope of the signal has changed from positive to negative or vice versa. If so, the amplitude corresponding to that threshold level is selected as a local extremum point. Hence, the accuracy of peak detection is dependent on the value of the inter-level distance $\Delta v$. The idea of extremum sampling is illustrated in Fig. 4.13. The input signal is compared with the threshold levels $l_1$ to $l_{10}$, which are equally spaced at $\Delta v$.

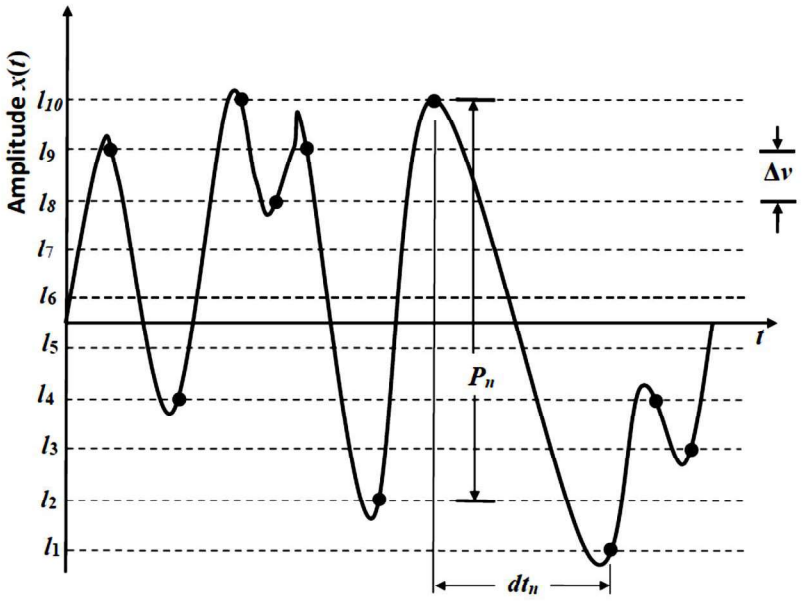


*Fig. 4.13 Illustration of extremum sampling*

Samples acquired with ES are represented by a triplet ($S_n$, $P_n$, $Dt_n$) as shown in Fig. 4.14. If the bit $S_n$ is '1,' it indicates that the present sample is representing a positive peak, and it is a negative peak if the bit is '0.' $P_n$ is the digital equivalent of the differences in amplitude between the successive peaks expressed in terms of $\Delta v$. If the difference between two adjacent peaks is $V_{pp}$, then $P_n$ is equal to $\lceil V_{pp} / \Delta v \rceil$, where $\lceil . \rceil$ is the ceiling operation, which is rounding towards the nearest higher integer value. The number of bits required to represent $P_n$is $\log_2 \lceil V_{pp} / \Delta v \rceil$. $Dt_n$ represents the time gap between the successive peaks $dt_n$, which is measured in terms of the number of cycles of the clock signal as in the case of LCS.

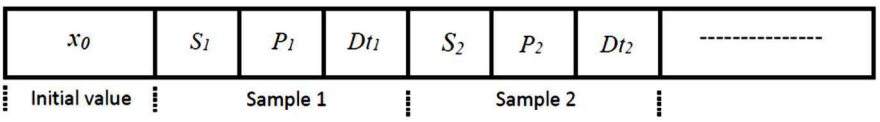


*Fig. 4.14 Representation of a sample in extremum sampling*

The signal-to-noise-ratio of the reconstructed signal depends on $\Delta v$, and the period of the clock signal $T_c$. If $\Delta v$ is large, there can be a significant change from the actual peak and the nearest threshold level, which causes quantization error in the amplitude. Similarly, there can be quantization error in time due to a large value of the clock time period $T_c$. For each sample, the amplitude of the peak and the time information are to be coded. Compressed output is obtained if ES is applied to speech or vibration signals. The block diagram of extremum sampling is shown in Fig. 4.15.

The comparators and the logic circuit produce an approximation, $R_i$ of the input signal. $V_H$ and $V_L$ are the upper and lower threshold levels with which the input is compared. If the present amplitude of the input crosses either $V_H$ or $V_L$, the value of $R_i$, $V_H$, and $V_L$ are increased or decreased by $\Delta v$. $Dt_n$ is represented by the output of the time-counter. The counter increments with the clock signal, and resets with a change of $S_n$, which indicates the occurrence of a

local extremum. The number of threshold levels between successive peaks is measured by the level-counter, which increments at the instant of each level-crossing. This counter is also reset with a change in $S_n$. During the reconstruction, each sample is updated with the present $S_n$, $P_n$, and $Dt_n$. Assuming $b_n$ =+1 for $S_n$ =1, and $b_n$ =-1 for $S_n$ =0, the present sample value $x(t_n)$ is computed from the previous sample value $x(t_{n-1})$ as

$$x(t_n) = x(t_{n-1}) + b_n P_n \Delta v \tag{4.19}$$

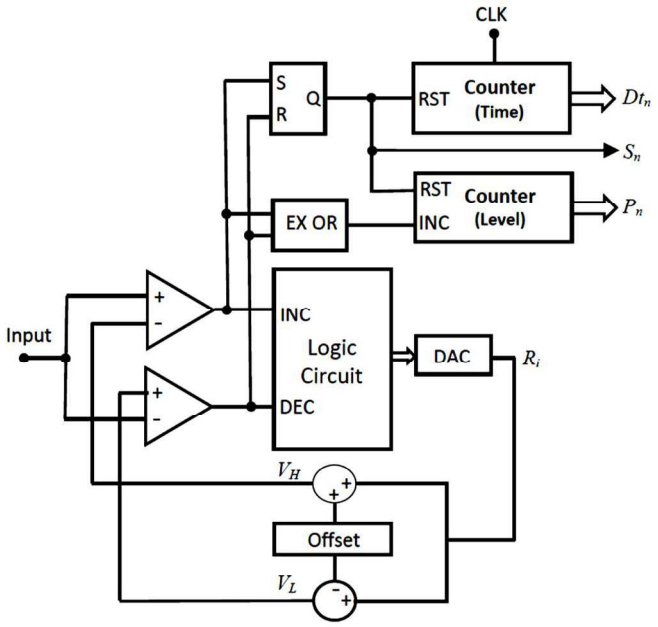


*Fig. 4.15 The block diagram for extremum sampling*

## 4.7 EFFECT OF NOISE IN LEVEL-CROSSING SAMPLING

Level-crossing sampling has inherent noise tolerance. If noise alone with peak-to-peak value less than $\Delta v$ is applied to LCS, no sample will be generated. However, if the same noise signal is present along with a slowly varying signal, large number of un-necessary samples are generated. This happens if one of the updated reference levels occupies the previous position of the other reference level. Such a situation can be avoided if the concept of hysteresis is incorporated in LCS, which is explained below.

For illustrating the effect of noise in the system, a sine wave of 100 Hz is used as a signal. Initially, the sinusoidal signal alone is subjected to the system. The signal and the variations in the reference levels $V_H$ and $V_L$ are shown in Fig. 4.16(a). There are 20 level-crossings taking place, and at each level-crossing, $V_H$ and $V_L$ change by $\Delta v$. Hence 20 samples are generated in LCS, and just two samples are taken in ES implemented with LCS, which are the peak values. In order to illustrate the noise tolerance of LCS and ES, a triangular signal of peak-to-peak amplitude ($V_{pp}$) which is slightly less than $\Delta v$ is used to represent the noise. If the triangular wave alone is applied to the system, there is no level-crossing taking place, and no samples are acquired in LCS or ES, since the amplitude variations are within $\Delta v$. The triangular wave is then added with the sine wave to generate a noisy signal. The added signal is then applied to the system. As illustrated in Fig. 4.16(b), $V_H$ and $V_L$ are updated by $\Delta v$ at each level-crossing. Near the positive and negative peak of the sine wave, the amplitude variations are within $\Delta v$, and there is no level-crossing taking place. However, a total of 180 samples are generated in LCS in the present situation, and 150 in ES. From Fig 4.16(b), it is observed that level-crossings are taking place even for the slightest amplitude variations in the signal. One such region near the negative peak of the sine wave is encircled in Fig 4.16(b), and it is shown magnified in Fig. 4.16(c). At the instant A, the input sine has a small increase in amplitude, and it crosses $V_H$, and both the reference levels increase by $\Delta v$. A sample is acquired at this instant. Soon after this instant, the peak of the triangular wave has a very small fall in its amplitude, but this causes the signal to cross $V_L$. $V_H$ and $V_L$ are decreased by $\Delta v$, and again one sample is generated. This has happened because, while $V_H$ and $V_L$ increased by $\Delta v$, the updated $V_L$ occupies the level of the previous $V_H$. Soon after crossing $V_H$, if the signal has a decrease in its amplitude, which is much less than $\Delta v$, it then crosses the present $V_L$, and a sample is generated. This can be avoided if hysteresis is incorporated in LCS.

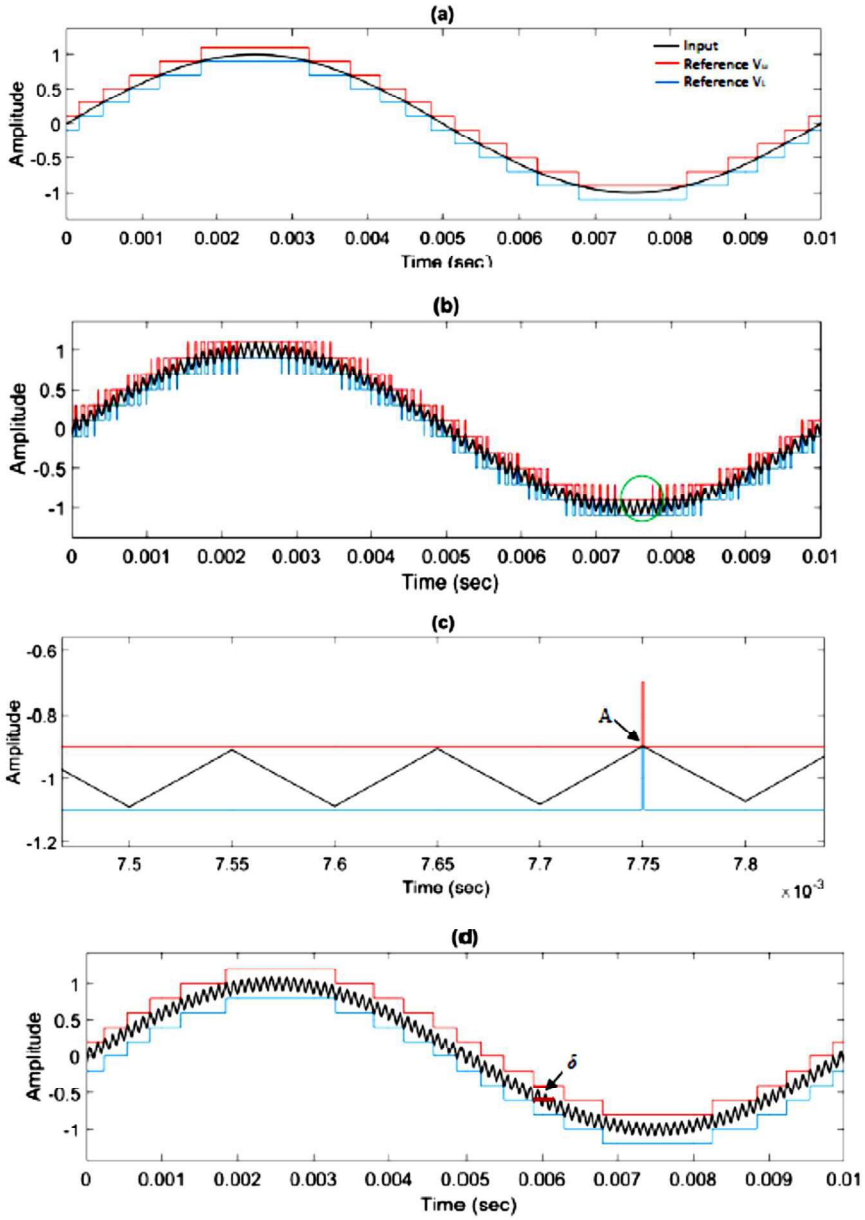


*Fig. 4.16 (a) Input and the reference levels while sine wave is applied to LCS (b) Noisy input applied to LCS without hysteresis (c) Magnified form of the encircled portion (d) Noisy input applied to LCS with hysteresis*

In order to incorporate hysteresis, a finite offset of $\delta$ is maintained between present $V_L$ and previous $V_H$ if the slope of the signal is positive. Similarly, the same offset is maintained between the present $V_H$ and the previous $V_L$ if the signal slope is negative. The same input signal is applied to LCS with hysteresis, and the corresponding $V_H$ and $V_L$ are shown in Fig. 4.16(d). Here the

offset $\delta$ is selected as $\Delta v$ itself. Similar to the output obtained for the noiseless input signal, as shown in Fig. 4.16(a), there are just 20 level-crossings. Hence the number of samples generated in LCS is 20, and just two samples are generated in ES. The disadvantage of using ES with hysteresis is that the maximum error in amplitude is $\Delta v + \delta$, compared to $\Delta v$, as in the case of ES without hysteresis. Depending upon the estimated value of the noise level, the value of $\delta$ can be selected. If the peak-to-peak value of the noise is greater than $\Delta v$, additional filtering must be done before applying to LCS or ES.

## 4.8 SUMMARY

In this chapter, the basic principle of LCS, the block diagram for its implementation, derivation of the signal-to-noise-ratio, and the steps for design are discussed. Adaptive level-crossing scheme (ALCS), in which the inter-level distance is altered according to the slope of the input signal, is introduced. Extremum sampling (ES) is another form of LCS, in which digital representations of the local extrema points are recorded. The algorithms for the reconstruction of the signal from LCS, ALCS and ES are also explained. The effect of noise in LCS, and ES based on LCS are also illustrated. LCS generates lesser number of samples compared to the uniform sampling scheme. However, the use of large number of bits to represent $Dt_n$ in each sample results in an excessive amount of data. A significant reduction in the data size is possible by changing the frequency of the clock used in the TDC according to the activity in the input signal which is discussed in the next chapter.

# CHAPTER 5

# LEVEL-CROSSING SAMPLER WITH MULTIPLE TEMPORAL RESOLUTIONS

## 5.1 INTRODUCTION

In this chapter, the inherent property of LCS is exploited for compressing speech signals. Due to the presence of long silence periods, the interval between level-crossings $dt_n$, and hence the word-size of the TDC count becomes large. The ratio of $dt_n$ between active and silent portions becomes worse than 1:1000. Even if a reduced word size is sufficient for active portions, it is insufficient for representing the long silence portions. If the word-size required for encoding $dt_n$ during the silent portions is used for representing all the $dt_n$ values, the data size becomes large resulting in a poor compression ratio. If a reduced word-size is used, the TDC counter overflows several times during the silent regions since there are no level-crossings taking place for a long duration. An efficient encoding for the silence period is proposed, utilizing the concept of frequency-scaling, which is a technique used for the reduction of dynamic power in processors. As explained in section 4.3, the temporal resolution of LCS is dependent on the time period $T_c$ of the clock used. Hence the proposed LCS scheme results in multiple temporal resolutions, which is also extended to adaptive LCS and extremum sampling. Extremum sampling with frequency-scaling results in extremely good compression compared to all the other LCS schemes.

## 5.2 LEVEL-CROSSING SAMPLING OF SPEECH SIGNALS

A speech signal consists of voice-active and silence regions. Silence is an integral part of a speech signal because speech is not intelligible without the presence of it. If we perform sampling at the Nyquist rate, samples are generated

uniformly during the silence region also. However, in LCS, there are no level-crossings during the silence period, and no samples are acquired from a noiseless voice signal. The interval between level-crossing instants $dt_n$ is represented by a '$B$' bit word $Dt_n$ which is the output of a TDC counter. The choice of '$B$' fixes the maximum value of $dt_n$ ($dt_{max}$) that is represented by,

$$dt_{max}=\left(2^{B}-1\right)T_c \tag{5.1}$$

The choice of a higher value of $B$ increases the circuit complexity and the volume of data. The data-size is large because each sample generated by LCS, irrespective of whether it is from the active or silence regions, must be represented by these $B$ bits. The TDC counter increments uniformly during the silence period as time progresses. If the silence period exceeds $dt_{max}$, the counter overflows and restarts counting from zero, which is repeated until a level-crossing is detected. The TDC is of constant resolution if the clock frequency $f_c$ is fixed.

As an illustration, a sample voice signal of duration 0.5 Seconds, which is the initial portion of the speech signal 'sp02' from the NOIZEUS database is subjected to LCS, and the corresponding outputs are shown in Fig. 5.1. Fig. 5.1(b) is the output of the level-crossing detector (LCD). It is a pulse signal generated while the input signal crosses any of the threshold levels. The darker portion indicates that $dt_n$ is very small, and the pulses are very close. The first level-crossing occurs at 0.2153s, after the duration of the initial silence region. The equivalent analog values of the TDC counter output are shown in Fig. 5.1(c). The counter resets at each level-crossing instant, and then counts up during each $dt_n$. Hence, they are in the shape of ramp waveforms with the height depending upon the duration $dt_n$. Frequency $f_c$ is selected as 100 kHz at which the reconstructed signal has reasonably good clarity. Fig. 5.1(c) shows the TDC output with a 16-bit counter.

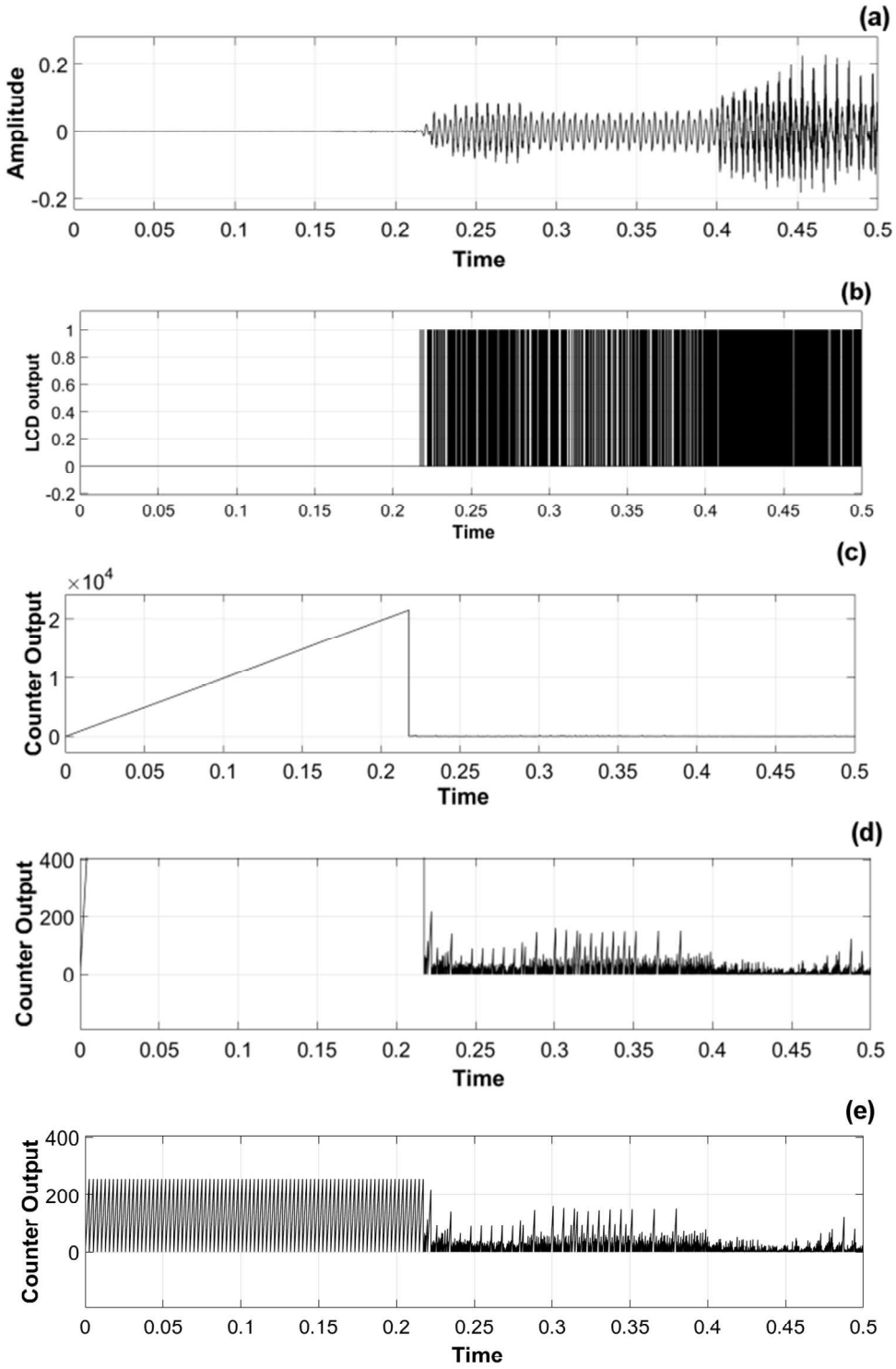


*Fig. 5.1. (a) Input signal (b) Output of level-crossing detector (c) Output of 16-bit TDC counter (d) Output of 16-bit TDC counter (magnified near the x-axis) (e) Output of 8-bit TDC counter*

The entire silence period is represented by a 16-bit word at the expense of using 16 bits for all the 2430 samples. At the end of the silence region, the TDC count is 21532, whereas values of the counts generated during the voice-active region are well below this count, and hence they are not visible in Fig. 5.1(c). Fig. 5.1(d) is the counter output, in which level-crossing intervals in the voice-active region are shown magnified. An 8-bit word could have represented the TDC counts except for the one that occurred at the end of the silence region.

Fig. 5.1(e) shows the counter output with an 8-bit TDC counter, which has a $dt_{max}$ of 2.55 ms with $f_c$ equal to 100kHz. This resulted in 2514 samples because the silence region is represented by a sequence of 84 counts each of value 255, followed by a count of value 28. Even though there is an increase of 84 samples compared to the earlier case, there is a significant saving in data-size because each count is of 8 bits. A single 8-bit count could have represented the entire silence region if the value of $T_c$ were sufficiently high. However, $T_c$ is selected to satisfy the *SNR* value in the reconstructed signal in accordance with Eqn. 4.10. An alternate solution is to use a clock signal of a higher $T_c$ during the silence period, which is explained in the next section.

## 5.3 FREQUENCY-SCALING

According to the Eqn. 3.1, the dynamic power consumption is directly proportional to the clock frequency, and hence, decreasing the clock frequency during the inactive periods saves power, increases battery life and reduces heat emission. Dynamic voltage and frequency-scaling (DVFS) is a technique adopted to increase the energy efficiency of processors in computing systems [90]. Generally, there are two schemes with which DVFS is implemented. The first scheme employs specific frequencies and associated voltages for selected modes like power saver mode. In the second scheme, the CPU load is continuously monitored, and the frequency of the clock is lowered if the CPU workload is less.

It is an adaptive method that selects the clock frequency depending upon the activity.

During the voice-active region, the time gap between the instants of level-crossing is minimal. Hence a high-frequency clock which satisfies the condition for the required SNR according to Eqn. 4.10 is used for TDC during this region. During the silence region, the clock signal to the TDC is from a low-frequency pulse generator so that there is a reduction in the dynamic power consumption, and lesser bits are sufficient to represent longer durations. Since there is no voice activity during this period, *SNR* is not affected.

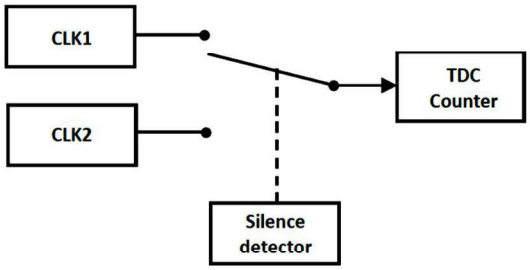


*Fig. 5.2 A simplified block diagram of the frequency-scaling scheme*

As shown in Fig. 5.2, CLK1 and CLK2 are the two clock signal generators with their corresponding periods having a relation, $T_{c1} << T_{c2}$. Instead of using two separate clock generators, CLK2 can be derived from CLK1 by dividing it by a factor *K*. Normal level-crossings are occurring during the voice-active region, and the switch remains connected to CLK1. While voice activity is absent for the duration of $dt_{max}$, the counter overflows, and the clock signal to the counter is switched to CLK2. The concept of frequency-scaling is illustrated in Fig. 5.3. Two speech segments are shown, which are separated by a silence region. The word-size of the counter *B* is selected such that it satisfies the condition for the required *SNR*. CLK1 is having a time period of $T_c$, and CLK2 is the scaled version of CLK1 with time period $KT_c$. Since CLK2 has a longer period, large durations can be represented with small TDC counts during the silence periods.

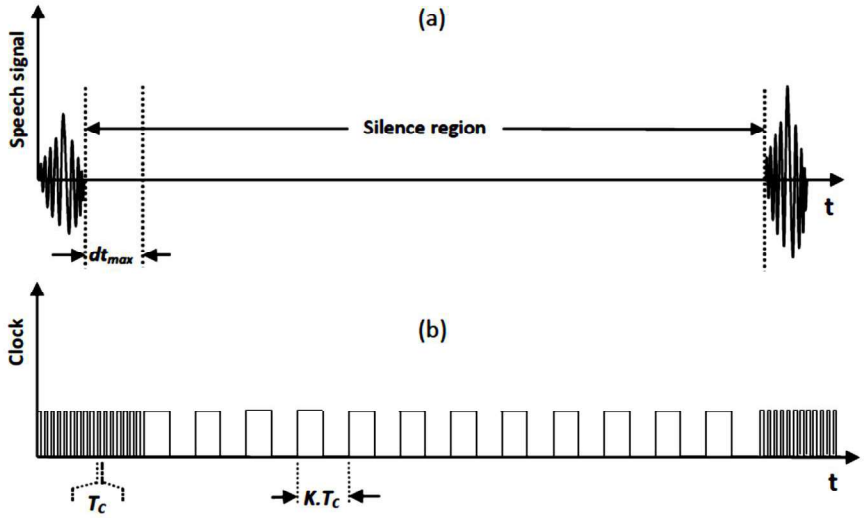


*Fig. 5.3 (a) An artificial speech segment with silence region (b) Illustration of the concept of frequency-scaling*

A detailed block diagram of the frequency-scaling scheme is shown in Fig. 5.4. A single clock generator is used (CLK1), and CLK2 is derived from CLK1 by scaling its period by a factor *K*. During the voice-active region, there are many level-crossings causing input R of the SR flip-flop to become high. During this region, the input S remains low, and CLK1 is directly applied to the TDC counter as the clock signal. While voice activity is absent for a duration of $dt_{max}$, overflow turns S to high, and R remains low, and the counter is switched to CLK2. If an extra bit is used to represent this change of clock frequency to the TDC, we need as many additional bits as the number of samples, and this affects the compression ratio. This is because, the indication bit must accompany each sample representation. In the proposed method, there is no need for a redundant bit because, the change of mode takes place at the instant of overflow in the counter, and the corresponding sample value is (*DIR*, $Dt_{max}$). $Dt_{max}$ is the TDC count corresponding to $dt_{max}$. The occurrence of a sample (*DIR*, $Dt_{max}$) is an indication that the next sample is acquired with CLK2. If there is silence for a prolonged duration, the counter overflows with CLK2, and there are repeated counts of $Dt_{max}$ in which the first one is due to CLK1, and others are due to CLK2. Instead, frequency-scaling can be extended to higher levels by using CLK3, which is a time-scaled version of CLK2. In this mode, the first, second,

and third $Dt_{max}$ in succession correspond to CLK1, CLK2, and CLK3, respectively.

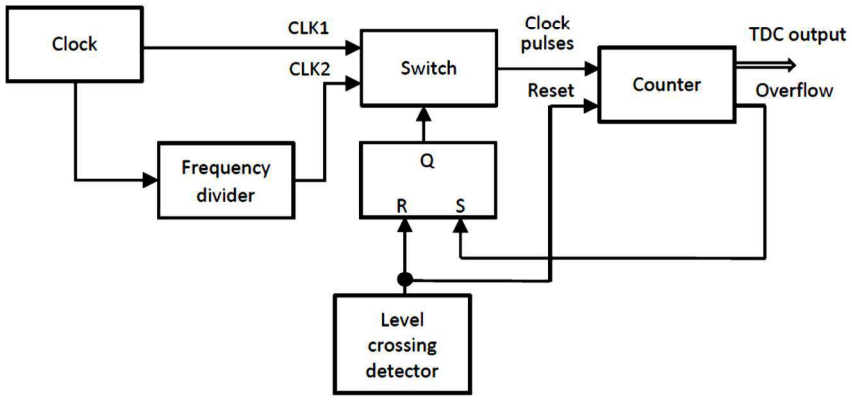


*Fig. 5.4 A detailed block diagram of the frequency-scaling scheme with multiple resolutions*

The signal, which is shown in Fig. 5.1(a) is subjected to LCS with frequency-scaling, and the corresponding TDC output is shown in Fig. 5.5. The frequency of the clock is 100 kHz, and the dividing factor $K$ is selected as 100. There are 2431 samples acquired by LCS with frequency-scaling, compared to 2430 samples with B = 16 as described in section 5.2. The initial overflow count of 255 is an indication of the beginning of the silence region, and after this, the counter is triggered by the low-frequency clock signal. With a clock signal of 100 kHz and an 8-bit counter, the first overflow ($Dt_n=Dt_{max}$) occurs at 2.55 milliseconds after the last level-crossing instant. With CLK1, the increment in the count takes place at every 10 µs (i.e., $1/f_{c1}$), and it is 1 ms with CLK2 if the value of $K$ is 100.

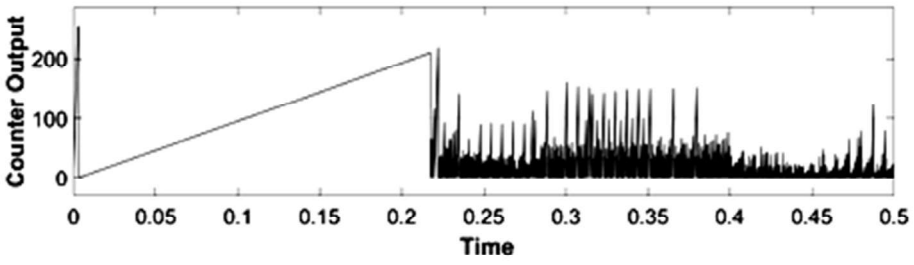


*Fig. 5.5 The frequency-scaled output of the 8-bit TDC counter*

Speech signal ‘sp03’with babble noise and having signal-to-noise-ratio (*SNR*) of 20dB is applied to LCS. The speech signal, TDC counter output, and the reconstructed signal are shown in Fig. 5.6. TDC counter automatically switches between the two clock signals depending upon the input activity. The noise gets removed from the signal since the amplitude variations due to this fall within the inter-level distance.

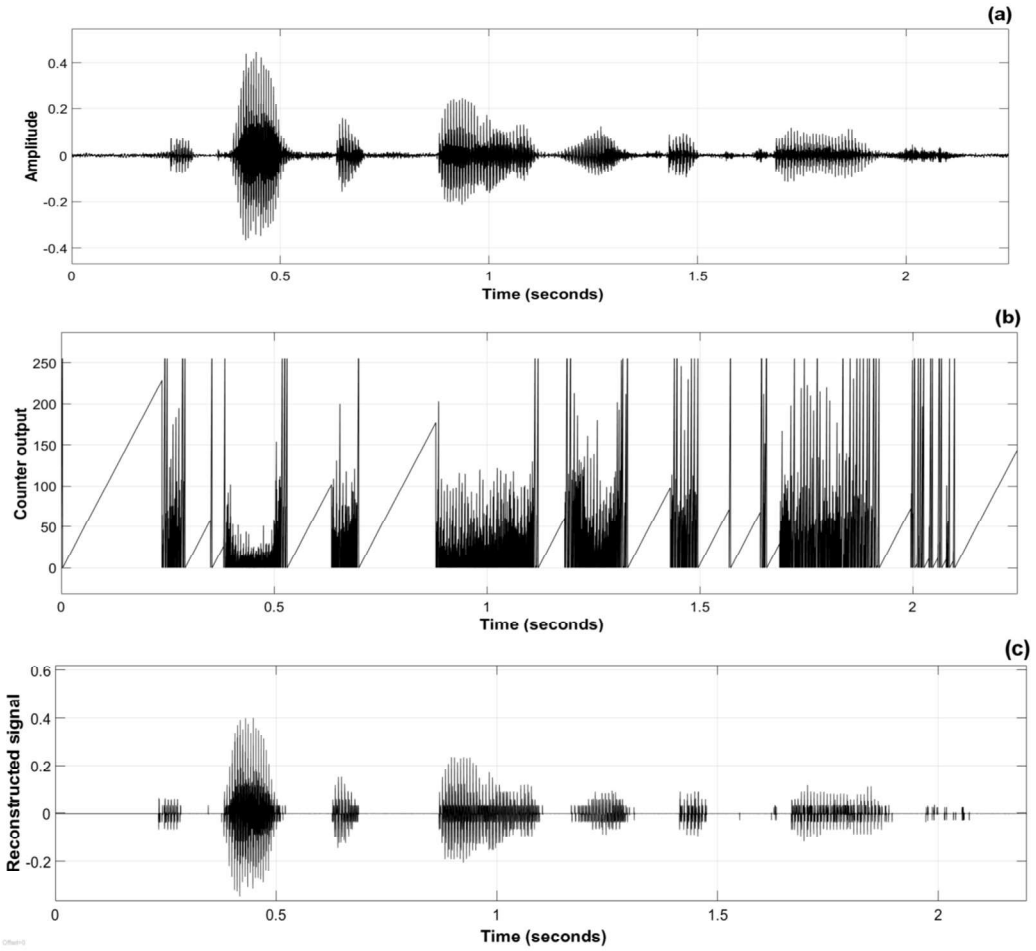


*Fig. 5.6 (a) The input speech signal (b) Output of the TDC counter (c) Reconstructed signal*

The quantization error in time with CLK2 connected to the TDC counter is in the range [0, $K.T_c$], which is high compared to its value with CLK1. The error in the last count causes a change in the duration of the silence region in the reconstructed output. In applications where this error cannot be tolerated, a correction word can be used, which follows the last count with CLK2. This word

must be the count of CLK1 pulses starting from the leading edge of the last CLK2 pulse, up to the instant at which level-crossing takes place after the silence period. This correction word is transferred to the output when the clock input to the TDC counter switches back to CLK1 from CLK2. This is equivalent to the coarse and fine time measurements used in some of the TDCs for accurate measurement of time as discussed in section 4.2.2. In this thesis, frequency-scaling is applied to normal LCS, adaptive LCS, and extremum sampling. In all these cases a significant reduction in the number of samples is observed.

## 5.4 ALGORITHMS FOR RECONSTRUCTION

Let $t_n$ be the $n^{th}$ time instant at which a non-uniform sample is acquired, $x(t_n)$ the corresponding amplitude of the sample and $\Delta v$ the distance between two adjacent threshold levels. $T_c$ is the period of the clock signal, $K$ the frequency-scaling factor, *len,* the length of the block, and let $b_n = 1$ for $DIR = 1$ &$b_n = -1$ for $DIR = 0$. Let the initial value of the input signal be $x_0$. The decision on whether the present LCS sample is acquired under the normal mode or the frequency-scaled mode is dependent on the previous $Dt_n$ value. Hence, $t_1$ and $x(t_1)$ are computed first.

### 5.4.1 LCS with frequency-scaling

Initialization: $t_0 = 0$, $x(t_0) = x_0$

$t_1 = Dt_1 T_c$
If $Dt_1 = Dt_{max}$
$x(t_1) = x_0$
else
$x(t_1) = x_0 + b_1 \Delta v$
end if
for $n = 2$: *len*
If $Dt_{n-1} = Dt_{max}$
$t_n = t_{n-1} + Dt_n K T_c$

$x(t_n) = x(t_{n-1})$

else

$t_n = t_{n-1} + Dt_nT_c$

$x(t_n) = x(t_{n-1}) + b_n\Delta v$

end if

end for

### 5.4.2 Adaptive LCS with frequency-scaling

As explained in section 4.5, the *ADA* bit is used in a two-level adaptive LCS to indicate whether the present sample differs in amplitude from the previous one by $\Delta v$ or $2\Delta v$. The adaptive LCS with frequency-scaling is the complex one since it is adaptive in amplitude and time. The flowchart for the reconstruction is shown in Fig. 5.7.

### 5.4.3 Extremum sampling with frequency-scaling

As mentioned in section 4.6, there is an additional parameter, level count $P_n$ to represent the change of amplitude from the previous peak. Upon receiving each sample, amplitude of the reconstructed signal must be updated by either $\Delta v$ or $2\Delta v$ in two-level adaptive LCS. However, in extremum sampling, the amplitude must be changed by $P_n\Delta v$ during the reconstruction. The sample values $x(t_1)$ and $x(t_n)$ in the algorithm explained in section 5.4.1 are computed using Eqn. 4.19.

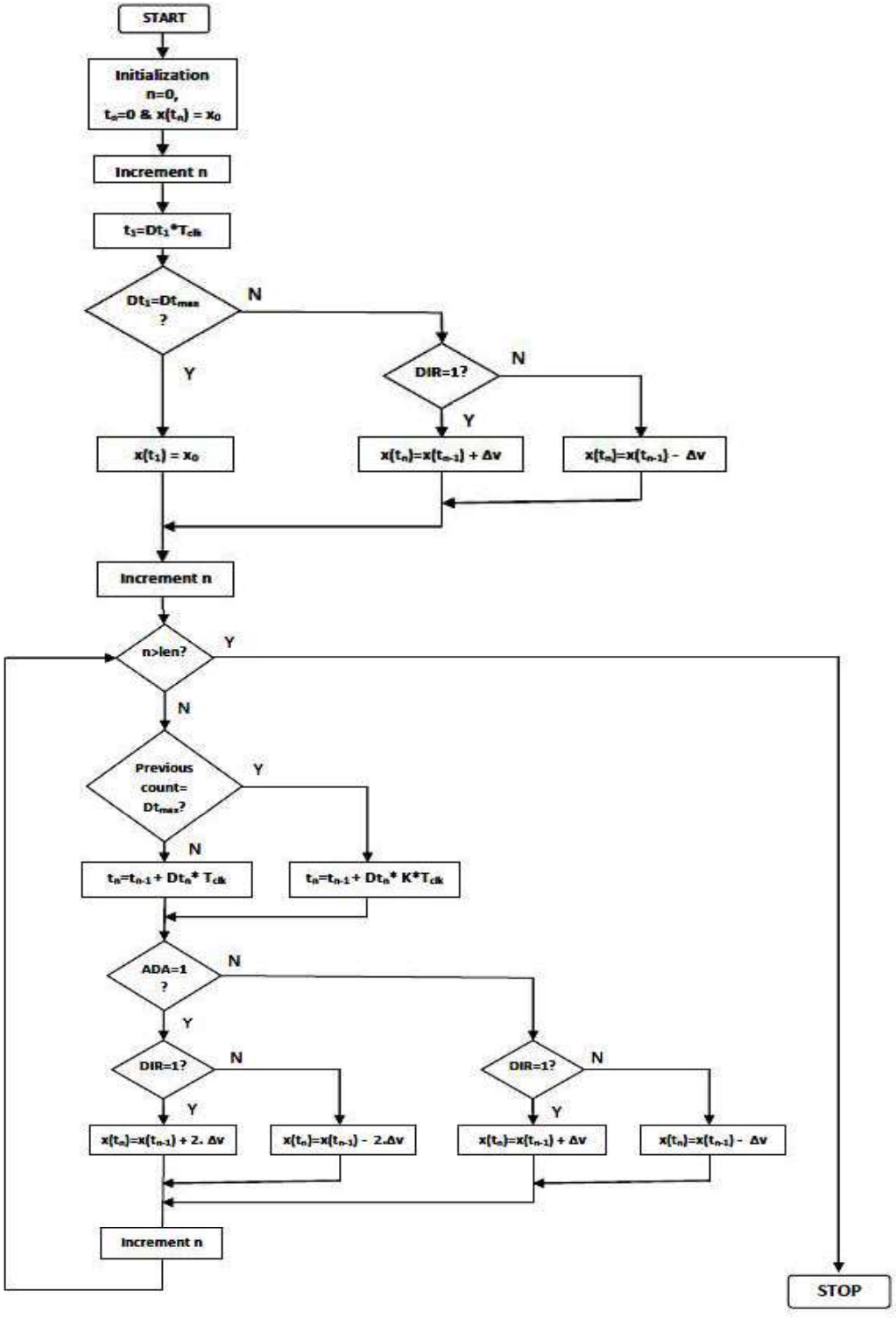


*Fig. 5.7. The flowchart for the reconstruction of Adaptive LCS with frequency-scaling*

## 5.5 SIMULATION RESULTS

The proposed algorithm is tested using speech signals from the NOIZEUS database and the 'Open Speech Repository.' NOIZEUS database contains speech signals, each with one Harvard test sentence. Noise-free and noisy signals are included in the database. Open Speech Repository includes test signals, each containing ten Harvard test sentences. The signals available in the '.wav' format are converted to '.mat' format with a sampling rate of 8000 Hz, and each sample is represented by 16 bits. Each signal is interpolated to treat them as a continuous signal, before sampling with various level-crossing methods. Simulation is done using Matlab and Simulink. Five numbers of male and five female speech signals, each consisting of five test sentences are applied to standard level-crossing sampling (LCS), adaptive LCS (ALCS), and extremum sampling (ES) with a fixed value of $T_c$ and $\Delta v$. The proposed method differs from the standard level-crossing methods with the inclusion of frequency-scaling (FS). All the signals are again sampled with the corresponding frequency-scaled methods (LCS-FS, ALCS-FS, and ES-FS).

Mean opinion score (*MOS*) was calculated from the response from a group of 35 persons. Based on the perceived quality of the reconstructed output, each person was asked to give their individual rating $R_n$, in the range from 1 to 5, as shown in Table 5.1.

*Table 5.1 Rating and the corresponding label for calculating MOS*

| Rating $R_n$ | Label |
|---|---|
| 5 | Excellent |
| 4 | Good |
| 3 | Fair |
| 2 | Poor |
| 1 | Bad |

Mean opinion score was calculated as the arithmetic mean of the individual rating as given below. N is the total number of persons, which is 35.

$$MOS = \frac{\sum_{n=1}^{N} R_n}{N} \tag{5.2}$$

Table 5.2 shows the comparison of the data size of the output obtained with LCS and LCS-FS. The value of compression ratio (*CR*) obtained with LCS-FS is compared with the corresponding *CR* obtained with LCS, and the percentage increase is listed in the table. The value of *CR* is computed as

$$\text{Compression Ratio } (CR) = \frac{\text{Input data size}}{\text{Output data size}} \tag{5.3}$$

*Table 5.2 Comparison of the data size in LCS and LCS-FS methods*

| Signal | Duration | Input data size (kb) | LCS | | LCS-FS | | Percentage increase in *CR* | *MOS* |
|---|---|---|---|---|---|---|---|---|
| | | | Data size (kb) | CR | Data size (kb) | CR | | |
| us_11 | 16s | 2048 | 361.1 | 5.67 | 337.1 | 6.08 | 7.12 | 4.06 |
| us_12 | 18s | 2304 | 454.3 | 5.07 | 425.8 | 5.41 | 6.69 | 4.09 |
| us_13 | 17s | 2176 | 397.1 | 5.48 | 368.9 | 5.90 | 7.64 | 4.00 |
| us_14 | 15s | 1920 | 327.5 | 5.86 | 306.1 | 6.27 | 6.99 | 4.03 |
| us_15 | 20s | 2560 | 387.8 | 6.60 | 358.7 | 7.14 | 8.11 | 4.06 |
| us_35 | 18s | 2304 | 963.6 | 2.39 | 936.9 | 2.46 | 2.85 | 4.38 |
| us_36 | 20s | 2560 | 728.2 | 3.52 | 686.6 | 3.73 | 6.06 | 4.22 |
| us_37 | 20s | 2560 | 935.2 | 2.74 | 901.7 | 2.84 | 3.72 | 4.25 |
| us_39 | 20s | 2560 | 974.9 | 2.63 | 944.4 | 2.71 | 3.23 | 4.28 |
| us_57 | 17s | 2176 | 667.4 | 3.26 | 642.1 | 3.39 | 3.94 | 4.31 |

The amount of reduction in the data-size in LCS-FS depends on the total duration of the silence region in each signal, and also on the value of *K*. The maximum value of *CR* obtained in LCS and LCS-FS are 6.60 and 7.14 respectively. The maximum improvement in the value of *CR* in LCS-FS over the standard LCS is obtained as 7.12%. The perceived quality of the output signal is represented in the form of Mean Opinion Score (*MOS*) and is shown in the table.

The same set of signals are again applied to ALCS and ALCS-FS, and the values of *CR* obtained are tabulated in Table 5.3.

*Table 5.3 Comparison of the data size in ALCS and ALCS-FS methods*

| Signal | ALCS | | ALCS-FS | | Percentage increase in *CR* | *MOS* |
|---|---|---|---|---|---|---|
| | Data size (kb) | CR | Data size (kb) | CR | | |
| us_11 | 269.4 | 7.60 | 241.4 | 8.48 | 11.60 | 4.00 |
| us_12 | 330 | 6.98 | 295 | 7.81 | 11.86 | 4.03 |
| us_13 | 288.5 | 7.54 | 255.7 | 8.51 | 12.83 | 3.88 |
| us_14 | 244.9 | 7.84 | 219.9 | 8.73 | 11.37 | 4.00 |
| us_15 | 303.5 | 8.43 | 271.4 | 9.43 | 11.83 | 4.06 |
| us_35 | 636.3 | 3.62 | 607 | 3.80 | 4.83 | 4.19 |
| us_36 | 499 | 5.13 | 451.2 | 5.67 | 10.59 | 4.13 |
| us_37 | 628 | 4.08 | 588 | 4.35 | 6.80 | 4.06 |
| us_39 | 663.9 | 3.86 | 628.9 | 4.07 | 5.57 | 4.06 |
| us_57 | 453.5 | 4.80 | 425 | 5.12 | 6.71 | 4.25 |

There is an increase in the value of *CR* compared to that obtained with LCS and LCS-FS methods. The maximum value of *CR* obtained with ALCS and ALCS-FS are 8.43 and 9.43 respectively. The maximum improvement in the value of *CR* with ALCS-FS over ALCS is obtained as 12.83%. The signals are again applied to ES and ES-FS methods, and the values of *CR* obtained are listed in table 5.4.

ES and ES-FS provides the maximum compression compared to other methods. The maximum value of *CR* obtained for ES is 17.07, and for ES-FS it is 19.81. The maximum increase in *CR* obtained for ES-FS compared to ES is 17.38%. It is observed that if the *SNR* is below 20dB, additional steps are needed to remove noise from the silence portion to apply the proposed method.

*Table 5.4 Comparison of the data size in ES and ES-FS methods*

| Signal | ES | | ES-FS | | Percentage increase in *CR* | *MOS* |
|---|---|---|---|---|---|---|
| | Data size (kb) | CR | Data size (kb) | CR | | |
| us_11 | 120 | 17.07 | 103.4 | 19.81 | 16.05 | 4.16 |
| us_12 | 151.8 | 15.18 | 132.5 | 17.39 | 14.57 | 4.25 |
| us_13 | 137.5 | 15.83 | 119.6 | 18.19 | 14.97 | 4.16 |
| us_14 | 130.5 | 14.71 | 116.7 | 16.45 | 11.83 | 4.28 |
| us_15 | 181.2 | 14.13 | 162 | 15.80 | 11.85 | 4.25 |
| us_35 | 296.6 | 7.77 | 276.8 | 8.32 | 7.15 | 4.31 |
| us_36 | 217.5 | 11.77 | 185.3 | 13.82 | 17.38 | 4.25 |
| us_37 | 301.1 | 8.50 | 274.7 | 9.32 | 9.61 | 4.28 |
| us_39 | 319.5 | 8.01 | 295.4 | 8.67 | 8.16 | 4.16 |
| us_57 | 211.8 | 10.27 | 192.4 | 11.31 | 10.08 | 4.28 |

Fig.5.8 shows the variations in the data size of three signals selected from Table 1 which are sampled with different methods. ALCS offers better compression compared to the conventional LCS method. But extremum sampling has less data-size compared to ALCS. But the frequency-scaling methods have better compression ratio compared to their corresponding conventional methods.

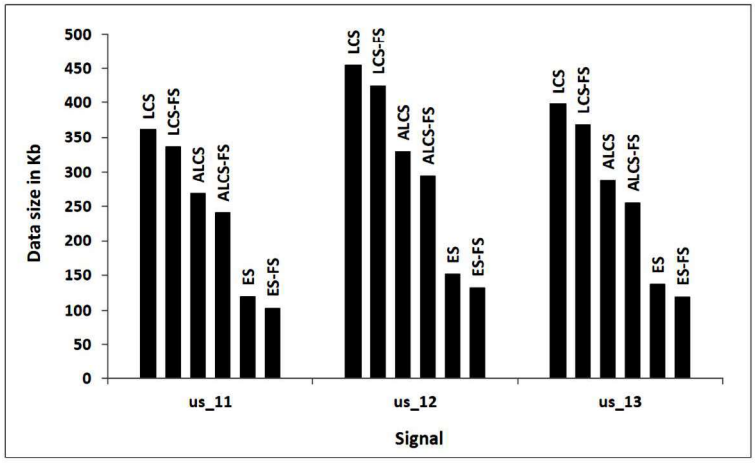


*Fig. 5.8 The comparison of data size obtained using various methods*

Taking the data size obtained with LCS as the reference, the performance of all the other methods listed in Table 5.2 to 5.4 are given in Table 5.5. The value of *CR* obtained with all the other methods are compared with the corresponding value obtained with LCS, and the percentage increase is listed in the table.

*Table 5.5 The performance of various level-crossing methods over the LCS method*

| Signal | Data size in LCS (kb) | Percentage increase in *CR* over LCS | | | | |
|---|---|---|---|---|---|---|
| | | LCS-FS | ALCS | ALCS-FS | ES | ES-FS |
| us_11 | 361.1 | 7.12 | 34.04 | 49.59 | 200.92 | 249.23 |
| us_12 | 454.3 | 6.69 | 37.67 | 54 | 199.28 | 242.87 |
| us_13 | 397.1 | 7.64 | 37.64 | 55.3 | 188.8 | 232.02 |
| us_14 | 327.5 | 6.99 | 33.73 | 48.93 | 150.96 | 180.63 |
| us_15 | 387.8 | 8.11 | 27.78 | 42.89 | 114.02 | 139.38 |
| us_35 | 963.6 | 2.85 | 51.44 | 58.75 | 224.88 | 248.12 |
| us_36 | 728.2 | 6.06 | 45.93 | 61.39 | 234.8 | 292.98 |
| us_37 | 935.2 | 3.72 | 48.92 | 59.05 | 210.59 | 240.44 |
| us_39 | 974.9 | 3.23 | 46.84 | 55.02 | 205.13 | 230.03 |
| us_57 | 667.4 | 3.94 | 47.17 | 57.04 | 215.11 | 246.88 |

The ratio, (data size in standard LCS)/ (data size in a specific method), is plotted in Fig. 5.9 for the signal “us_11”. Extremum sampling with frequency scaling, ES-FS has the highest ratio with value 3.49.

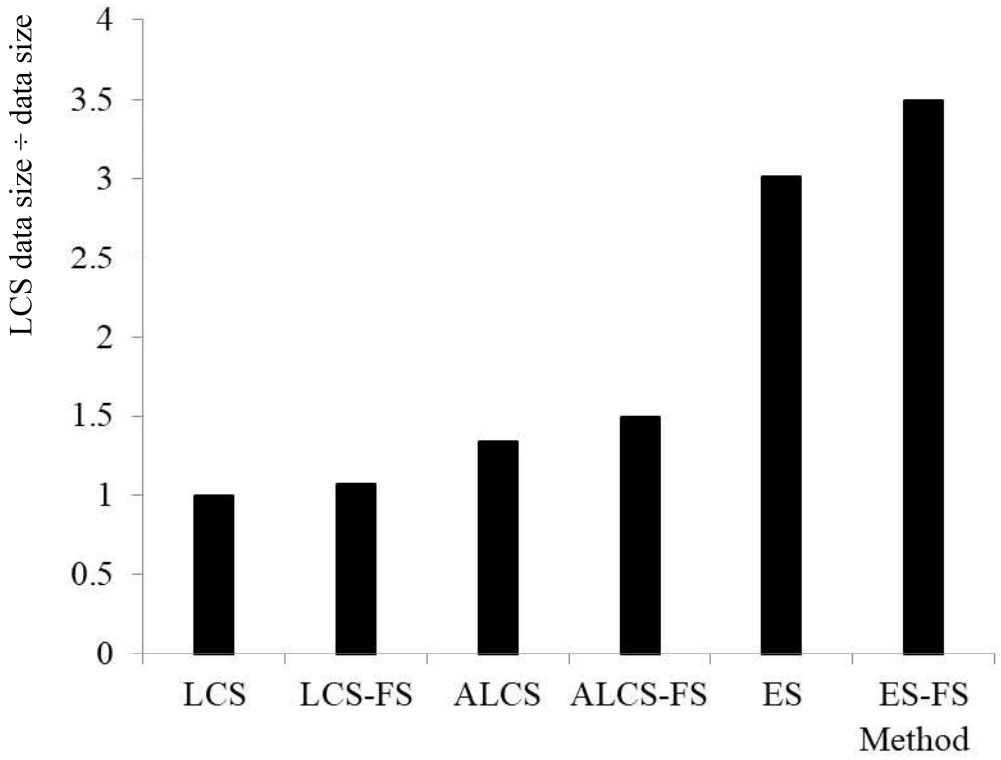


*Fig. 5.9 Comparison in terms of the ratio: data-size in standard LCS ÷ data-size in the corresponding method*

The frequency-scaled method just differs from the corresponding conventional method in the representation of the sample values, and hence none of the parameters that affect the *SNR* is altered. Hence, it is observed that there is no degradation in the quality due to the introduction of frequency-scaling.

As seen in Figs. 5.5 and 5.6(b), the occurrence of the TDC count corresponding to $Dt_{max}$ is a real-time indication of the beginning of the silence region in the voice signal. The value of $B$ must be selected, such that $Dt_{max}$ is greater than the most prolonged interval between level-crossing instants in a speech signal. The duration of the silence region is verified with the software 'praat,' and it is matching with the TDC count.

Most of the speech encoders operate on digital samples which are acquired at regular intervals based on the sampling frequency. The proposed encoding schemes are based on LCS, and hence produce a lesser number of

samples depending on the activity. Compression of the signal is achieved in the sampling process itself and evades the requirement of an additional compression algorithm. Hence the computational complexity is very less compared to the conventional compression schemes.

## 5.6 SUMMARY

The temporal resolution of LCS depends on the clock frequency of the TDC counter. Standard LCS methods have a constant resolution, even during the silence region, resulting in a higher bits/ sample value. A level-crossing sampler for speech signals, which have multiple temporal resolutions achieved by frequency-scaling of the TDC clock, is presented in this chapter. The method identifies the silence regions and then feeds a low-frequency clock to the TDC counter. Silence regions with long durations are represented with smaller words that reduce the total data size, maintaining the reconstruction accuracy. In conventional ALCS, the distance between the threshold levels is varied according to the slope of the input signal. By introducing frequency-scaling to ALCS, they also become adaptive in time, resulting in further data compression. The frequency-scaling method is also extended to extremum sampling. Several speech signals have been sampled with the conventional LCS methods and also with the frequency-scaling scheme. In all these cases, the frequency-scaled method offers a better performance compared to the conventional LCS methods in reducing the data size.

Vibration signals acquired from mechanical systems are used for fault detection and condition monitoring. A simple method for fault detection using average level-crossing rate of the signal, without storing the data samples, is discussed in the next chapter. The chapter also proposes extremum sampling as an efficient method for sampling and compressing vibration signals, without the use of any complex compression algorithm.

# CHAPTER 6

# COMPRESSION OF VIBRATION SIGNALS USING EXTREMUM SAMPLING, AND ANOMALY DETECTION IN MECHANICAL SYSTEMS

## 6.1 INTRODUCTION

Vibration signals are generally utilized for condition monitoring of the mechanical systems, including launch vehicles. Wireless sensor nodes are employed for sensing the vibrations and transmitting the data to remote locations. Vibration signals have the highest frequency among all the other sensor outputs. The analysis of these signals becomes extremely difficult due to the enormous amount of data acquired by sampling the signals at the Nyquist rate. Besides, there is a limitation of the available bandwidth in launch vehicles and wireless nodes. Wireless transmissions in sensor nodes consume a major portion of its power, and hence data compression must be done before transmission.

In this chapter, two methods for processing the vibration signals are discussed.

(a) Wherever vibration data is to be transmitted to a receiver at a remote location, extremum sampling can be used, which evades the application of a compression algorithm to all the samples acquired at the Nyquist rate.

(b) Wherever vibration data is used for the anomaly detection in mechanical systems, the variations in the average level-crossing rate of the vibration signals can be monitored, which provides a real-time indication of the faults.

Vibration signals from standard databases are subjected to extremum sampling, and the performance has been analyzed with compression ratio, mean square error, peak signal-to-noise ratio, and R-squared value. Excellent values of compression ratios have been achieved with minimum error in reconstruction. Since the method accomplishes compression during the sampling process, the additional burden at the transmitter for subjecting all the acquired samples to a compression algorithm is avoided.

The method for anomaly detection, which is based on the average level-crossing rate, works on the analog output of the sensor and does not require conventional steps like sampling, feature extraction, classification, or computation of the spectrum. It is a simple system that performs real-time detection of anomalies in the bearing of a machine using vibration signals. Faults in the machines usually create an increase in the frequency of the vibrations. The amplitude of the signal also changes in some situations. The increase in amplitude or frequency leads to a corresponding increase in the level-crossing rate, which is a parameter indicating the rate of change of a signal. Based on the percentage increase in the average value of the level-crossing rate (*ALCR*), a suitable warning signal can be issued.

The algorithm has been tested with standard data sets. There is a clear distinction between the *ALCR* values of normal and faulty machines, which has been used to release accurate indication about the fault. If the noise conditions do not vary much, the pre-processing of the input signal is not needed. The vibration signals from faulty bearings have *ALCR* values, ranging from 3.48 times to 10.71 times the average value of *ALCR* obtained with normal bearing. Hence the system offers bearing fault detection with100% accuracy.

## 6.2 COMPRESSION OF VIBRATION SIGNALS

Vibration is observed as an oscillating motion about an equilibrium point. In mechanical systems, vibrations occur due to the effects of manufacturing tolerances, and rubbing contacts between different parts. Small vibrations can trigger resonances in other mechanical parts, which cause significant vibrations. Hence, it is necessary to monitor the vibrations for the condition monitoring of mechanical systems that have rotating parts. Piezoelectric accelerometers are the universally used transducers for vibration measurement. It is robust and has a wide frequency range with excellent linearity throughout the ranges. Piezoelectric accelerometers do not require a power supply, since they are self-generating, and there is no wear and tear due to the absence of moving parts.

The staging phase of a rocket is the shutdown of one stage and the separation and ignition of the next stage [91]. During the staging phase, signals exhibit wide variations, and only a little signal compression is possible. The sampling frequency must be sufficient to capture these signals during the staging phase. However, very high compression is possible in between the staging phases due to the quiescent nature of various parameters. The use of a constant sampling frequency captures redundant data between the staging phases. Hence, an event-driven sampling method is ideally suited for this situation. Since the vibration signals have a linear variation between the peak values, the extremum sampling method, which captures samples at the local extrema of the signal, is the right choice.

Vibration signals have the highest frequency among all the other telemetry signals transmitted from a launch vehicle. Parameters like altitude, attitude, velocity, and acceleration are sampled at a much lower frequency. The sampling frequency of vibration signals selected for Indian launch vehicles is 6000 Hz with an 8-bits resolution. The data-rate for the vibration signal is

48 kbps, and there are around 10 vibration signals to be encoded, and the total bit rate required is 480 kbps. The total bit-rate available for telemetry is reported to be around 1Mbps. Other telemetry signals like pressure and temperature are sampled at 60 Hz, and velocity and acceleration signals at 120 Hz approximately, which is very less compared to the sampling frequency used for vibration signals. Hence, there is a necessity for compressing the vibration signals to reduce the total bit-rate. In industries, vibration data has to be sent to remote servers for processing. Reducing the amount of data and hence the transmission bandwidth is a significant requirement.

The Consultative Committee for Space Data Systems (CCSDS) has recommended standards [92] for lossless data compression applications of space missions with packetized telemetry. The encoder consists of a pre-processor followed by an adaptive entropy encoder. At the pre-processor stage, a reversible function is applied to the input samples to reduce the entropy, which results in the reduction of the average number of bits in the representation. The adaptive entropy coder provides a set of coding options based on the redundancy in the block of data, which is the output from the pre-processor. Rice's adaptive coding technique is used, which produces variable-length codes. The samples are encoded with fundamental sequence codes, which consist of words with a number of '0's followed by a '1' at the end. Sequences of '0's are further compressed with run-length coding.

Vibration signals received from the launch vehicles are generally used for condition monitoring. In this chapter, extremum sampling has been proposed for encoding vibration signals which produce compressed set of samples in real-time. As explained in section 4.6, in extremum sampling, the local maxima and minima of signals are acquired along with the time gap between the peaks. With this information, a vibration signal, which is having an oscillatory nature, can be reconstructed. It is a non-uniform sampling method achieving compression during the sampling process itself. Being an activity-dependent sampling method,

the number of samples is proportional to the frequency content present in the signal. A significant reduction in the data size has been achieved, and the reconstructed signal preserves the essential features of the original signal. The advantages of the proposed method are a reduction in the dynamic power dissipation, transmission bandwidth, and storage requirement.

### 6.2.1 Extremum sampling of vibration signals-Performance measures

As an alternative to the conventional methods in which a compression process follows the uniform sampling, extremum sampling is applied to vibration signals to produce a compressed set of samples. The parameters that measure the effectiveness of compression of the signal are, mean square error (*MSE*), peak signal-to-noise ratio (*PSNR*), R-squared value ($R^2$), and the compression ratio (*CR*). *MSE*, *PSNR*, and $R^2$ evaluate the distortions caused by the sampling process. *CR* measures the performance of size-reduction defined in Eqn. 6.1.

$$CR = \frac{Original\ data\ size}{Compressed\ data\ size} \tag{6.1}$$

Let $y_i$ be the $i^{th}$ value of the reconstructed signal and $x_i$ the value of the input at the same instant. *MSE* measures the average of the squares of the error between the input and the reconstructed signal. The reconstruction is better if the value of *MSE* is closer to zero. For a group of n samples, *MSE* is defined as shown in Eqn. 6.2.

$$MSE = \frac{1}{n}\sum_{i=1}^{n}\left(x_i - y_i\right)^2 \tag{6.2}$$

PSNR compares the maximum level of the signal power to the level of the noise power, noise being the difference between the original and reconstructed signals. PSNR is expressed in Eqn. 6.3. $x_{max}$ is the maximum amplitude of the input signal.

$$PSNR_{\mathrm{dB}}=10\log_{10}\frac{(x_{max})^2}{\frac{1}{\mathrm{n}}\sum_{i=1}^{n}(x_i-y_i)^2} \tag{6.3}$$

R-squared $(R^2)$ is a statistical measure having a value between 0 and 1, representing the proportion of the variance between the variables. $R^2$ with a value closer to 1 indicates that the reconstructed signal has a close similarity to the input signal. $R^2$is computed as

$$R^2 = 1-\frac{\sum_{\mathrm{i}=1}^{\mathrm{n}}(x_i-y_i)^2}{\sum_{\mathrm{i}=1}^{\mathrm{n}}(x_i-\bar{x})^2} \tag{6.4}$$

$\bar{x}$ is the mean of the input signal.

### 6.2.2 Simulation results

Bearing vibration-data from the data set provided by Case Western Reserve University [93] is used for the simulation. It is available as uniform samples with a sampling rate of 12000 per second. These samples are interpolated to convert them into the analog form, and extremum sampling is performed on selected input signals. Simulation is done with Matlab/ Simulink.

As an illustration, a short duration of the vibration signal 'X097_DE', which is subjected to extremum sampling, and the corresponding reconstructed outputs are shown in Fig. 6.1. The input signal and the reconstructed output are shown with dotted and bold lines, respectively.

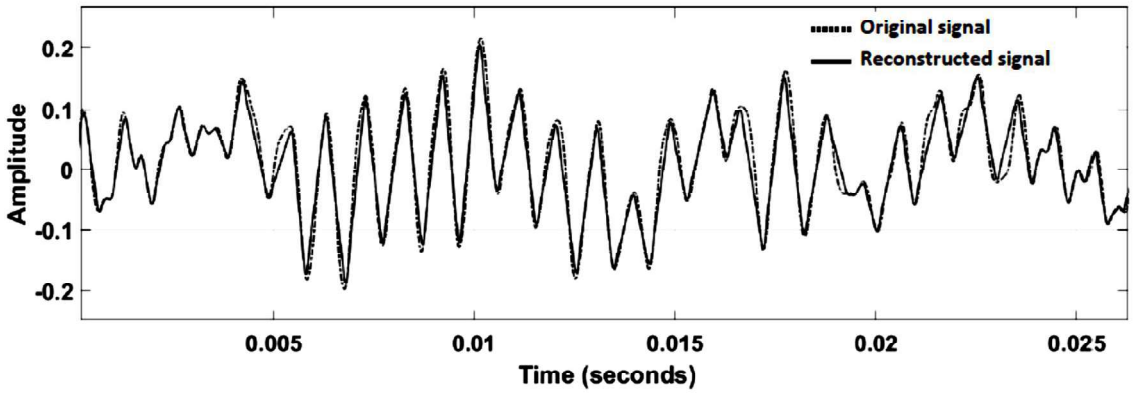


*Fig. 6.1 Input vibration signal and the reconstructed output*

Details of input signals which are subjected to extremum sampling, and the corresponding values of *CR*, *MSE*, *PSNR*, and $R^2$ are listed in Table 6.1. It is observed from the table that the signals have been reproduced with minimal error. High values of compression ratios have been achieved with an excellent correlation between the input and output signals. The inter-level distance $\Delta v$ is selected as 5 mv, and the frequency of the timer counter $f_c$ is 100 kHz.

*Table 6.1* *Compression ratio (CR), Mean square error (MSE), Peak signal-to-noise ratio (PSNR) and $R^2$ value of vibration signals*

| Signal | CR | MSE | PSNR | $R^2$ value |
|---|---|---|---|---|
| X097_DE | 4.8979 | $7.2511 \times 10^{-4}$ | 31.3960 | 0.8975 |
| X097_FE | 4.7291 | $9.0239 \times 10^{-4}$ | 30.4461 | 0.9176 |
| X098_DE | 3.7065 | $5.6830 \times 10^{-4}$ | 32.4542 | 0.8667 |
| X098_FE | 3.2653 | $2.7450 \times 10^{-4}$ | 35.6135 | 0.9225 |
| X099_DE | 3.4285 | $2.0814 \times 10^{-4}$ | 36.8164 | 0.9376 |
| X099_FE | 3.5165 | $5.0327 \times 10^{-4}$ | 32.9820 | 0.9105 |
| X100_DE | 3.1894 | $1.8088 \times 10^{-4}$ | 37.4262 | 0.9548 |
| X100_FE | 3.6090 | $4.2044 \times 10^{-4}$ | 33.7629 | 0.9106 |
| X106_BA | 3.7860 | 0.0011 | 29.6950 | 0.8712 |
| X121_BA | 3.5165 | 3.8623x10-$^4$ | 34.1315 | 0.8628 |

As discussed in section 4.3, the signal-to-noise ratio of a standard level-crossing sampler is dependent only on the frequency of the clock used. In extremum sampling, the local peak is detected by a change in the direction of the slope at the level-crossing instant. Hence, extremum sampling suffers an error in the amplitude also. The variation of *CR* and $R^2$ values attained for the signal 'X097_DE' with respect to $\Delta v$ are plotted in Fig. 6.2. Even though CR increases with $\Delta v$, as shown in Fig. 6.2(a), the error in amplitude values also has a proportional increase, which is reflected in the $R^2$ values, and is shown in Fig. 6.2(b).

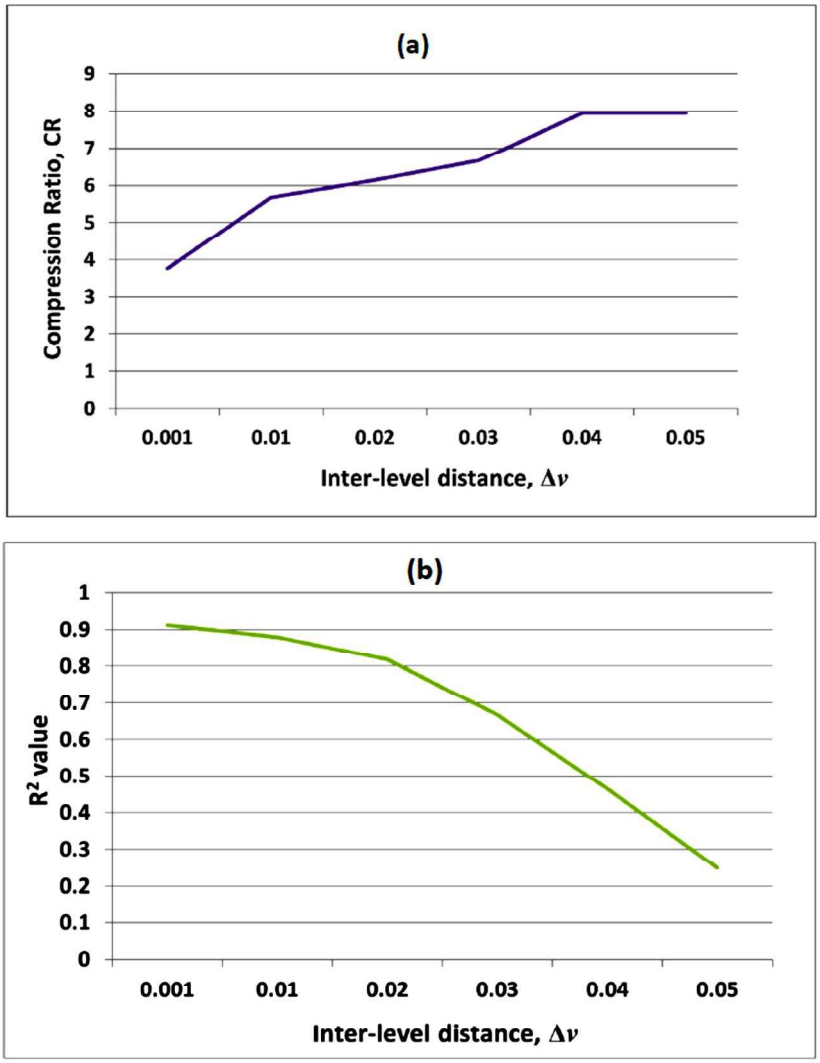


*Fig. 6.2 (a) Compression ratio (CR) versus Δv*
*(b) $R^2$ value versus Δv*

The reproduced signals exhibit great similarity with the input signals. As an example, a vibration signal 'X097_DE' and its spectrum are shown in Fig. 6.3(a) and Fig. 6.3(b), respectively. The reconstructed outputs in the time domain and spectral domain are shown in Fig. 6.3(c) and Fig. 6.3(d), respectively. All the peak values in the time domain and all the significant frequency components in the input are preserved.

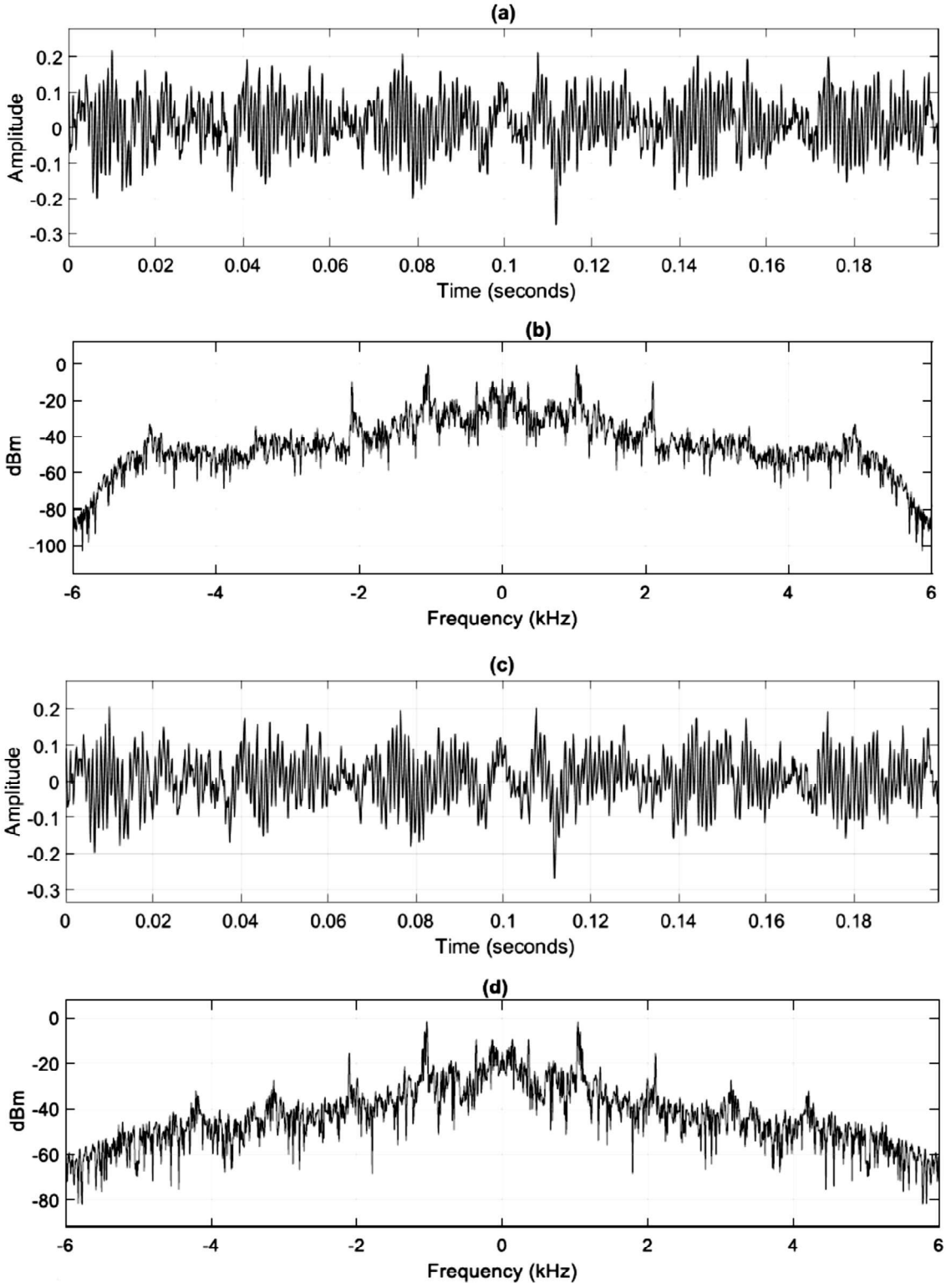


*Fig. 6.3 (a) Input signal (b) Spectrum of the input signal (c) Output signal (d) Spectrum of the output signal*

Vibration signals acquired with normal and faulty bearings are available in the database. On analysis, it is observed that the signals from faulty bearings

have higher values of $P_n$ and lower values of $Dt_n$. The compression ratio achieved for a signal from a faulty bearing is slightly less than that with a normal one, but it maintains the reconstruction accuracy. The reconstruction accuracy is proportional to $f_c$, and inversely proportional to $\Delta v$.

## 6.3 ANOMALY DETECTION IN MECHANICAL SYSTEMS USING VIBRATION SIGNALS

Most of the engineering systems have rotating parts, and various parameters must be closely monitored for maintaining their health. The situation is very critical in systems such as aircraft and spacecraft in which failure may cause loss of lives or a tremendous amount of money invested [57]. The faults in machines used in industries must be detected long before they become severe so that planned repair work can be scheduled. Most of the faults like imbalance, resonance, misalignment, looseness, drive belt problems, and eccentricity occurring in machines cause some changes in the vibration signals. Hence vibration analysis serves as a means for identifying machine deterioration. Further damage and its severe effects can be avoided if preventive maintenance is carried out soon after a warning signal is received.

Fault diagnosis and prognosis are mainly dependent on sensors and their sensing strategies. A wide variety of sensors are used for condition monitoring of equipment nowadays. The data output from the sensors must be processed for extracting useful information. The processed data must be in the reduced form, preserving the features which are needed for detecting the anomalies.

All the present methods for anomaly detection involve either sophisticated analysis methods or require processing on a massive amount of data collected for this purpose. As discussed in section 6.2, the available bit rate in launch vehicles is very much limited. Several vibration signals are to be telemetered to the ground, which requires a very high data rate. The number of vibration signals transmitted to the ground can be reduced to a minimum if on-

board anomaly detection is used, and its output alone needs to be transmitted to earth instead of sending the whole sensor data.

A simple signal processing method that provides real-time indications of anomalies in bearings is presented in this section. It is based on the changes in the average level-crossing rate of the vibration signals. It is also free from the steps involved in conventional fault detection methods, including sampling, compression, feature extraction, and classification. The system is free from the complex analysis procedures or the big data analysis problem in traditional methods.

### 6.3.1 Average level crossing rate (*ALCR*)

A change in the instantaneous value of a vibration signal cannot be used for detecting the faulty condition of a machine. Hence a parameter which is estimated over a short time interval must be selected for this purpose. If there is a faulty condition in the bearing of a machine, there is an increase in the frequency of the vibration signal. In most of the cases, there is also an increase in the amplitude. Irrespective of the peak value, the average amplitude of a vibration signal is nearly zero, and cannot be used as a parameter for detecting anomalies. Similarly, the energy of a signal cannot be considered for this purpose because it may not change with respect to a change in frequency. Average Level-Crossing Rate (*ALCR*) of a signal is the best choice for detecting the variations in the vibration signal due to a faulty condition in a machine. The level-crossing rate (*LCR*) is a measure of the rapidity of a signal. *LCR* is defined as the number of times a signal crosses a certain amplitude level in unit time [94]. *ALCR* is obtained by summing up the *LCR* values of all the levels in unit time. It is a time-domain parameter that increases with an increase in either the amplitude or frequency of a signal, which is illustrated in Fig. 6.4.

The computation of *ALCR* value has been explained in [94]. Let $x(t)$ be the analog input signal for which *ALCR* has to be computed. A level crossing,

$c(j, t_0)$ at a particular level $l_j$ is detected at time $t_0$, if $(x(t_0)\text{-}l_j)(x(t_0\text{-}\delta t)\text{-}l_j)<0$; where $\delta t$ is a short time interval. If the above condition is satisfied, $c(j, t_0) = 1$, and it is 0 otherwise. Level-crossing rate (LCR), $L(j, t_0)$ can be computed at a particular instant $t_0$ for an interval $\Delta t$ as shown in Eqn. 6.5.

$$L(j,t_0) = \sum_{t_0-\Delta t}^{t_0} c(j,t_0) \tag{6.5}$$

The average level-crossing rate, *ALCR*, is defined in Eqn. 6.6, where $N$ is the total number of reference levels.

$$ALCR = \sum_{j=1}^{N} L(j,t_0) \tag{6.6}$$

The value of *ALCR* depends on $\Delta v$, the inter-level distance, and $\Delta t$, the duration for which it is computed.

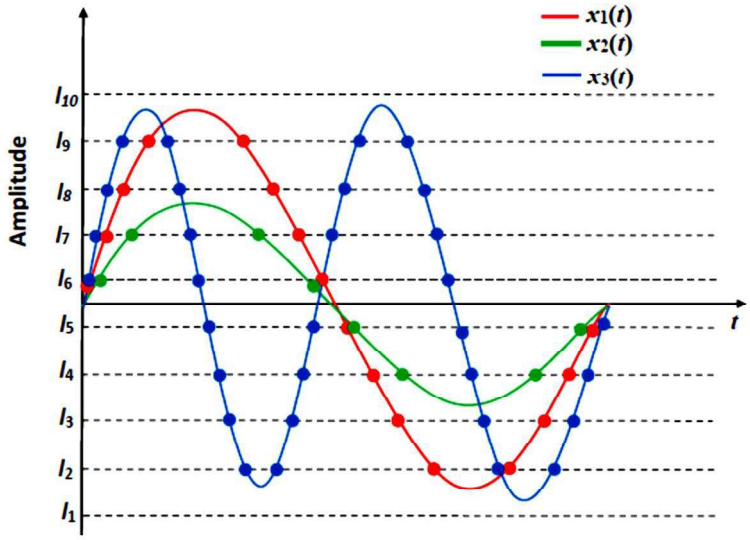


*Fig. 6.4 Number of level-crossings*

Three sinusoidal signals $x_1(t)$, $x_2(t)$, and $x_3(t)$ of equal durations are shown in Fig. 6.4. Denoting the number of level-crossings occurring in a duration '$t$' as '$N_t$', its value for $x_1(t)$ is 16. The frequency of the signal $x_2(t)$ is equal to that of $x_1(t)$, but its peak value is almost half of $x_1(t)$. The value of $N_t$ for $x_2(t)$ is eight. The peak amplitude of $x_3(t)$ is almost equal to that of $x_1(t)$, but the

frequency is almost double. The value of $N_t$ for $x_3(t)$ is 32, which is double that of $x_1(t)$. If a fault condition occurs in a machine, there will be an increase in frequency and amplitude of the vibration signal, which causes a corresponding increase in the value of *ALCR*. *ALCR* has been used in [94] for automatic speech segmentation.

As shown in Fig.6.5(a), an arbitrary analog signal $x(t)$, is applied to a level-crossing detector (LCD). The reference voltage levels $l_1$ to $l_6$ are placed uniformly at $\Delta v$ apart. The instantaneous amplitude of the signal $x(t)$ is compared with these levels. The dark dots on $x(t)$ indicate the instants at which level-crossings take place. These instants are marked as $t_1$ to $t_{13}$ on the time axis. The signal crosses the level $l_2$ at time instant $t_1$. The corresponding output of the level-crossing detector (LCD) is shown in Fig. 6.5(b). *LCR* is dependent on the value of $\Delta v$, the signal amplitude $A$, and the frequency of the signal.

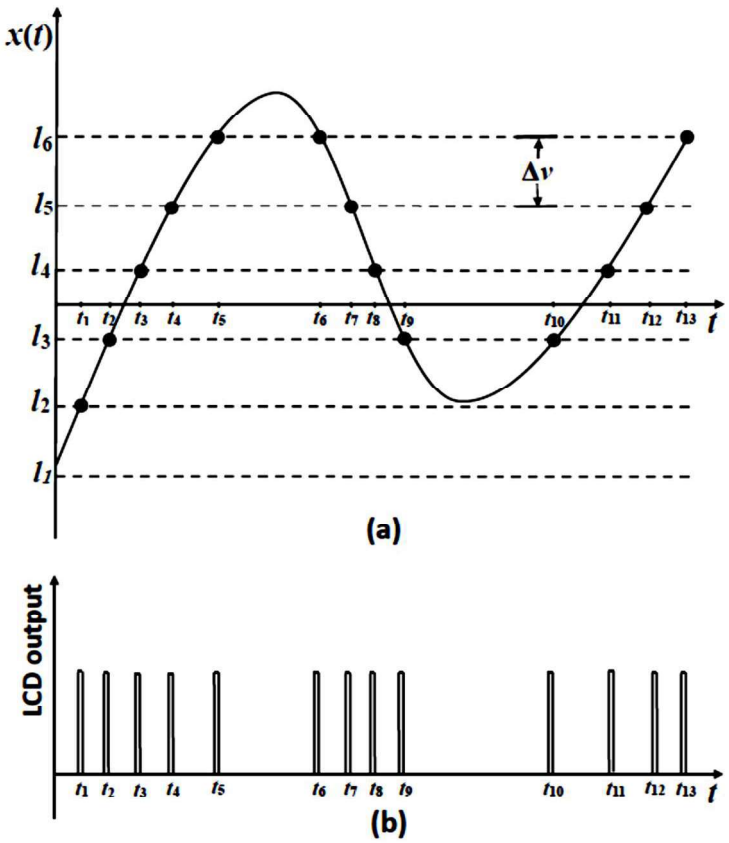


*Fig. 6.5(a) Input signal (b) LCD output*

The *ALCR* of a signal can be monitored by comparing the instantaneous value of the signal with a set of reference levels. LCD output is fed to a counter which counts the number of level-crossings in a particular duration, $\Delta t$ for which *ALCR* is computed. For this purpose, a timer, which resets the counter at the end of every $\Delta t$ is used.

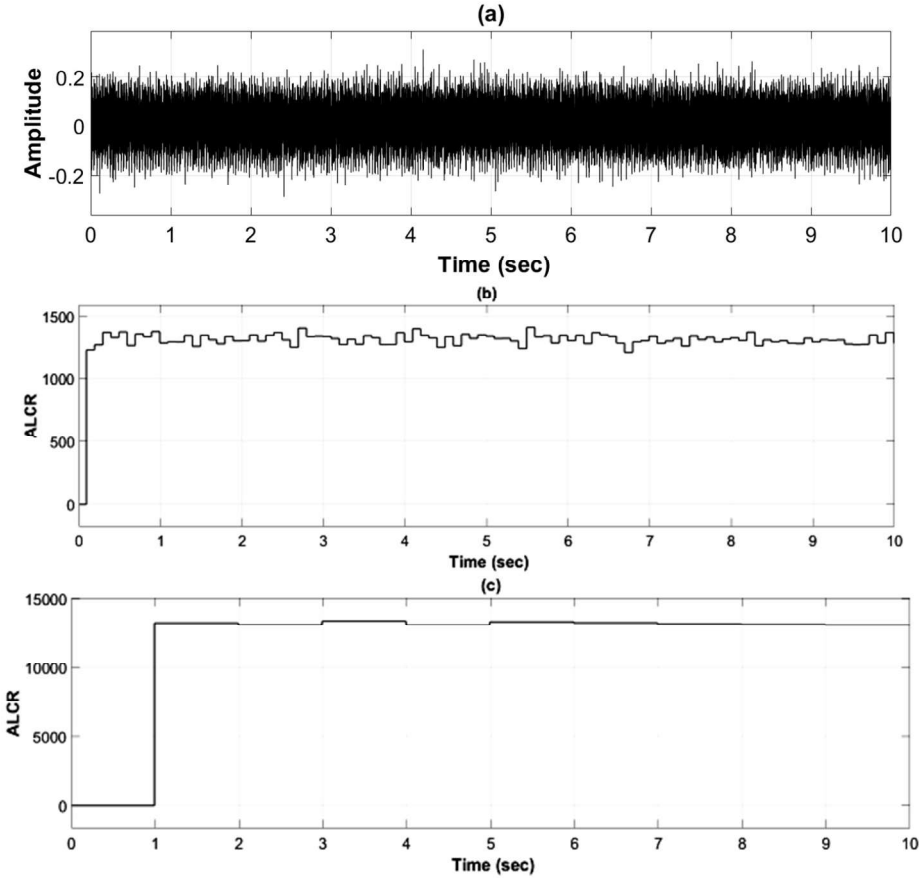


*Fig. 6.6 (a) Vibration signal (X097_DE) (b) ALCR with $\Delta t$= 0.1 second (c) ALCR with $\Delta t$= 1 second*

The data set provided by the Case Western Reserve University is the output from accelerometers which are attached to the housing of the motor using magnetic bases. Vibration data is also collected after introducing faults in the bearings with the electro-discharge machining technique. A vibration signal, 'X097_DE', is shown in Fig. 6.6(a), and its *ALCR* in Fig. 6.6(b), and Fig. 6.6(c). In Fig. 6.6(b), *ALCR* values are computed, taking $\Delta t$ as 0.1 seconds, and in Fig. 6.6(c), it is taken as one second. Even though *ALCR* computed with $\Delta t$ of one

second shows a smooth variation in *ALCR*, the maximum delay for delivering the warning signal is one second compared to 0.1 seconds in the earlier case. If a signal is applied to the LCD, the value of *ALCR* will be computed at the end of every $\Delta t$ seconds. Hence, in Fig. 6.6 (b) and Fig. 6.6 (c), *ALCR* is seen to be zero during the initial time period of $\Delta t$.

### 6.3.2 Anomaly detection using *ALCR*

A vibration signal, 'X100_FE' acquired from a normal bearing, and its spectrum are shown in Fig. 6.7(a), and Fig. 6.7(b), respectively. The significant frequency components in the spectrum extend approximately up to 2 kHz. *ALCR* values of this signal are computed and are shown in Fig. 6.7 (c). The average value of *ALCR* is 1500. Fig. 6.7(d) shows another signal, 'X106_FE', acquired from the same machine with a faulty bearing. The spectrum of this signal is shown in Fig. 6.7(e) in which the significant frequency components are seen to be extended above 4kHz. There is also an increase in the maximum amplitude of the signal acquired from the faulty machine. The corresponding *ALCR* is plotted in Fig. 6.7(f). There is a huge increase in the *ALCR* values of this signal compared to the previous case and is computed as 8391.

All the vibration signals collected from the machine, which is having a faulty bearing, is spread in its bandwidth with some increase in the peak amplitude. This is illustrated in Fig. 6.7, where a significant increase in the *ALCR* value of a vibration signal, collected from a faulty bearing, is compared to that from a normal bearing. Variations in *ALCR* values are used for the detection of faults. Fig. 6.8 depicts the method of detection of anomalies in the machine using *ALCR* values.

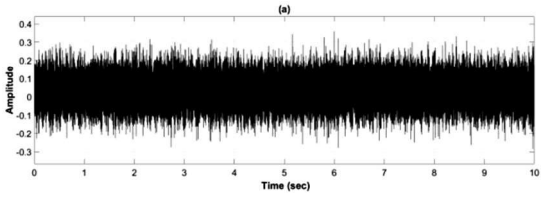


*(a) The vibration signal from a normal bearing (X100_FE)*

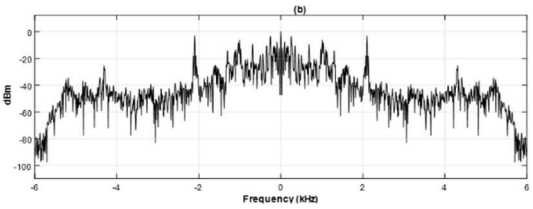


*(b) Spectrum of X100_FE*

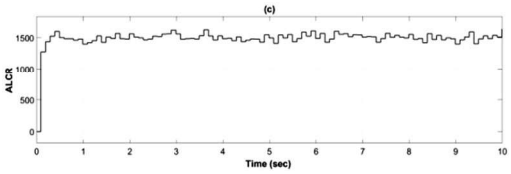


*(c) ALCR of X100_FE*

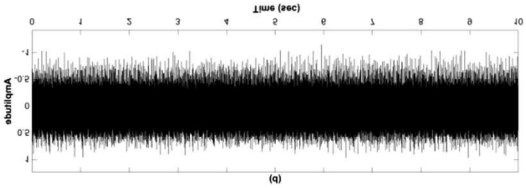

*(d) The vibration signal from a faulty bearing (X106_FE)*

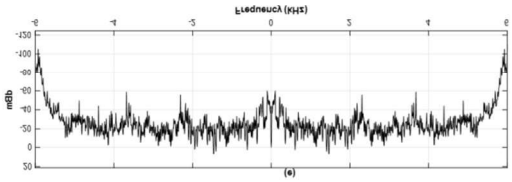

*(e) Spectrum of X106_FE*

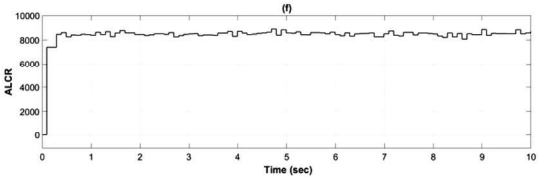


*(f) ALCR of X106_FE*

*Fig.6.7 Illustration of Variation in ALCR Values of Vibration Signals from Normal and Faulty Bearings*

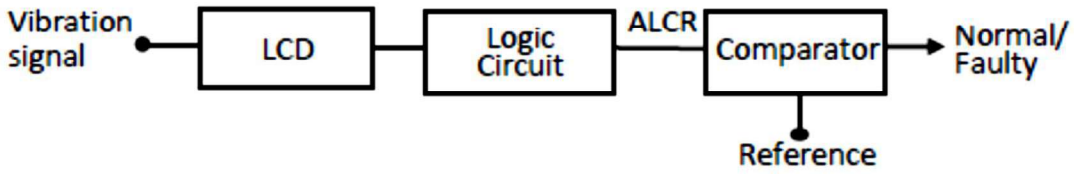


*Fig. 6.8 The block diagram for the anomaly detection using ALCR values*

The input signal is applied to the LCD, which produces non-uniformly spaced pulse signals at the instant of each level-crossing. The logic circuit counts the number of pulses produced in a fixed duration, which is the value of *ALCR*. A threshold value of *ALCR* can be manually set with a prior knowledge of the vibrations produced under normal working conditions. Alternatively, the initial

*ALCR* value can be stored as a reference for detecting a specified percentage increase in the observed value.

### 6.3.3 Simulation Results

The vibration data from standard databases, which are samples acquired at the Nyquist rate, are interpolated to convert them into the analog form. These analog signals are analyzed by observing the variations in their *ALCR* values, as shown in Fig. 6.8. Simulation has been performed with Simulink. The bandwidth of the signals collected with faulty bearing has increased, and a small increase in the amplitude is observed in some signals.

*Table 6.2 Vibration signals and their ALCR values*

| Signal | Normal/ faulty | *ALCR* value |
|---|---|---|
| X097_DE | Normal | 1308 |
| X098_FE | Normal | 1302 |
| X098_DE | Normal | 1157 |
| X099_DE | Normal | 1265 |
| X099_FE | Normal | 1366 |
| X100_DE | Normal | 1345 |
| X100_FE | Normal | 1500 |
| X105_DE | Faulty | 12200 |
| X105_FE | Faulty | 9296 |
| X106_DE | Faulty | 12160 |
| X106_FE | Faulty | 8391 |
| X108_DE | Faulty | 12890 |
| X119_DE | Faulty | 7340 |
| X121_DE | Faulty | 8006 |
| X130_FE | Faulty | 14140 |
| X133_DE | Faulty | 13240 |
| X169_FE | Faulty | 5960 |
| X172_DE | Faulty | 6353 |
| X185_DE | Faulty | 5648 |
| X200_DE | Faulty | 4595 |

A significant increase in *ALCR* values has been noticed in the signals collected from the faulty machines, compared to the values corresponding to a normal machine. The inter-level distance $\Delta v$ is selected as 25mv, and *ALCR* is computed as the total number of level-crossings during a period of 0.1 seconds.

The simulation results are shown in Table 6.2. The first column indicates the signal, and the second one indicating whether the signal was acquired under the normal or faulty conditions. The corresponding *ALCR* values are entered in the third column. The abbreviations DE and FE, along with the signal number, represent "Door End and Fan End," which are the positions of the sensors. *ALCR* values of each signal are also plotted in Fig. 6.9. The increase in *ALCR* values is used for anomaly detection in the proposed method. Besides offering a real-time operation, the system avoids the necessity of sampling the signal, storing the data, feature extraction, classification, and big data analysis.

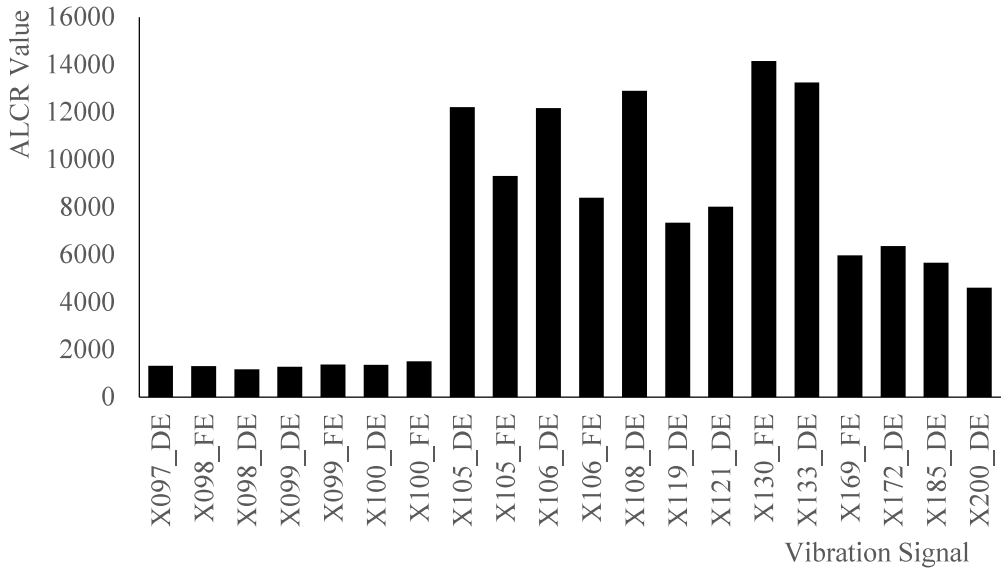


*Fig. 6.9 The plot of ALCR vs signals*

The algorithm has also been tested with NASA bearing data set [95]. The data set includes three sets of vibration data, which are the output of accelerometers placed at different locations inside the bearing housing of an AC

motor. The rotation speed of the motor was 2000 rpm, with a radial load of 6000 lbs. Each data set was the output of a test-to-failure experiment and consists of data acquired under failure conditions. It was reported that the inner race defect occurred in bearing 3 at the end of the experiment, which is shown in Fig. 6.10(a). Vibration signals of channel 5 from bearing 3 acquired during the last 45 seconds of the test are shown in Fig.6.10(a). At around 13 seconds, there is a gradual change in the amplitude and spectrum, and another sudden hike occurs at around 42 seconds. The corresponding values of *ALCR* are plotted in Fig. 6.10(b). It can be noticed that there is a significant change in the *ALCR* values at 13 and 42 seconds.

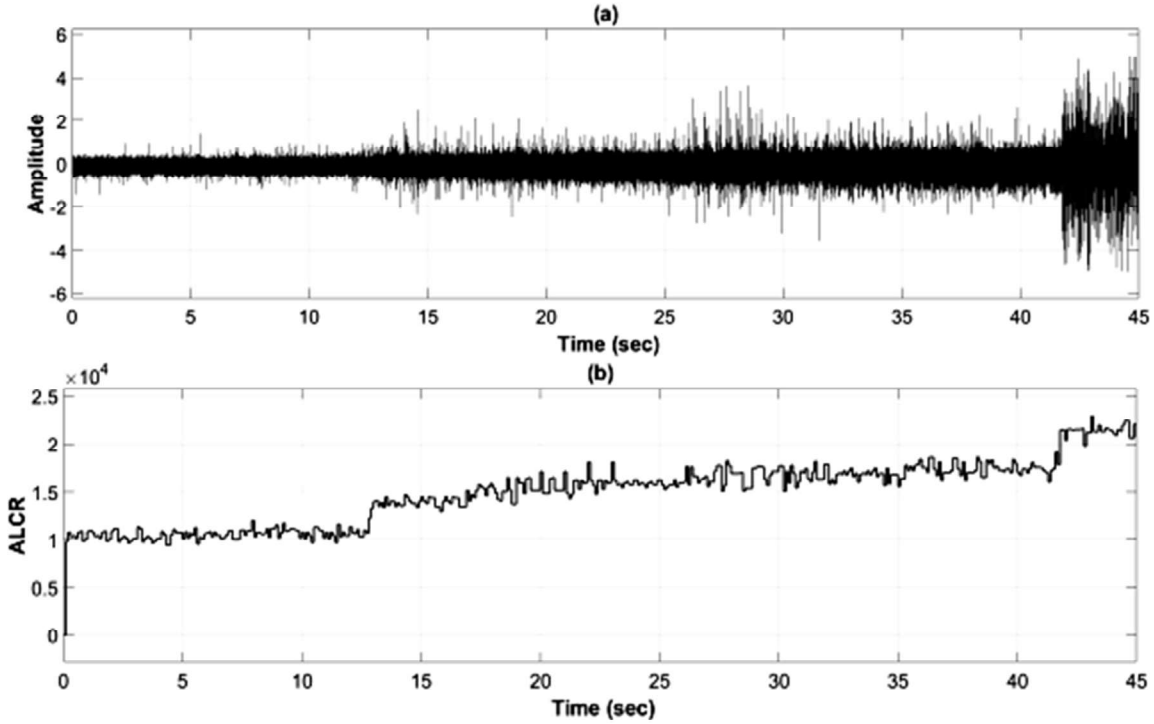


*Fig. 6.10 (a) NASA signal (bearing 3, channel 5) (b) ALCR of NASA signal*

The output from channel 6 of the same bearing is shown in Fig. 6.11(a), and the corresponding *ALCR* values are plotted in Fig. 6.11(b). Similar to the *ALCR* values obtained for channel 5, sudden increase in the value of *ALCR* is observed at 13$^{th}$ and 42$^{nd}$ seconds for channel 6 also. An increase in the *ALCR* values is the indication for the faults that occurred at the instants explained above.

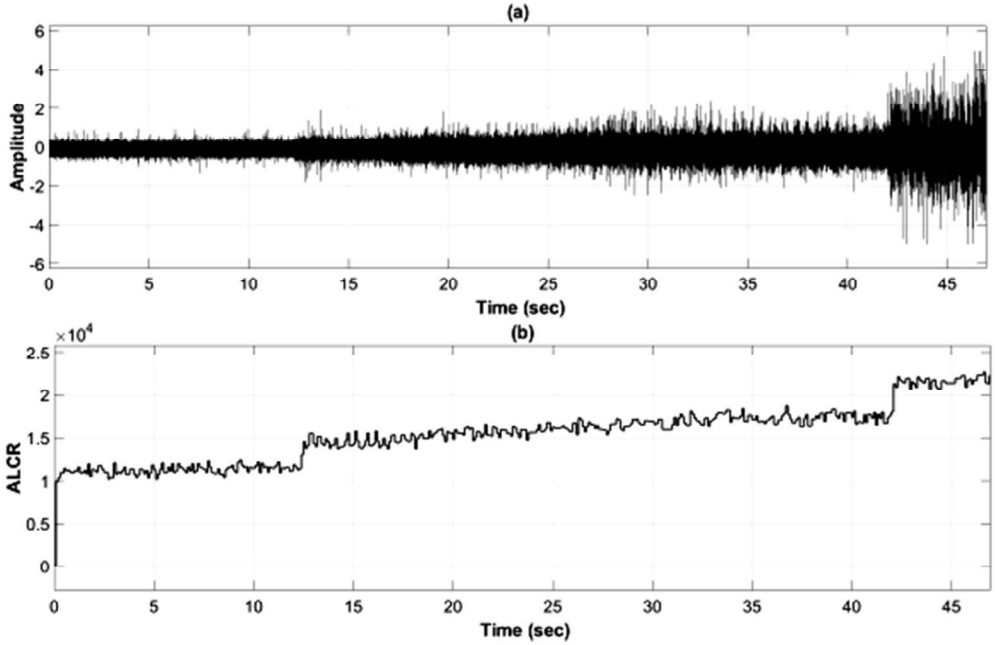


*Fig. 6.11 (a) NASA signal (bearing 3, channel 6) (b) ALCR of the signal*

## 6.4 SUMMARY

Conventional compression algorithms and CS-based methods adopt complex procedures for the compressed encoding of the vibration data. Compressed-sensing demands iterative optimization algorithms to be executed for the reconstruction of the original signal. But extremum sampling produces compressed set of data directly from the analog input signal enabling real-time encoding and reconstruction. In this chapter, extremum sampling has been proposed for vibration signals as an alternative to conventional sampling methods and CS-based methods. Samples at the local extrema of the input signal are acquired, which are sufficient for the reproduction of vibration signals. Even though the proposed method falls in the category of lossy compression, the peak values of the input and the time gap between them are retained in the reconstructed output. The method offers high compression ratios with minimal error with less computational complexity. The proposed method is suitable for telemetry systems in launch vehicles and other wireless sensor networks. Even if the samples are non-uniformly spaced, the number of bits per sample remains the

same, which enables easy multiplexing. The compression ratio achieved with any of the level-crossing methods is the benefit gained from a non-uniform sampling method, and the possibility of achieving further compression from these samples needs to be explored.

A signal processing method based on *ALCR* is also proposed for detecting bearing faults in machines. ALCR-based method is the low-cost alternative to the conventional condition-monitoring systems. Bearing faults in machines cause observable changes in the *ALCR* values of vibration signals. By monitoring the variations in the *ALCR*, anomalies in machines can be detected very easily. It is capable of delivering real-time indications about the operating conditions of a machine. It is especially suitable for systems where computational requirements and big data analysis cannot be afforded. The bit-rate requirement in launch vehicle telemetry can be reduced to a minimum if on-board anomaly detection mechanism is used, which works directly on the sensor output. Instead of transmitting the entire vibration data from a spacecraft, a few numbers of *ALCR* values are sufficient for fault analysis. The analog sensor output can be directly applied to the LCD for *ALCR* measurement, and it provides a real-time indication of faults in the machine. *ALCR* can be used as a parameter for predicting the remaining useful life, which requires a massive amount of vibration data otherwise. The same task can be achieved by making use of *ALCR* values, which are very few in number compared to the number of samples in the vibration data. Further study is required to find the effect of noise under varying noise conditions.

*ALCR* can be used for the activity detection in any signal. As pointed out in section 6.3.2, it was used for automatic speech segmentation in [94]. In the next chapter, *ALCR* has been used to automatically control the gain of an amplifier, based on the activity in a voice signal. Another application of *ALCR* explained in the next chapter is acoustic feedback detection in public address systems.

# CHAPTER 7

# ACTIVITY-DETECTION BASED ON LEVEL-CROSSING RATE

## 7.1 INTRODUCTION

Temporal features are more reliable to analyze the signal-variations because they retain both the magnitude and phase information. As discussed in section 6.3.2, *ALCR* is a time-domain parameter sensitive to changes in both the amplitude and frequency of the signal. *ALCR* has been applied for anomaly detection of mechanical systems in chapter 6 and has various applications like detection of channel fading and speech segmentation. In this chapter, *ALCR* is applied for detecting the activity of signals, based on which specific control action can be triggered. *ALCR* is used for the activity-detection of signals in the following applications.

(a) A voice-controlled audio mixer is implemented, in which the activity of the input speech signal is monitored with its *ALCR* values. Based on the *ALCR*, the attenuation of a background music signal is controlled. Such voice-controlled audio mixers have broad applications in announcement systems at radio and TV broadcasting stations and announcement systems.

(b) An acoustic feedback suppressor in which the feedback detection is done with *ALCR*, and the feedback frequency estimation is made with zero-crossing time. The feedback suppression is demonstrated with notch and low-pass filters.

In a voice-controlled mixer, the amplitude of the background music is controlled by the intensity of a speech signal. The intensity of the speech signal is monitored with *ALCR*. A two-level mixer is implemented such that the amplitude

of the music signal is reduced to one-fourth its actual amplitude, if a speech signal is detected. In the acoustic feedback suppression system, howling is detected with the *ALCR* of the output signal. The acoustic feedback was created with a single microphone, an amplifier, and a loudspeaker. Howling signals with and without the presence of speech were recorded. Acoustic feedback is detected using the variations in the *ALCR* values. Based on the zero-crossing time, a corresponding path is selected with notch filters, designed for the fundamental and second harmonic frequencies of the howling signal. The notch filters in each path are cascaded by a low-pass filter to remove the frequency components outside the speech-band. This study aims to illustrate the potential of *ALCR* for activity detection by emphasizing the howling-detection part rather than its suppression.

## 7.2 VOICE-CONTROLLED MIXER

There is a standard requirement in any announcement system to adjust the volume of music, which is presently being played in the background, while an announcement is made using a voice signal. Earlier, this was done by manually adjusting the volume of the background signal. However, the manual method has the drawback that the level of attenuation is highly subjective. Automatic voice-controlled amplifiers have been developed in the announcement systems to tackle this problem, the general block diagram of which is shown in Fig. 7.1.

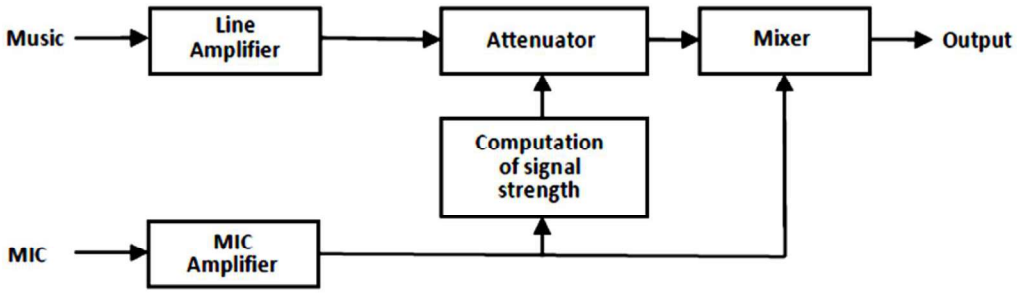


*Fig. 7.1 General block diagram of a voice-controlled audio mixer*

A recorded music signal is fed to a line amplifier, and its output is connected to an attenuator. The attenuation is controlled by the intensity of a voice signal, which is the output from a MIC amplifier. The attenuated music and the voice signal are added in a mixer amplifier, and the output is broadcasted.

There are various methods for sensing the intensity of the voice signal which is used to control the background signal. Attenuation is varied according to the average value of the voice signal, using a circuit similar to an envelope detector in [96]. A capacitor maintains a voltage that is proportional to the new peak value of the signal. Another method makes use of short-term energy (STE) and zero-crossing rate (ZCR) for detecting the voice activity [76]. ZCR is used to check whether the input signal is a voice signal or not. Based on the energy of the voice signal, the attenuation of the background music is varied.

### 7.2.1 Voice-controlled mixer based on *ALCR*

In the method explained in this thesis, *ALCR* is used to detect the activity of the speech signal, which evades the step of computing the short-term energy. *ALCR* has been defined in section 6.3.2. The *ALCR* values for the speech signal are computed for every $\Delta t$ seconds, and the attenuation is increased if the *ALCR* increases above a threshold value. The noise input with peak-to-peak amplitude less than the inter-level distance $\Delta v$ does not create a level-crossing. Hence the *ALCR* value is not affected by the noise.

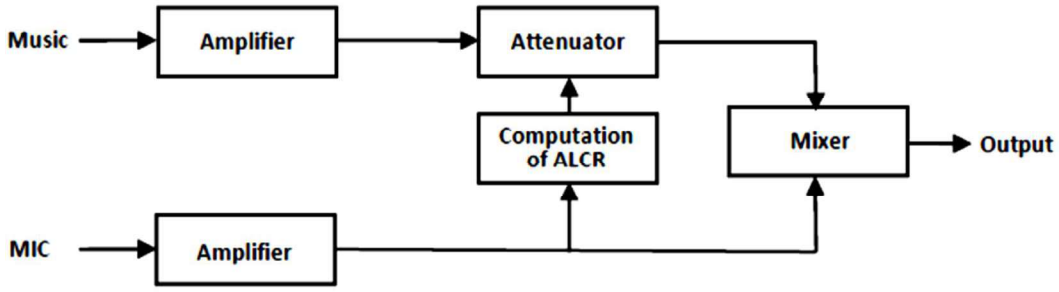


*Fig. 7.2 Block diagram of a voice-controlled audio mixer based on ALCR values*

### 7.2.2 Simulation results

The noise tolerance of level-crossing sampling has been explained in section 4.7. The voice-activated mixer does not respond to the noise present at the microphone input if the peak-to-peak amplitude is within $\Delta v$. The noise tolerance is illustrated in Fig. 7.3, in which the speech signal is in the magnified form, and the number of level-crossings between $\Delta t$ are shown. At the beginning portion there is no speech signal present, except the noise whose amplitude variations are within $\Delta v$. Hence there is no level-crossing taking place during this time. Since the *ALCR* is computed for a specific duration of $\Delta t$, the system does not react to the undesired input variations in the form of impulse noise.

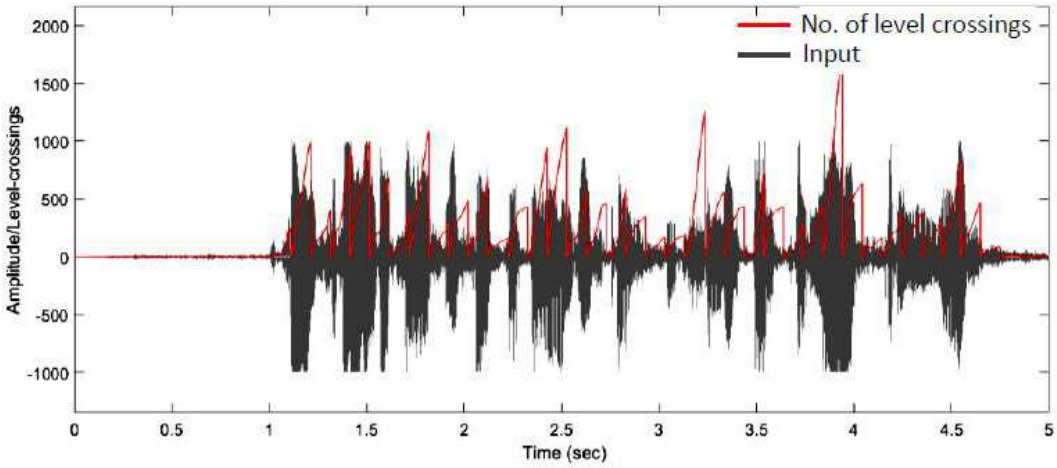


*Fig. 7.3 Speech signal and the number of level-crossings*

The input and output of a two-level-mixer are shown in Fig. 7.4. The speech signal used for controlling the mixer and its *ALCR* values are depicted in Fig. 7.4(a) and Fig. 7.4(b). The music signal, which is played in the background, is shown in Fig 7.3(c). If the *ALCR* increases above the threshold value which is previously set, the music signal is attenuated to 25% of the original amplitude, as illustrated in Fig. 7.4(d). The attenuated signal is added with the original speech signal in the mixer, as seen in Fig. 7.4(e). The value of $\Delta v$ is selected as 0.1v, and $\Delta t$ is chosen as 0.1s. *ALCR* has a variation from 0 to 1816. The threshold value is chosen as 100.

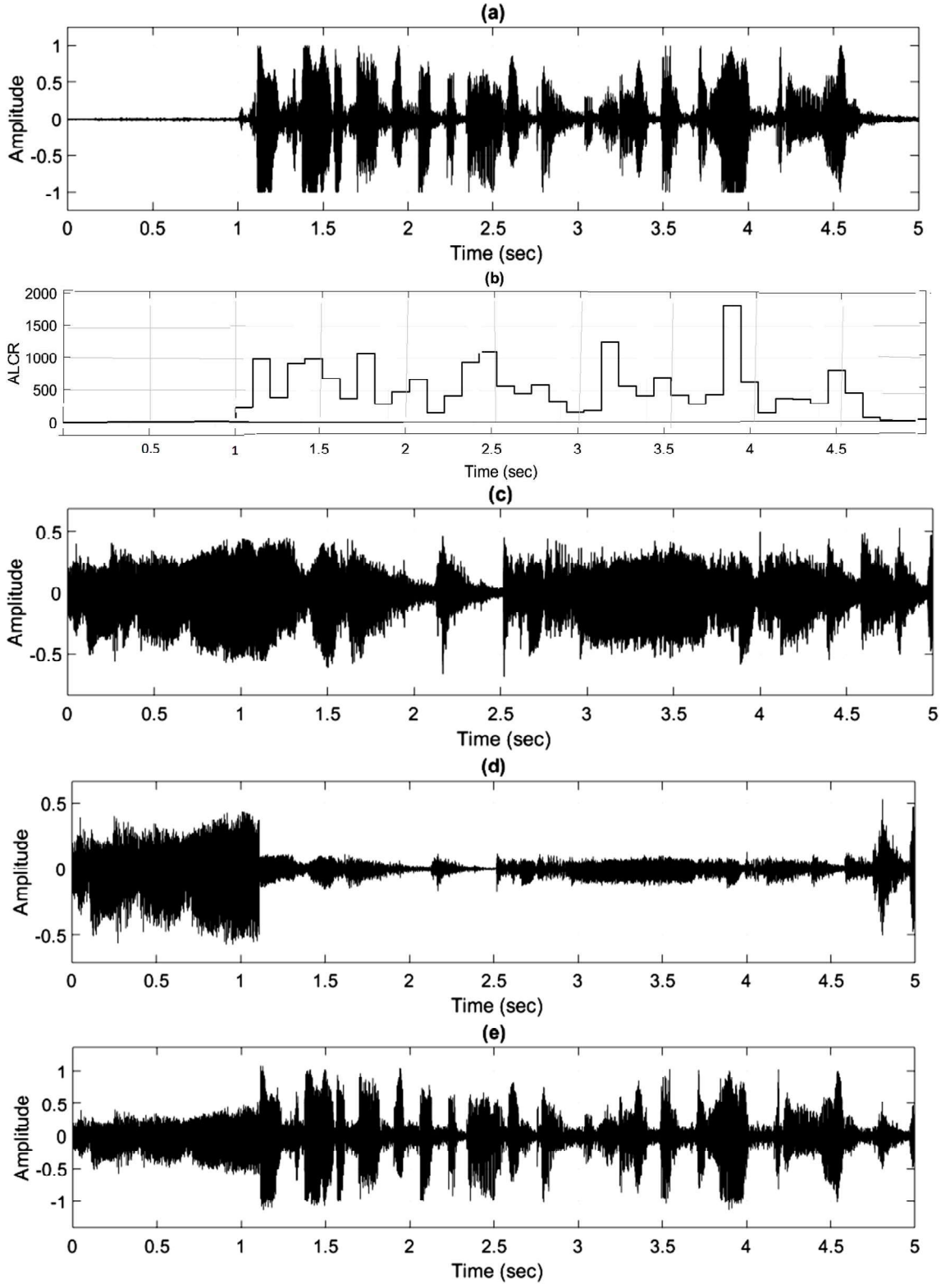


*Fig. 7.4 (a) Input speech signal (b) ALCR of the speech signal (c) Background music signal (d) Attenuated music signal (e) Mixer output*

## 7.3 ACOUSTIC FEEDBACK SUPPRESSION

Acoustic feedback, which is also known as Larson effect, occurs in public address (PA) systems and hearing aids when a closed loop is formed between the audio input and the speaker output. It is the undesired acoustic coupling between loudspeakers and microphones, as shown in Fig. 7.5. The feedback signal is again amplified and fed to the loudspeaker. If the loop-gain approaches unity, the system becomes unstable, and a steady sinusoidal signal is produced, resulting in the howling noise. The howling noise is annoying to the speaker and the audience, and manual intervention is needed to control its effect. Manual controls include a reduction in the gain of the amplifier and changing the location of the loudspeakers. Even after several years of research in automatic acoustic feedback suppression, a reliable solution has not been derived. Manual intervention is still required to reduce the gain while using PA systems.

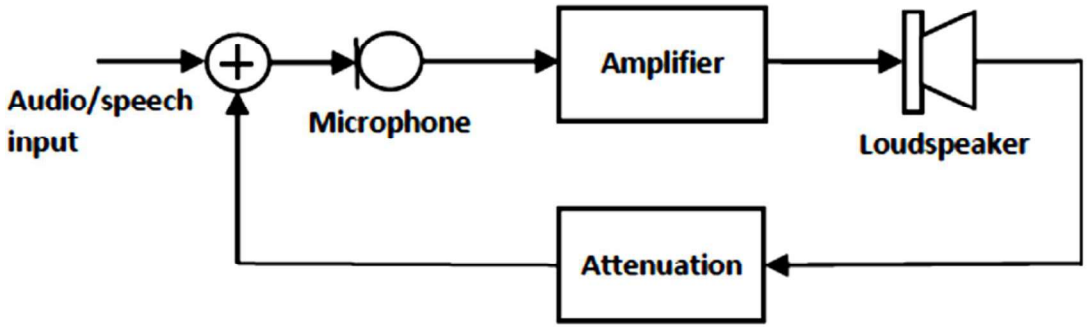


*Fig. 7.5 Model for acoustic feedback*

The frequency of oscillation developed by the acoustic feedback is dependent on the delay of the feedback signal. Based on the zero-degree locations, there are peaks in the closed-loop response with a frequency-spacing, which is equal to the reciprocal of the delay time. If the delay is increased, the frequency-spacing in the closed-loop response gets decreased, and the number of peaks at which oscillations occur increases. However, the rate at which the oscillations build-up is inversely proportional to the delay.

### 7.3.1 Methods for controlling acoustic feedback

There are various methods used for suppressing acoustic feedback. A widely adopted method is adaptive feedback cancellation (AFC), in which the feedback signal from the speaker is estimated by an adaptive filter to subtract it from the input signal for removing the feedback [97]. In the frequency shifting method, frequencies are shifted up or down by a few hertz. The frequency shifter continuously moves the generated feedback frequency until the feedback is attenuated. Another method used is the gain reduction method, in which the forward path gain is reduced to move the system away from the point of instability [98]. The gain reduction can be implemented in different ways. The gain is reduced equally in all the frequency bands in automatic gain control (AGC) methods. In automatic equalization methods (AEQ), the gain is reduced in the frequency bands where the loop gain is close to unity. The gain is reduced in narrow frequency bands in notch-filter-based howling suppression (NHS) methods [99]. The steps involved in implementing NHS methods are feedback discrimination, frequency identification, and deployment of notch frequencies.

There is proactive and reactive instability detection in gain reduction methods [100]. Proactive methods detect howling before it is perceived, based on a measurement of the magnitude response of the feedback path or by observing the critical frequency components in the microphone signal. The commonly used gain reduction techniques are based on reactive method, in which howling is perceived before detecting it.

### 7.3.2 Feedback discrimination

At a particular instant, oscillation occurs at a single frequency, and hence the microphone signal frequency having the highest magnitude can be treated as a howling signal. Several algorithms, based on both spectral and temporal criteria for discriminating howling signal from the speech and music signals are available. In spectral methods, the power ratio of the candidate howling signal to

the entire spectrum, and the ratio between its harmonics and the neighboring frequency components are evaluated. There are also methods based on temporal criteria for feedback discrimination [98]. Some of the temporal methods are based on the observations that the howling frequency component has exponentially increasing amplitude before getting a steady value. Another property used in the temporal method is that the howling frequency persists for a long time, compared to the speech signal frequency.

### 7.3.3 Frequency identification

Identification of the howling frequency can be performed by using FFT algorithms in which the peak values of frequency are selected. The frequency can also be identified from the coefficient values of adaptive notch filters. In both these methods, identification of lower frequencies is challenging. In the FFT method, the frame size selected must be long enough for achieving the required frequency resolution, resulting in a slow response. Greater precision is required in the case of adaptive notch filters.

### 7.3.4 Acoustic feedback detection based on *ALCR*

Conventional acoustic feedback detection algorithms require digitization of the input signals and framing of the samples. As discussed in section 7.3.3, the frame size selection is a compromise between the speed of operation and the frequency resolution. These limitations can be overcome with algorithms based on the level-crossing rate, in which no sampling, digitizing, and framing is required. In this chapter, the emphasis is given on the feedback discrimination and the frequency identification of the howling signal. From the analog input, acoustic feedback is detected with *ALCR*, and the howling frequency is identified with the zero-crossing time. The howling signal rapidly increases in amplitude to reach a steady level, which results in a noticeable change in the *ALCR* values. During the period of howling oscillation occurs at a single frequency, which can be measured with the zero-crossing time of the feedback signal.

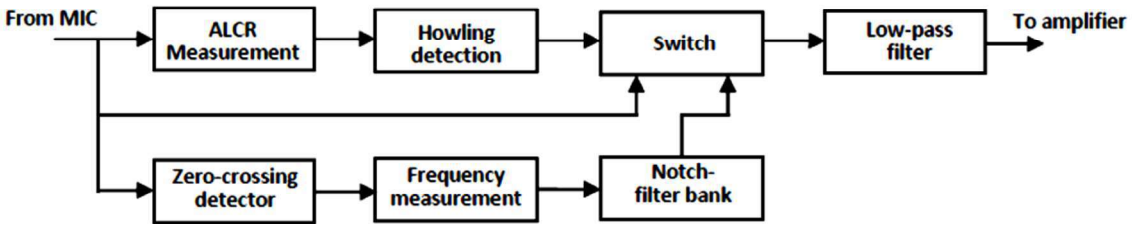


*Fig. 7.6 Block diagram of the acoustic feedback suppression system based on ALCR*

The block diagram for the acoustic feedback suppression based on *ALCR* is depicted in Fig. 7.6. *ALCR* is computed from the output of the microphone. A threshold can be fixed for the *ALCR* value, above which the signal corresponds to howling. The microphone output is fed to a zero-crossing detector, from which frequency is measured. The frequency of howling is found from the time gap between zero-crossing instants, measured using a clock signal with a known frequency. Based on the measured frequency, a particular notch filter is selected, the centre frequency of which is nearer to the howling frequency. The notch filter and the microphone output are the two inputs of a switch controlled by the howling detector. If acoustic feedback is detected, the output of the notch filter is passed to the amplifier; otherwise, output of the microphone is passed. The switched output is passed through a low-pass filter to remove the abrupt changes due to switching

### 7.3.5 Simulation Results

Acoustic feedback was created with a microphone, amplifier, and a speaker, and the microphone output was recorded for analysis. Several signals were recorded, and the variations in the *ALCR* values were observed during the howling period.

A feedback signal which consists of howling noise alone is shown in Fig. 7.7 (a). The spectrum of the signal is depicted in Fig. 7.7 (b). The significant component present is 890 Hz, which is the only frequency present during the initial period. There is an exponential increase in the peak values. After reaching

the saturation level, there is a flattening at the peak amplitude, which creates the harmonics of 890 Hz. The *ALCR* values with $\Delta t = 0.1s$ are plotted in Fig. 7.7 (c). The *ALCR* value updated at a particular instant is corresponding to the signal activity during the past 0.1s. The zero-crossing time remains the same, with which the fundamental frequency of oscillation can be measured. A digital counter is used to measure the time period of ten cycles at a time. A magnified portion of the howling signal is presented in Fig. 7.7 (d) showing the counter output that measures the zero-crossing time of ten cycles and the peak values of the counter output. The zero-crossing time remains constant for almost the entire duration, indicating the presence of a constant howling frequency. In Fig. 7.7 (d), after every ten cycles, the counter output has a mean peak value of 1125. With 100 kHz clock, the time duration of a single cycle is measured as 0.00125s. The corresponding frequency is 888.89 Hz, which is very close to howling measured from the spectrum. The signal is passed through notch filters with centre frequencies equal to the fundamental and second harmonics. It is also passed through a low pass filter to limit the high-frequency content. The output of the filter and the corresponding spectrum are shown in Fig. 7.7 (e) and Fig. 7.7 (f), illustrating that the howling frequency component is attenuated by 35 dB.

A speech signal which has howling noise during the period from 2.8s onwards is shown in Fig. 7.8 (a). *ALCR* values with $\Delta t$ selected as 0.1 s are plotted in Fig.7.8 (b). The first *ALCR* value appears at 0.1s in the figure because it is calculated for the previous 0.1s. There is a distinct margin between the *ALCR* values during the period of howling, and otherwise. A suitable value of the threshold is fixed to differentiate between the normal and feedback conditions. The zero-crossing time of the feedback signal is measured, based on which a suitable notch filter is selected for removing the howling frequency.

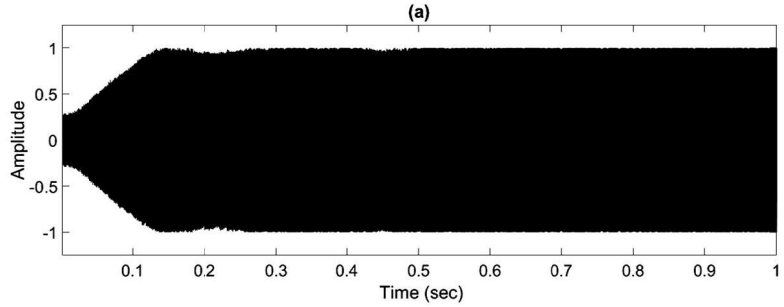


*(a) Howling signal*

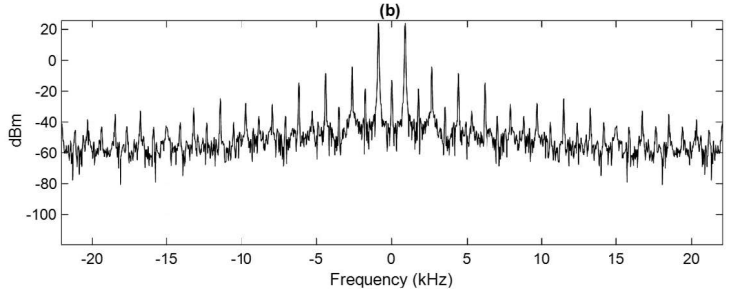


*(b) Spectrum of howling signal*

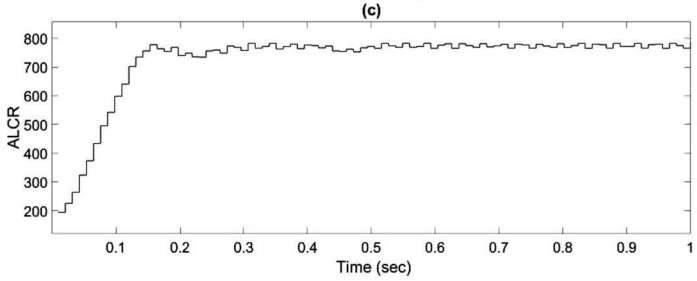


*(c) plot of ALCR*

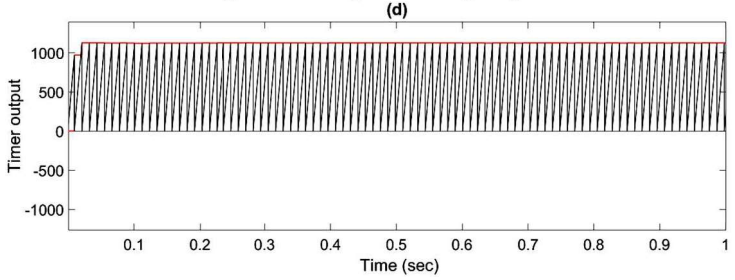


*. (d) Illustration of zero-crossing time for ten cycles*

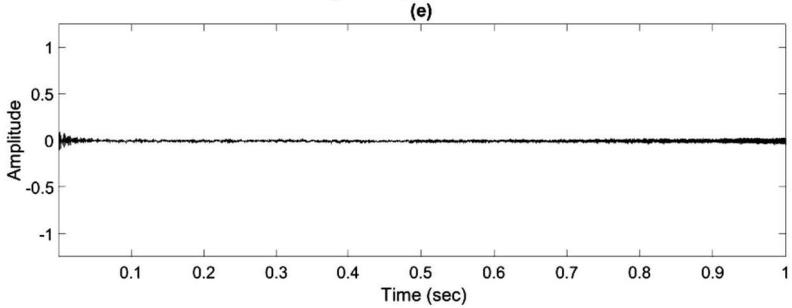


*(e) The filtered output*

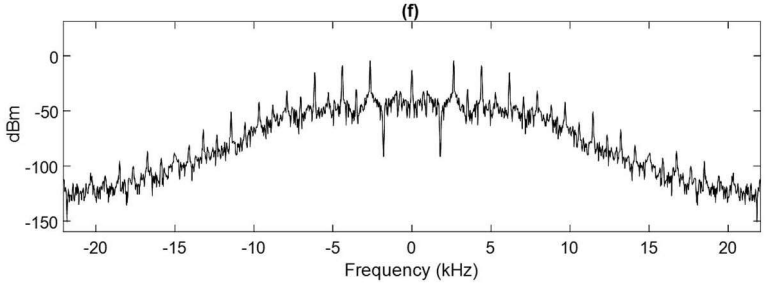


*(f) Spectrum of the filtered output*

*Fig. 7.7 Illustration of the frequency identification, and suppression of a howling signal*

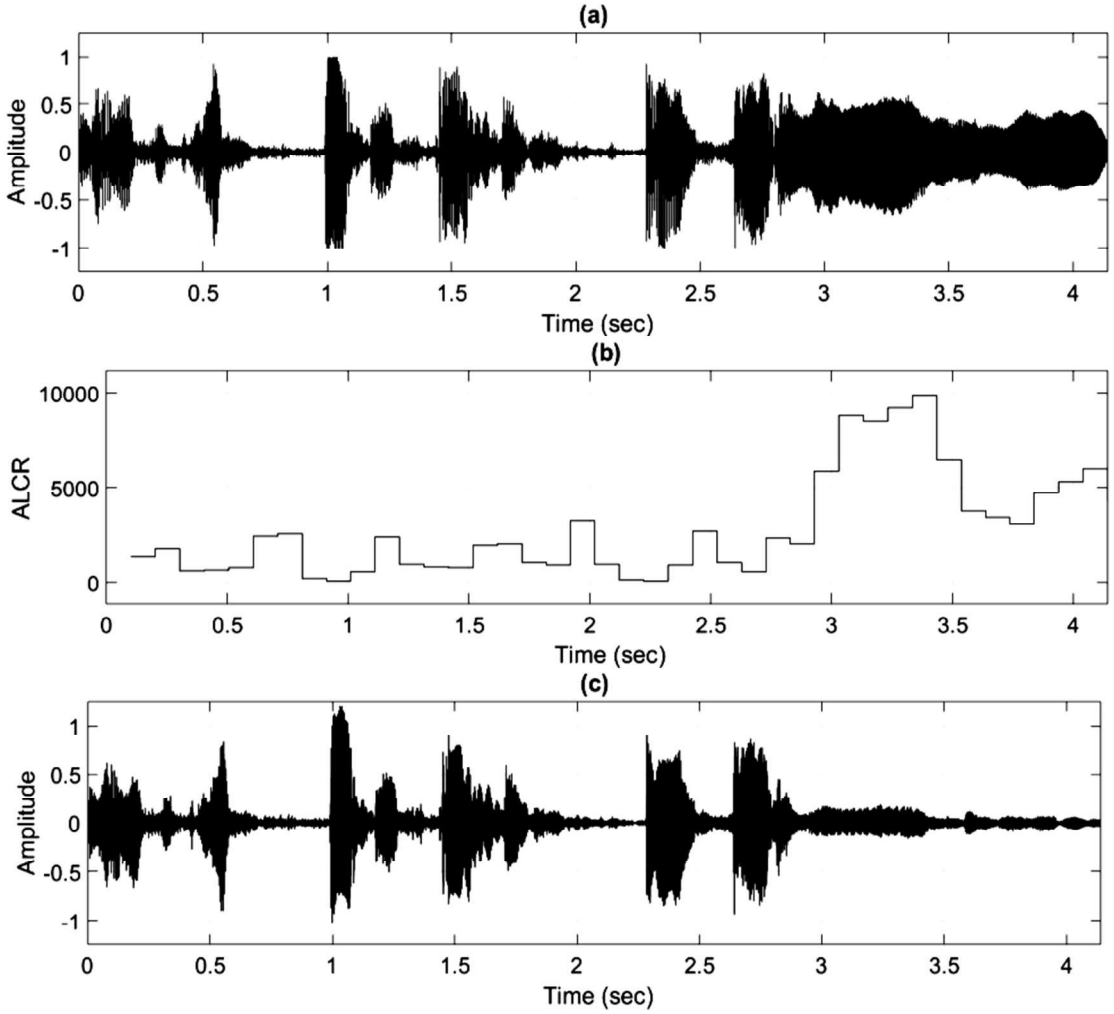


*Fig 7.8 (a) Speech signal with howling noise (b) ALCR of the speech signal (c) Output of the notch filter*

For accurate measurement of the frequency of howling, the time duration for several successive zero-crossings is measured to estimate a single time period. The clock frequency for measuring the time period is selected as 100 kHz, and the time taken for ten cycles are measured. The filtered output is depicted in Fig. 7.8 (d).

There is always a delay of $\Delta t$ in detecting the howling because, the change in *ALCR* value due to the presence of howling noise is reflected after this time. A reduction in the value of $\Delta t$ causes unnecessary variations in the *ALCR* values, especially when the peak value of the signal is nearer to the saturation level. The simulation was conducted with a limited number of recorded signals,

and a few numbers of notch filters were used. The emphasis of this work was on the feedback discrimination using *ALCR*, and frequency identification using zero-crossing time, which is suitable for any NHS system.

## 7.4 SUMMARY

In this chapter, two examples in which the activity detection is performed with *ALCR* of the input signal are presented. The voice-controlled mixer based on *ALCR* has the advantage that noise levels up to the inter-level distance $\Delta v$ are suppressed. Instead of computing the zero-crossing rate and energy of the signal, computations of *ALCR* values are sufficient for controlling the mixer. Since the *ALCR* value is computed for a specific duration $\Delta t$, any sudden change in the input of the microphone does not appear at the output. The system is capable of real-time operation, and compressed samples can be transmitted if time-to-digital converter (TDC) is also incorporated. *ALCR* values are calculated for the analog input, and hence, the input signal need not be digitized.

Time-domain methods for feedback discrimination and frequency identification, suitable for notch-based howling suppression systems are presented in this chapter. The system operates with the analog signal. In the conventional methods, the choice of frame size decides the frequency resolution and the delay. In the method based on *ALCR*, the conventional steps of sampling, digitization, and framing are avoided, and the computation of the spectrum is not needed.

# CHAPTER 8

# CONCLUSIONS AND FUTURE SCOPE

In this thesis, the potential of non-uniform sampling schemes to save resources like bandwidth, memory, and power is exploited. The possibility of low-cost activity and anomaly detection schemes that require an analog input signal instead of its digital samples are explored.

A level-crossing sampling (LCS) system for the compressed encoding of speech signals is designed and simulated. Two-level adaptive level-crossing sampler (ALCS), in which the inter-level distance $\Delta v$ is changed according to the slope of the input signal, is also simulated. Speech and vibration signals have been applied to extremum sampling (ES), which is suitable for encoding signals with an oscillatory nature. It was observed that ES provides the maximum value of compression ratio, compared to LCS and ALCS. The signal-to-noise ratio (SNR) due to the quantization of time is proportional to the clock frequency of the time-to-digital converter (TDC) employed in LCS. LCS, ALCS, and ES with multiple temporal resolutions are simulated to reduce the dynamic range of the TDC, leading to a reduction in the bits per sample. The frequency-scaling technique is incorporated in conventional level-crossing samplers to achieve multiple resolutions for the efficient encoding of the silence regions in the signals. Each frequency-scaled method has a lesser data-size than its equivalent level-crossing method that does not employ frequency-scaling.

A method is devised for the real-time anomaly detection in mechanical systems based on the average level-crossing rate (*ALCR*) of vibration signals. The proposed system works on the analog output of the sensor and does not require conventional steps like sampling, feature extraction, classification, or computation of the spectrum. A voice-controlled mixer is simulated in which the attenuation of the background music is controlled with the *ALCR* value of the

speech signal. An acoustic feedback suppression system has been simulated, in which the feedback discrimination is performed with *ALCR* values. The zero-crossing time is used for measuring the howling frequency. All the methods based on *ALCR* work on analog input, and the sampling, encoding, and framing operations are evaded.

The compression ratio achieved with level-crossing methods is not the outcome of a compression algorithm but the result achieved with a non-uniform sampling process. The possibility of achieving further compression from these non-uniform samples needs to be explored. *ALCR* can be used as a parameter for predicting a machine's remaining useful life (RUL). Generally, for the prediction of RUL, a massive amount of vibration data is needed. The same task can be achieved using *ALCR* values, which are very few compared to the number of samples in the vibration data. Level-crossing methods can also be applied for the analysis of power quality. Synchronous logic has reached its technological limits while dealing with power consumption, clock distribution, and electromagnetic emission, and hence, non-uniform sampling is a promise for the future digital world.

# REFERENCES


[1] C. E. Shannon, “Communication in the presence of noise,” Proc. IRE, vol. 37, pp. 10-21, 1949.

[2] Miskowicz M., "Event-Based Control and Signal Processing," Taylor & Francis, 2015.

[3] T. Beyrouthy L. Fesquet, and R. Rolland, “Data sampling and processing: Uniform vs. non-uniform schemes,” Oct. 2015, doi: 10.1109/EBCCSP.2015.7300665.

[4] A. Kabbani, “Logical effort based dynamic power estimation and optimization of static CMOS circuits,” *Integr. VLSI J.*, vol. 43, no. 3, pp. 279–288, Jun. 2010, doi: 10.1016/j.vlsi.2010.02.002.

[5] L. Alacoque, M. Renaudin, and S. Nicolle, “Irregular sampling and local quantification scheme A-D converter,” *Electron. Lett.*, vol. 39, no. 3, pp. 263–264, Feb. 2003, doi: 10.1049/el:20030237.

[6] E. Allier, L. Fesquet, G. Sicard, M. Renaudin, “Low Power Asynchronous A/D Conversion”, Proceedings of the 12th International Workshop on Power and Timing, Modeling, Optimization and Simulation (PATMOS’02), September 11-13 2002, Sevilla, Spain.

[7] Can A., Sejdic, E., Chaparro, L.: ‘Asynchronous sampling and reconstruction of sparse signals,’ Proc. of the 20th European Signal Processing Conf. (EUSIPCO), August 2012, pp. 854–858.

[8] Y. Tsividis, “Continuous-time digital signal processing,” *Electron. Lett.*, vol. 39, no. 21, pp. 1551–1552, Oct. 2003, doi: 10.1049/el:20031015.

[9] Y. Tsividis, Digital signal processing in continuous time: A possibility for avoiding aliasing and reducing quantization error, Proceedings of IEEE International Conf. on Acoustics, Speech, and Signal Processing ICASSP 2004, 2004, pp. 589–592.

[10] Candes, E. J., & Wakin, M. B. (2008). An Introduction to Compressive Sampling. IEEE Signal Processing Magazine, 25(2), 21–0. doi:10.1109/msp.2007.914731.

[11] Orović, I., Papić, V., Ioana, C., Li, X., & Stanković, S, "Compressive Sensing in Signal Processing: Algorithms and Transform Domain Formulations," *Mathematical Problems in Engineering, 2016, 1–16.* doi:10.1155/2016/7616393.

[12] E. J. Candes and M. B. Wakin, "An introduction to compressive sampling: A sensing/sampling paradigm that goes against the common knowledge in data acquisition," *IEEE Signal Process. Mag.*, vol. 25, no. 2, pp. 21–30, 2008, doi: 10.1109/MSP.2007.914731.

[13] M. A. Davenport, M. F. Duarte, Y. C. Eldar, and G. Kutyniok, "Introduction to compressed sensing," in *Compressed Sensing: Theory and Applications*, Cambridge University Press, 2009, pp. 1–64.

[14] J. W. Mark and T. D. Todd, "A Nonuniform Sampling Approach to Data Compression," *IEEE Trans. Commun.*, vol. 29, no. 1, pp. 24–32, 1981, doi: 10.1109/TCOM.1981.1094872.

[15] N. Sayiner, H. N. Sorensen, and T. R. Viswanathan, "A level-crossing sampling scheme for A/D conversion," *IEEE Trans. Circuits Syst*. II, vol. 43, pp. 335-339, 1996.

[16] F. Akopyan, R. Manohar, and A. B. Apsel, “A level-crossing flash asynchronous analog-to-digital converter,” in *Proceedings - International Symposium on Asynchronous Circuits and Systems*, 2006, vol. 2006, pp. 12–22, doi: 10.1109/ASYNC.2006.5.

[17] H. Inose, T. Aoki, and K. Watanabe, “Asynchronous delta-modulation system,” *Electron. Lett.*, vol. 2, no. 3, pp. 95–96, 1966, doi: 10.1049/el:19660077.

[18] A. El-Hadbi, O. Elissati, and L. Fesquet, “Time-to-Digital Converters: A Literature Review and New Perspectives,” May 2019, doi: 10.1109/EBCCSP.2019.8836857.

[19] E. Allier, G. Sicard, L. Fesquet, and M. Renaudin, “A new class of asynchronous A/D converters based on time quantization,” in *Proceedings - International Symposium on Asynchronous Circuits and Systems*, 2003, pp. 196–205, doi: 10.1109/ASYNC.2003.1199179.

[20] T. Wang, D. Wang, P. J. Hurst, B. C. Levy, and S. H. Lewis, “A level-crossing analog-to-digital converter with triangular dither,” *IEEE Trans. Circuits Syst. I Regul. Pap.*, vol. 56, no. 9, pp. 2089–2099, 2009, doi: 10.1109/TCSI.2008.2011586.

[21] C. Weltin-Wu and Y. Tsividis, “An event-driven, alias-free ADC with signal-dependent resolution,” in *IEEE Symposium on VLSI Circuits, Digest of Technical Papers*, 2012, pp. 28–29, doi: 10.1109/VLSIC.2012.6243773.

[22] N. Ravanshad, H. Rezaee-Dehsorkh, and R. Lotfi, “A fully-synchronous offset-insensitive level-crossing analog-To-digital converter,” in *Midwest Symposium on Circuits and Systems*, Jul. 2016, vol. 0, doi: 10.1109/MWSCAS.2016.7870108.

[23] Y. Li, D. Zhao, M. N. Van Dongen, and W. A. Serdijn, “A 0.5V signal-specific continuous-time level-crossing ADC with charge sharing,” in *2011 IEEE Biomedical Circuits and Systems Conference, BioCAS 2011*, 2011, pp. 381–384, doi: 10.1109/BioCAS.2011.6107807.

[24] M. Malmirchegini, M. M. Kafashan, M. Ghassemian, and F. Marvasti, “Non-uniform sampling based on an adaptive level-crossing scheme,” *IET Signal Process.*, vol. 9, no. 6, pp. 484–490, Aug. 2015, doi: 10.1049/iet-spr.2014.0170.

[25] B. Bidegaray-Fesquet and L. Fesquet, “Levels, peaks, slopes. which sampling for which purpose?” Oct. 2016, doi: 10.1109/EBCCSP.2016.7605261.

[26] I. Homjakovs, M. Hashimoto, T. Onoye, and T. Hirose, “Signal-dependent analog-to-digital conversion based on MINIMAX sampling,” 2011, doi: 10.1109/ MWSCAS.2011.6026466.

[27] Greitans M., Shavelis R., Fesquet L., Beyrouthy T., “Combined peak and level-crossing sampling scheme,” *In: Proceedings of international conference on sampling theory and applications SampTA*, 2011.

[28] J. Zhou *et al.*, “Compressed Level Crossing Sampling for Ultra-Low Power IoT Devices,” *IEEE Trans. Circuits Syst. I Regul. Pap.*, vol. 64, no. 9, pp. 2495–2507, Sep. 2017, doi: 10.1109/TCSI.2017.2707481.

[29] Y. Li, D. Zhao, and W. A. Serdijn, “A sub-microwatt asynchronous level-crossing ADC for biomedical applications,” *IEEE Trans. Biomed. Circuits Syst.*, vol. 7, no. 2, pp. 149–157, 2013, doi: 10.1109/TBCAS.2013.2254484.

[30] W. Tang *et al.*, “Continuous time level crossing sampling ADC for bio-potential recording systems,” *IEEE Trans. Circuits Syst. I Regul. Pap.*, vol. 60, no. 6, pp. 1407–1418, 2013, doi: 10.1109/TCSI.2012.2220464.

[31] J. Jimenez, S. Dai, and J. K. Rosenstein, “A microwatt front end and asynchronous ADC for sparse biopotential acquisition,” in *Midwest Symposium on Circuits and Systems*, Sep. 2017, vol. 2017-August, pp. 503–506, doi: 10.1109/MWSCAS.2017.8052970.

[32] T. Marisa *et al.*, “Pseudo Asynchronous Level Crossing ADC for ECG Signal Acquisition,” *IEEE Trans. Biomed. Circuits Syst.*, vol. 11, no. 2, pp. 267–278, Apr. 2017, doi: 10.1109/TBCAS.2016.2619858.

[33] H. Teimoori, N. Ravanshad, and H. Rezaee-Dehsorkh, “Ultra-low-power fully-synchronous level-crossing analog-to-digital converter for biomedical signal acquisition,” in *Proceedings of the International Conference on Microelectronics, ICM*, Jan. 2018, vol. 2017-December, pp. 1–4, doi: 10.1109/ICM.2017.8268875.

[34] Y. Hou *et al.*, “A 61-nW Level-Crossing ADC with Adaptive Sampling for Biomedical Applications,” *IEEE Trans. Circuits Syst. II Express Briefs*, vol. 66, no. 1, pp. 56–60, Jan. 2019, doi: 10.1109/TCSII.2018.2841037.

[35] B. L, “Single-Chip Implementation of Level-Crossing ADC for ECG Sampling,” *J. Electr. Electron. Syst.*, vol. 06, no. 01, 2017, doi: 10.4172/2332-0796.1000219.

[36] N. Ravanshad, H. Rezaee-Dehsorkh, R. Lotfi, and Y. Lian, “A level-crossing based QRS-detection algorithm for wearable ECG sensors,” *IEEE J. Biomed. Heal. Informatics*, vol. 18, no. 1, pp. 183–192, Jan. 2014, doi: 10.1109/JBHI.2013.2274809.

[37] F. Aeschlimann, E. Allier, L. Fesquet, and M. Renaudin, “Asynchronous FIR filters: towards a new digital processing chain,” Jun. 2004, pp. 198–206, doi: 10.1109/async.2004.1299303.

[38] C. Vezyrtzis and Y. Tsividis, “Processing of signals using level-crossing sampling,” in *Proceedings - IEEE International Symposium on Circuits and Systems*, 2009, pp. 2293–2296, doi: 10.1109/ISCAS.2009.5118257.

[39] M. Greitans and R. Shavelis, “Speech sampling by level-crossing and its reconstruction using spline-based filtering,” in *2007 IWSSIP and EC-SIPMCS - Proc. 2007 14th Int. Workshop on Systems, Signals and Image Processing, and 6th EURASIP Conf. Focused on Speech and Image Processing, Multimedia Communications and Services*, 2007, pp. 292–295, doi: 10.1109/IWSSIP.2007.4381099.

[40] S. M. Qaisar, R. Yahiaoui, and T. Gharbi, “An efficient signal acquisition with an adaptive rate A/D conversion,” in *ICCAS 2013 - 2013 IEEE International Conference on Circuits and Systems: “Advanced Circuits and Systems for Sustainability,”* 2013, pp. 124–129, doi: 10.1109/CircuitsAndSystems.2013.6671611.

[41] M. B. Mashhadi, N. Salarieh, E. S. Farahani, and F. Marvasti, “Level crossing speech sampling and its sparsity promoting reconstruction using an iterative method with adaptive thresholding,” *IET Signal Process.*, vol. 11, no. 6, pp. 721–726, Aug. 2017, doi: 10.1049/iet-spr.2016.0569.

[42] J. C. Charr, R. Couturier, A. Fanfakh, and A. Giersch, “Dynamic frequency scaling for energy consumption reduction in synchronous distributed applications,” in *Proceedings - 2014 IEEE International Symposium on Parallel and Distributed Processing with Applications, ISPA 2014*, Oct. 2014, pp. 225–230, doi: 10.1109/ISPA.2014.38.

[43] P. Di Sanzo and B. Ciciani, “CPU-core frequency scaling for efficient thread scheduling in transactional memories,” in *2016 International Conference on High Performance Computing and Simulation, HPCS 2016*, Sep. 2016, pp. 42–47, doi: 10.1109/HPCSim.2016.7568314.

[44] K. Choi, R. Soma, and M. Pedram, “Dynamic Voltage and Frequency Scaling based on Workload Decomposition,” in *Proceedings of the International Symposium on Low Power Electronics and Design*, 2004, vol. 2004-January, no. January, pp. 174–179, doi: 10.1109/LPE.2004.240891.

[45] David Salomon, *Data Compression: The Complete Reference*. New York: Springer-Verlag, 2004.

[46] M. Malovic, L. Brajovic, T. Sekara, and Z. Miskovic, “Lossless compression of vibration signals on an embedded device using a TDE based predictor,” *Elektron. irElektrotechnika*, vol. 22, no. 2, pp. 21–26, 2016, doi: 10.5755/j01.eie.22.2.7646.

[47] Y. Zhang, P. Hutchinson, N. A. J. Lieven, and J. Nunez-Yanez, “Optimal compression of vibration data with lifting wavelet transform and context-based arithmetic coding,” in *25th European Signal Processing Conference, EUSIPCO 2017*, Oct. 2017, vol. 2017-January, pp. 1996–2000, doi: 10.23919/EUSIPCO. 2017.8081559.

[48] K. A. Jaafar, I. Najem Saleh, and A. Ali Abduladhem, “Vibration data compression in wireless sensors network,” in *2012 IEEE International Conference on Signal Processing, Communications and Computing, ICSPCC 2012*, 2012, pp. 717–722, doi: 10.1109/ICSPCC.2012.6335712.

[49] Y. Shan, Y. Ren, G. Zhen, and K. Wang, “An enhanced run-length encoding compression method for telemetry data,” *Metrol. Meas. Syst.*, vol. 24, no. 3, pp. 551–562, Sep. 2017, doi: 10.1515/mms-2017-0039.

[50] M. Oltean, J. Picheral, E. Lahalle, and H. Hamdan, “Vibration signals compression with time-frequency adaptive quantization,” in *WISP 2011 - IEEE International Symposium on Intelligent Signal Processing, Proceedings*, 2011, pp. 138–141, doi: 10.1109/WISP.2011.6051693.

[51] M. Oltean, J. Picheral, E. Lahalle, H. Hamdan, and J. Griffaton, “Compression methods for mechanical vibration signals: Application to the plane engines,” *Mech. Syst. Signal Process.*, vol. 41, no. 1–2, pp. 313–327, Dec. 2013, doi: 10.1016/ j.ymssp.2013.07.005.

[52] Yi-Qing Ni, Si-Xin Chen, “Compressive sensing for vibration signals in high-speed rail monitoring,” *9th European Workshop on Structural Health Monitoring* (EWSHM 2018) July 10-13 Manchester UK, 2018.

[53] L. Zhou, Q. Yu, D. Liu, M. Li, S. Chi, and L. Liu, “Compressive sensing-based vibration signal reconstruction using sparsity adaptive subspace pursuit,” *Adv. Mech. Eng.*, vol. 10, no. 8, Aug. 2018, doi: 10.1177/1687814018790877.

[54] G. Vachtsevanos, F. L. Lewis, M. Roemer, A. Hess, and B. Wu, *Intelligent Fault Diagnosis and Prognosis for Engineering Systems*, John Wiley & Sons Ltd., New Jersey, 2006.

[55] Yang Zhang, Paul Hutchinson, Nicholas A.J. Lieven, Jose Nunez-Yanez, “Adaptive event-triggered anomaly detection in compressed vibration data,” *Mechanical Systems and Signal Processing*, May 2019 122:480.

[56] D.A. Tobon-Mejia, K. Medjaher, N. Zerhouni, G. Tripot, “A Data-driven Failure Prognostics Method Based on Mixture of Gaussians Hidden Markov Models,” *IEEE Trans. Reliab*. 61 (2) (2012) 491–503, https://doi.org/10.1109/TR.2012.2194177.

[57] S. Lindsay and D. M. K. Woodbridge, “Spacecraft state-of-health (SOH) analysis via data mining,” 2014, doi: 10.2514/6.2014-1733.

[58] L. Hong and J. S. Dhupia, “A time-domain fault detection method based on an electrical machine stator current measurement for planetary gear-sets,” in *2013 IEEE/ASME International Conference on Advanced Intelligent Mechatronics: Mechatronics for Human Wellbeing, AIM 2013*, 2013, pp. 1631–1636, doi: 10.1109/AIM.2013.6584330.

[59] Davis, Bryan J., "A Novel Time-Domain Method of Fault Diagnosis in Induction Motors" (2017). Honors Scholar Theses. 546.

[60] M. D. Prieto, G. Cirrincione, A. G. Espinosa, J. A. Ortega, and H. Henao, “Bearing fault detection by a novel condition-monitoring scheme based on statistical-time features and neural networks,” *IEEE Trans. Ind. Electron.*, vol. 60, no. 8, pp. 3398–3407, 2013, doi: 10.1109/TIE.2012.2219838.

[61] Li W., Zhang S., Rakheja S., “Feature denoising and nearest-farthest distance preserving projection for machine fault diagnosis,” *IEEE Trans. Ind. Inform*. 2016, 12, 393–404.

[62] Jiang L., Shi T., Xuan J., “Fault diagnosis of rolling bearings based on marginal fisher analysis,” *J. Vib. Control* 2014, 20, 470–480.

[63] Ali, J.B., Fnaiech N., Saidi L., Chebel-Morello B., and Fnaiech F., “Application of empirical mode decomposition and artificial neural network for automatic bearing fault diagnosis based on vibration signals,” *Appl. Acoust*. 2015, 89, 16–27.

[64] Sun, Y., Xiong, Z., “An optimal weighted wavelet packet entropy method with application to real-time chatter detection,” *IEEE/ASME Trans. Mechatron*. 2016, 21, 2004–2014.

[65] Jung U., Koh, B.Wavelet energy-based visualization and classification of high-dimensional signal for bearing fault detection. Knowl. Inf. Syst. 2015, 44, 197–215.

[66] Zhang, L.; Hu, J.F.; Xiong, G.L., "Bearing fault diagnosis using a novel classifier ensemble based on lifting wavelet packet transforms and sample entropy," *Shock Vib*. 2016, 2016, 4805383.

[67] Xinpeng Zhang, Niaoqing Hu, Lei Hu, Ling Chen, and Zhe Cheng, "A bearing fault detection method with low-dimensional compressed measurements of vibration signal," *Advances in Mechanical Engineering* 2015, Vol. 7(7) 1–12.

[68] Wang H., Ke, Y., Luo G., Li L., and Tang G., "A Two-Stage Compression Method for the Fault Detection of Roller Bearings," *Shock Vib*. 2016, 4, 1–11.

[69] Jian Li, Jun Deng, and WeizhiXie, "Damage Detection with Streamlined Structural Health Monitoring Data," *Sensors*, 15 (4) (2015), pp.8832-8851.

[70] Yusuke Takahashi, "Anomaly Detection using Vibration Analysis with Machine Learning Technology for Industrial IoT System," *OKI Technical Review*, December 2017 / Issue 230 Vol. 84 No.2.

[71] Sun S.Y., Wang Y., "Fault diagnosis of gear box based on BP neural network," *Advances in computers. Electron Mechatron*2014;667:349–52.

[72] Qu Y. Z., He M., Deutsch J., He D., "Detection of pitting in gears using a deep sparse autoencoder," *Appl Sci-Basel* 2017;7(5):515.

[73] Wang J., Li S., An Z., Jiang X., Qian W., Ji S., "Batch-normalized deep neural networks for achieving fast intelligent fault diagnosis of machines," *Neurocomputing* 2019; 329: 53–65.

[74] Vincent P, Larochelle H, Lajoie I, Bengio Y, Manzagol P-A. Stacked denoising autoencoders: learning useful representations in a deep network with a local denoising criterion. J Mach Learn Res 2010;11(12):3371–408.

[75] J. A. Enokela and J. U. Agber, “An Automatic Voice-Controlled Audio Amplifier,” 2012. Accessed: Nov. 26, 2020. [Online]. Available: http://www.ijser.org.

[76] Ilmi, M., Huda, M., & Rahardhita, W., “Automatic Control Music Amplifier Using Speech Signal Utilizing by TMS320C6713,” 2015 International Electronics Symposium (IES).

[77] P. R. Williams, ‘‘Method and System for Elimination of Acoustic Feedback,’’ U.S. patent appl. 2010/0 046 768 A1 (2010 Feb.).

[78] D. Somasundaram, ‘‘Feedback Cancellation in a Sound System,’’ U.S. patent appl. 2008/0 085 013 A1 (2008 Apr.).

[79] M. H. Er, T. H. Ooi, L. S. Li, and C. J. Liew, ‘‘A DSP-Based Acoustic Feedback Canceller for Public Address Systems,’’ *Microprocessors and Microsys*., vol. 18, pp. 39–47 (1994 Jan./Feb.).

[80] S. Ando, ‘‘Howling Detection and Prevention Circuit and a Loudspeaker System Employing the Same,’’ U.S. patent 6,252,969 (2001 June)

[81] A. Kawamura, M. Matsumoto, M. Serikawa, and H. Numazu, ‘‘Sound Amplifying Apparatus with Automatic Howl-Suppressing Function,’’ Euro. patent EP0 599 450 (2001 Nov.)

[82] N. Osmanovic and V. Clarke, ‘‘Acoustic Feedback Cancellation System,’’ U.S. patent 7,664,275 (2010 Feb.).

[83] Beutler, F. J. (1966). *Error-Free Recovery of Signals from Irregularly Spaced Samples. SIAM Review, 8(3), 328–335.* doi:10.1137/1008065.

[84] Ellis, P. (1959). Extension of phase plane analysis to quantized systems. IRE Transactions on Automatic Control, 4(2), 43–54. doi:10.1109/tac.1959.1104845.

[85] Inose, H., Aoki, T., & Watanabe, K., "Asynchronous delta-modulation system," *Electronics Letters, 2(3), 95.* doi:10.1049/el:19660077, 1966

[86] K. J. Astrom, and B. Bernhardsson, "Comparison of periodic and event-based sampling for first-order stochastic systems," *In proceedings of IFAC World Congress*, 1999, pp. 301–306.

[87] M. Mi´skowicz, "Send-on-delta concept: An event-based data reporting strategy," *Sensors*, vol. 6, pp. 49–63, 2006.

[88] Mark Davenport, Marco Duarte, Yonina Eldar, and Gitta Kutyniok, "Introduction to compressed sensing," (Chapter in *Compressed Sensing: Theory and Applications*, Cambridge University Press, 2012).

[89] J. Kalisz, "Review of methods for time interval measurements with picosecond resolution," *Metrologia*, vol. 41, no. 1. pp. 17–32, Feb. 2004, doi: 10.1088/0026-1394/41/1/004.

[90] WenleiBao, Changwan Hong, Sudheer Chunduri, Sriram Krishnamoorthy, Louis-Noel Pouchet, Fabrice Rastello, and P. Sadayappan. "Static and Dynamic Frequency Scaling on Multicore CPUs," *ACM Transactions on Architecture and Code Optimization* (*TACO*), 13(4), 2016.

[91] Thomas Lynch J., "Data Compression, Techniques and Applications," Van Nostrand Reinhold Company, 1985.

[92] CCSDS Secretariat (2012) Lossless Data Compression CCSDS Blue Book. CCSDS 121.0-B-2.

[93] https://csegroups.case.edu/bearingdatacenter/pages/download-data-file.

[94] Anindya Sarkar and T.V. Sreenivas, “Automatic Speech Segmentation Using Average Level Crossing Rate Information,” *IEEE International Conference on Acoustics, Speech, and Signal Processing (ICASSP'05)*, vol. 1, pp. 397-400, March 2005.

[95] Hai Qiu, Jay Lee, Jing Lin. “Wavelet Filter-based Weak Signature Detection Method and its Application on Roller Bearing Prognostics.” *Journal of Sound and Vibration* 289 (2006) 1066-1090.

[96] Enokela Jonathan Adakole and Jonathan U. Agber. “An Automatic Voice-Controlled Audio Amplifier.” *International Journal of Scientific & Engineering Research*, Volume 3, Issue 1, January-2012.

[97] Guilin Ma, Gran, F., Jacobsen, F., & Agerkvist, F. T., “Adaptive Feedback Cancellation with Band-Limited LPC Vocoder in Digital Hearing Aids,” *IEEE Transactions on Audio, Speech, and Language Processing, 19(4), 677–687.* doi:10.1109/tasl.2010.2057245, 2011.

[98] Toon van Waterschoot, Marc Moonen, "Comparative Evaluation of Howling Detection Criteria in Notch-Filter-Based Howling Suppression," *J. Audio Eng. Soc*., vol. 58, no. 11, pp. 923-940, (2010 November).

[99] P. Gil-Cacho, T. van Waterschoot, M. Moonen and S. H. Jensen, "Regularized adaptive notch filters for acoustic howling suppression," *2009 17th European Signal Processing Conference*, Glasgow, 2009, pp. 2574-2578.

[100] T. van Waterschoot and M. Moonen, "Fifty Years of Acoustic Feedback Control: State of the Art and Future Challenges," in *Proceedings of the IEEE*, vol. 99, no. 2, pp. 288-327, Feb. 2011, doi: 10.1109/JPROC.2010.2090998.

# LIST OF PUBLICATIONS

**Journal Publications:**

1. Premanand B., and V.S. Sheeba, "Compressed Encoding of Vibration Signals using Extremum sampling," *SN Journal of Applied Sciences* (Springer Nature), DOI:10.1007/s42452-020-3076-6.

2. Premanand B., and V.S. Sheeba, "Real-Time Anomaly Detection using Average Level-Crossing Rate," *International Journal of Innovative Technology and Exploring Engineering*, DOI: 10.35940/ ijitee. D1863.029420.

**National Conference:**

1. Harsha K.K. & Premanand B., "Trends in Acoustic Feedback Suppression Methods," National Conference on Innovations in Engineering & Technology, NCIET-2020, Feb 11$^{th}$ and 12$^{th}$ Govt. Polytechnic College, Palakkad.

**Paper under revision:**

1. Premanand B., and V.S. Sheeba, "Level-Crossing Sampling with Multiple Temporal Resolutions for Speech Signals," Journal of Circuits, Systems, and Computers.